WASHINGTON UNIVERSITY

SCHOOL OF ENGINEERING AND APPLIED SCIENCE

DEPARTMENT OF CIVIL ENGINEERING

SEISMIC FRAGILITY RELATIONSHIPS FOR CIVIL STRUCTURES RETROFITTED

WITH SEMI-ACTIVE DEVICES

by

Waleed T. Barnawi

Prepared under the direction of Professor Shirley J. Dyke

A thesis presented to the School of Engineering of

Washington University in partial fulfillment of the

requirements for the degree of

MASTER OF SCIENCE

August 2008

Saint Louis, Missouri

WASHINGTON UNIVERSITY

SCHOOL OF ENGINEERING AND APPLIED SCIENCE

DEPARTMENT OF COMPUTER SCIENCE AND ENGINEERING

ABSTRACT

SEISMIC FRAGILITY RELATIONSHIPS CIVIL STRUCTURES RETROFITTED

WITH SEMI-ACTIVE DEVICES

by

Waleed T. Barnawi

ADVISOR: Professor Shirley J. Dyke

August 2008

St. Louis, Missouri

Development of techniques for seismic mitigation has become increasingly important for communities throughout the world. Of the many available techniques, structural control has emerged as a promising option for the last thirty years. Extensive investigation has been conducted for modeling, performance, and strategies of structural control. Studies of this method have centered on the use of passive, active, and semi-active control devices. Semi-active control devices have gained popularity because they combine positive aspects of both passive and active control. In particular, magnetorheological dampers have been used extensively in research and implemented in practice. However, structural control studies are evaluated on a case by case scenario or over a few earthquakes. In recent years, a new approach known as consequence based engineering seeks to evaluate seismic risk reduction through probabilistic safety assessment spanning a large class of structures. The assessment is performed through the development of fragility relationships for a class of structures. Seismic fragility relationships determine the probability of exceeding some limit state over a range of seismic inputs based on a number of ground motions, thus allowing for more than one case scenario to be analyzed. This thesis focuses on the methodology used to develop fragility relationships for civil structures that have been retrofitted with semi-active control devices for seismic risk mitigation purposes.

To Jennifer, my family, and the Fouts

Contents

List of Tables

List of Figures

Acknowledgements

Lastly, I would like to thank the most important people in my life. My family who have always wanted what was best for me. Jennifer Fout, my fiancé, whose words lended me strength and comfort when I could not find any. And to God, who was there every step of the way.

<div align="right">Waleed T. Barnawi</div>

Chapter 1

Literature Review

Earthquakes are one of nature's most destructive events. Earthquakes cause devastating loss of lives and billions of dollars in structural and non-structural damage. In recent times, the world has experienced several major earthquakes. The 2004 Great Sumatra-Andaman Earthquake which caused a devastating tsunami resulted in over 200,000 deaths. The 2007 Peru Earthquake caused over 500 deaths. The 2008 Chengdu Earthquake in China killed an estimated 80,000 people. With so much destruction being caused by these earthquakes, mankind has sought to implement measures to prevent such catastrophes from reoccurring.

In order to reduce the effects earthquakes have on safety, structural damage and business interruption, design codes have been developed. Many of these new codes have started using performance based approaches to ensure that certain levels of safety are met. Despite these efforts, buildings are still susceptible to damage. This concern is especially true for buildings designed before new codes were in place that properly evaluated the lateral forces applied to structures.

Consequence based engineering is a new approach to evaluate seismic risk reduction through a probabilistic safety assessment. Seismic risk assessments have become more valuable to mitigate future losses due to its ability to cover more than case by case scenarios.

In such methods, fragility assessments are an integral part of probabilistic safety assessments. Fragility assessments have shown to be advantageous due to their efficacy in spite of prior knowledge of the hazard, cost efficiency, and simplicity (Wen, Ellingwood, and Bracci 2004). In fact, numerous studies have been conducted that apply fragility analyses to structures (Jeong and Elnashai 2004; Kafali and Grigoriu 2004).

The last several years have seen a rise in the use of fragility curves for mitigation studies (Bai 2004; Reinhorn, Barron-Correva, and Ayala 2002; Taylor and Dyke 2006; Taylor 2007). Tragedies such as Hurricane Katrina and the collapse of the I-35 West Mississippi River Bridge in Minnesota have made emergency management agencies more conscientious regarding rehabilitation of structures. As mentioned earlier, older structures are more at risk of natural hazards due to deterioration and dated design specifications. In these cases, community leaders must decide which buildings are in need of more immediate rehabilitation. Fragility assessments aid in decision-making for communities about which structures are in need of more immediate attention. In addition to being able to identify structures in need of repair, fragility assessments can show the reduction in damage of structures that have been properly retrofitted. Some of these retrofit strategies include shear walls, column jacketing, and cross bracing. Recently, the idea of structural control has emerged as a promising retrofit option.

Developed nearly four decades ago, structural control has been investigated and proven to reduce the responses of civil engineering structures excited by external disturbances such as earthquakes. Structural control systems are typically classified into three main categories:

passive, active, and semi-active control. Of the three types of control systems, passive systems are the most widely used. Passive devices utilize the building's response to develop control forces for the reduction of seismic effects. The drawback to passive devices, however, is that this class of devices has no controllable feature and is therefore very limited in their ability to mitigate the effects of various seismic events. Active control devices are comprised of sensors used to measure the building's response and actuators that then apply control forces to reduce these effects. Active devices also require a large power supply which may or may not be available in a seismic event. Semi-active control combines active control's ability to alter its control characteristics with the inherent stability associated with passive control. Another important feature of semi-active control is that it only requires a small power supply.

A particular semi-active device that has shown to be quite effective is the magneto-rheological (MR) damper. This device is a damper that contains a special fluid that has the reversible capacity to change from a Newtonian fluid to a semi-solid state that has a yield stress associated with it in a matter of milliseconds. The yield stress of the MR fluid is limited by a magnetic saturation and is 50~100 kPa for an applied magnetic field of 150 ~250 kA/m. The fluid itself consists of some carrier medium such as hydrocarbon oil or silicone oil with micron-sized magnetically polarized particles dispersed in them. When this fluid is exposed to a magnetic field, the particles bond together providing additional resistance due to the increased yield stress. The resultant control forces the dampers produce are dependent on the strength of the magnetic field applied. Because the control forces are adjusted by the magnetic field and do not require a mechanical valve, the MR

device displays high reliability (Jansen and Dyke 2000). To produce these magnetic fields, only 1 ~ 3 Amps and 20 ~ 60 Volts are usually needed.
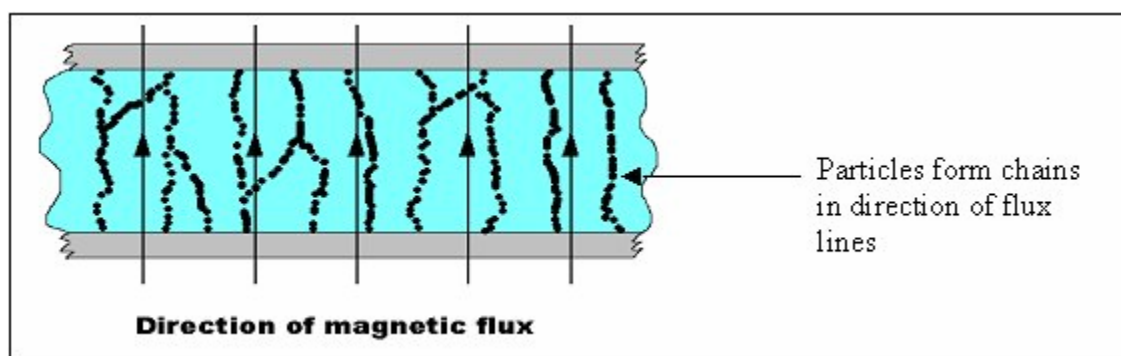
Figure 1.1 Alignment of Particles in MR fluid (Wikipedia)

Thus, only a small power source, such as a battery, is required for the MR damper. The MR damper has also been experimentally validated for various types and capacities (Jansen and Dyke 2000; Sodeyama, Suzuki, and Katsuaki 2004; Spencer et al. 1997a,b).

This thesis focuses on the development and utilization of fragility curves that properly show the mitigation effects of seismically excited structures that have been retrofitted with control devices. The remainder of this chapter centers on structural control, fragility curves, and the usage of retrofit techniques, including control systems, with fragility curves. The final topic serves as the motivation behind this research.

1.1 New Madrid Seismic Zone

The New Madrid Seismic Zone is located in the areas of the Mississippi, Ohio, and Wabash River Valleys in the Central United States. This region is the second most seismically active part of the continental U.S. Approximately 150 to 200 earthquakes are recorded annually in this region by a network of monitoring instruments (USGS 2008a). In addition, the New Madrid Zone is where several of the largest earthquakes to strike the main part of the United States have occurred. These seismic excitations occurred between 1811 and 1812. Due to the lack of natural barriers of the region, it was estimated that the earthquakes could be felt over 5,000,000 square kilometers. It was reported that structural damage occurred as far as Cincinnati, Ohio; St. Louis, Missouri; and places in Kentucky and Tennessee (USGS 2008b). The town of New Madrid was also greatly damaged. Fortunately, the New Madrid area was not very populated and loss of life and property was kept at a minimum. Today, however, this region is heavily populated and seismic activity of that magnitude would have catastrophic effects on the mid-America region. While these kinds of effects may never be fully mitigated, structural control has emerged as an effective method for reduction of seismic excitation in this and other regions throughout the globe.

1.2 Structural Control

Every day, structures across the world are subjected to various loading conditions. Most of the time engineers estimate these loads that are related to the building itself and its contents resulting in fairly accurate values. External disturbances, however, do play an important

factor in the life of any structure. These excitations can be wind induced, seismic, or from blast impacts. The two common features shared by all of these are that they are dynamic in nature and have no discernable pattern or origin. This uncertainty makes development of appropriate design codes challenging at times. Based on modern control theory, structural control has emerged to mitigate the damage occurred during severe events. Proposed originally by Yao (1972), structural control has been developed and investigated over the last three decades to mitigate the harmful effects that outside disturbances impose on structures. Structural control has three main branches: passive control, active control, and semi-active control.

Passive control is the earliest and most widely used of the three types of control devices. This perspective is largely due to the simplicity and cost of passive control devices. Composed mainly of mechanical elements, passive control devices use the building's response responses to develop control forces to limit the effects of seismic excitation. Because this system is purely reactive, passive control devices can only dissipate energy from ground motions. This characteristic allows passive control to be considered bounded input-bounded output (BIBO) stable. Passive devices also do not require a power source. Passive control devices include tuned mass dampers, base isolation, and supplemental dampers. One of the world's tallest structures, the Taipei 101, employs a tuned mass damper to protect against the seismically active region of Taiwan. The CitiCorp Building in New York and various other structures throughout the U.S. have some form of passive devices implemented on them.

Figure 1.2 Taipei 101

Figure 1.3 Citicorp Building

To compensate for the lack of controllability of passive devices, active control devices have been studied and implemented. Using a system of sensors and actuators, active devices develop and alter control forces to reduce the effects of seismic disturbances imposed on structures. If not properly designed, active control can input external energy into a system, thereby aggravating the effects of ground excitations. Control algorithms are being continually developed and improved to provide the most effective active control schemes.

In an early study by Abdel-Rohman and Leipholz (1979), an optimal closed loop control is proposed for a simplified one-span bridge model. The problem consisted of minimizing a quadratic objective function through usage of the Riccati matrix. Deflection and acceleration at the mid-span was examined subjected to a moving harmonic loading condition and a moving train load. Results show that the uncontrolled cases develop instability, while the active control cases dampen the vibration induced on the bridge model. Dyke et al. (1996c)

investigated the use of acceleration feedback algorithms as opposed to direct measurements of displacements and velocities which are impractical for full scale implementations. The study experimentally verified the H_2/LQG (Dyke et al. 1996b; Dyke et al. 1998; Jansen and Dyke 2000; Yoshida 2003; Yoshida et al. 2003; Yoshida and Dyke 2004) acceleration feedback algorithm on a three story, one-bay structure with an active mass driver. In a work by Bontempi, Casciati, and Giuduci (2003), various passive and active control devices were compared on a benchmark cable-stayed bridge. The passive devices were viscous dampers, visco-elastic dampers, and elasto-plastic dampers. The algorithm used for the active cases was the LQG algorithm. It was concluded in this study that the best passive case outperformed the best active case.

Semi-active devices have emerged as a popular form of control in recent years. This popularity is due to its controllability, stability, and low power requirements. Another attractive feature of semi-active control systems is that in the event of a power outage, the control system will revert to a passive system. As with active control, the performance of semi-active control is reliant on the ability of control algorithms implemented in the system.

Numerous studies have demonstrated the effectiveness of semi-active control devices on structures. Iemura and Pradono (2005) proposed a semi-active control algorithm, the pseudo-negative stiffness (PNS) algorithm for implementation on control devices situated on the Tempozan Bridge in Osaka, Japan. The algorithm was compared with viscous dampers using the LQR algorithm. The result was that the PNS offered comparable results while using fewer sensors and reducing the earthquake input energy. Agrawal, Yang, and He

(2003) compared various control strategies on a benchmark cable-stayed bridge. The study used active devices, linear and nonlinear viscous dampers, resetting semi-active stiffness damper (RSASD), switching semi-active stiffness damper (SSASD), and the semi-active friction damper (SAFD) in combination with linear springs. For a comparative study, all of the devices were given a force constraint of 1000 kN, which is consistent with the benchmark study. The study showed that the SSASD is inferior to the RSASD. It was also determined that the SAFD case in combination with linear springs is comparable to the sample active controller. As shown in this prior study there are many different types of semi-active devices.

One particular device that has been the subject of many investigations is the MR damper. The MR damper is inherently stable, highly reliable, has low power requirements and controllable characteristics which is common in most semi-active devices. The MR damper, though, is especially beneficial for civil applications due to the properties of the MR fluid itself. Civil structures, especially bridges, are subject to exposure to moisture and broad temperature changes which will have limit impact on altering the abilities of the MR fluid inside the dampers.

Dyke et al. (1998) experimentally compared semi-active and passive control of the MR damper implemented on a three story model. The semi-active device in this study was controlled using the clipped-optimal algorithm (Dyke et al. 1996b). The study was divided into two tests. The first test involved a low and high amplitude version of the 1940 El Centro earthquake. The second test was a broadband random excitation under three

different input amplitudes. The study showed that the semi-active control was significantly better than the best passive cases for most of the trials.

Yoshida and Dyke (2004) also evaluated several semi-active control designs and an active case implemented on the 20 story nonlinear benchmark building. In the study, an ideal semi-active device, an MR damper with the clipped-optimal algorithm, and a MR damper with a modified clipped-optimal (Yoshida 2003; Yoshida et al. 2004) were compared. It was shown that the semi-active cases produced similar results to that of the active cases, while using a smaller amount of power. In a comparison of the two algorithms, the modified clipped-optimal reduced the accelerations of the structure, while achieving nearly the same inter-story drifts. In a study by Park, K. –S. et al. (2003), hybrid control was evaluated for the benchmark cable-stayed bridge. Two types of hybrid controls were proposed. The first consisted of lead rubber bearings (LRBs) and hydraulic actuators. The second consisted of LRBs and MR dampers. The two hybrid systems were compared to the results with passive and semi-active systems alone. It was determined that the hybrid controllers had better performance for most of the responses than the other control systems. In addition, the hybrid controllers provided a robustness that was superior to the other control systems. Jung, Spencer, and In-Won (2003) studied the effects of structural control on the benchmark cable-stayed bridge. For this particular study, passive, ideal active, ideal semi-active, and three MR damper models were compared. The models were the Bingham, Bouc-Wen, and Modified Bouc-Wen. In comparing the MR damper models the Bouc-Wen and Modified Bouc-Wen were more computationally tractable than the Bingham model. The clipped-optimal algorithm was proposed for the semi-active control devices. Based on the

results provided, the proposed semi-active control was considered a good choice because the Cape Girardeau region was similar to the geological location of Mexico City according to the study. The proposed semi-active control performs better than the sample active design and similar to the passive-on case. The passive-on control requires a peak maximum force higher than the proposed semi-active device, however.

Figure 1.4 180 kN MR damper (Lord Corporation)

Domaneschi (2005) examined the effects of various types of control strategies on the benchmark cable-stayed bridge. The work consisted of a comparison of passive, active, and semi-active control on the Phase II benchmark cable-stayed bridge. The passive and semi-active devices were developed using the Bouc-Wen MR damper model. The control scheme for the active devices used the LQG control algorithm. A decentralized semi-active control system was developed for the bridge model. The devices were implemented by using a simple on/off skyhook control law. The study showed that for most simulations the semi-active control performed close to the active cases and generally much better than the passive cases. In each of these cases, structural control has been shown to be an effective method for mitigating seismic forces. However, all of these studies have been investigated as isolated

events. The inclusion of various connected systems for evaluation and mitigation has been a focus of consequence based engineering.

1.3 Consequence Based Engineering

Consequence based engineering (CBE) is a new paradigm for seismic risk assessment across regions or interconnected systems (Abrams 2002). The focus of CBE is to quantify the risks of an infrastructure system by assessing selected components of that system (Wen, Ellingwood, and Bracci 2004). In such an assessment, the benefits of various seismic risk mitigation techniques can be compared and evaluated by applying them to certain components throughout a community. Examples of this include retrofitting lifelines, essential facilities, and important transportation routes that would have a major impact on the community at large. To better understand the tasks involved in CBE, Figure 1.3 details how rapid assessment, decision making, damage synthesis, and consequence minimization is all interconnected. The rapid assessment portion of the paradigm takes pre-existing data or inventory and quickly determines if the consequences are acceptable using a decision making criteria. If the decision making criteria determines the consequences should be redefined, then new acceptable consequences are defined. The decision making segment also decides whether parameters of interest should be refined, if a more detailed analysis is needed, and if some system intervention is necessary.

An important step in the damage synthesis process is the redefinition of fragility relations. Unlike approximate vulnerability functions which are used for quick loss estimations, structure specific fragility relationships allows for an accurate assessment of systems with specific structural characteristics. In the case of critical structures, such as hospitals and bridges, the ability to compare consequence minimizations through retrofitting by using specific structure fragility functions is an integral part of CBE. It is the aim of CBE to quantify and minimize consequences across regions or interconnected systems, through system intervention techniques such as retrofitting a structure to an acceptable level (Abrams 2002).
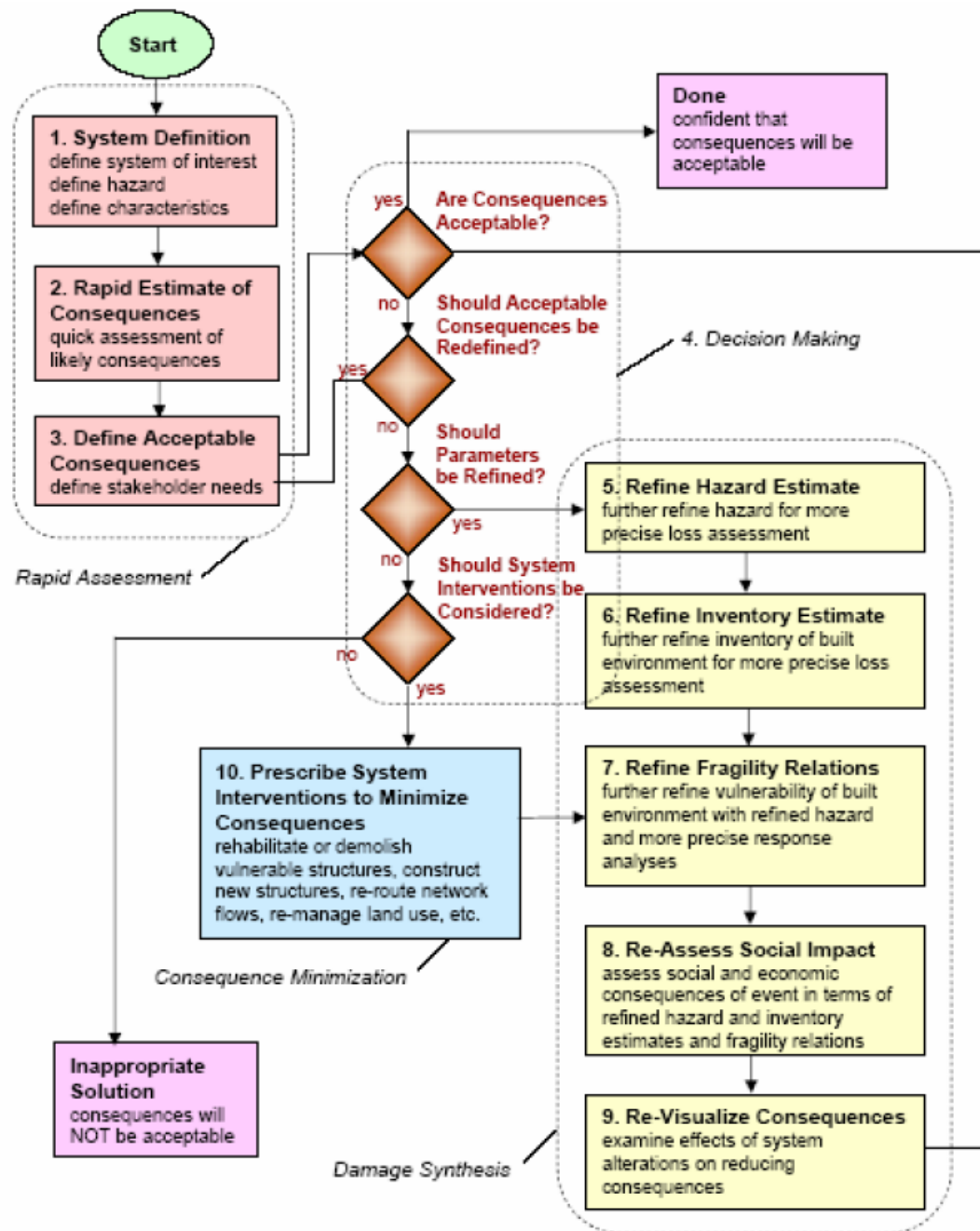
Figure 1.5 Consequence Based Engineering Paradigm (after Abrams 2002)

As stated earlier, critical structures are a valid and appropriate situation that warrants the use

of CBE. These dominant contributors to communities can be identified through the use of

probabilistic safety assessments (PSA). PSA is a structured framework for evaluating uncertainty, performance and reliability of an engineered system (Wen, Ellingwood, and Bracci 2004). PSA differ from traditional deterministic approaches to safety in that they focus on why and how a system may fail by its explicit treatment of uncertainties. An important feature of PSA is that it allows for an easily understandable approach so that decision makers may be able to evaluate situations and re-evaluate them as new circumstances arise. PSA begins by identifying limit states, which determine the performance of the system. A fully coupled risk assessment which defines the conditional probability of attaining a performance limit state and the probability of a hazard occurring is usually considered next. In the case of seismic risk assessment, the hazard is generally some seismic demand. A fragility analysis is an essential part of the fully coupled risk assessment. In many cases, a properly conducted fragility analysis is less complex, less costly, and involves fewer disciplines than a fully coupled risk analysis (Wen, Ellingwood, and Bracci 2004).

1.4 Fragility Curves

Fragility curves are defined as the conditional probability of a system reaching a prescribed limit state for a given system demand. These limit states range from unserviceability to some degree of structural damage including incipient collapse. The demands can be maximum force, displacements caused by earthquake ground motions, or more generally for seismic analysis, some prescribed intensity measure of ground motion over a period of time. The

advantages of a fragility assessment include that while knowledge of the hazard is helpful, such knowledge is not essential for the assessment. Also, due to its relative simplicity miscommunication between risk analysis teams and non-specialist stakeholders or decision-makers are less likely to occur. The complement of a fragility assessment is the reliability of the system, which is essentially the probability of proper performance over a given time period (Melchers 1999).

Researchers have developed various methodologies for fragility relationships between the structure's response and the ground motion intensity level. Singhal and Kiremidjian (1996) presented a method for the development of fragility curves that does not rely on heuristics or on empirical data. A Monte Carlo simulation approach was used to determine the probabilities of structural damage, and an ensemble of ground motions was generated using an autoregressive moving average model. These excitations were imposed on various low, mid, and high rise concrete frame structures. Although observed damage data is very limited and could not be used to verify the fragility curves, simulated damage states were found to be close to the predicted fragility analyses. In a follow-up study by Singhal and Kiremidjian (1998), a Bayesian statistical analysis method for updating fragility relationships was presented. The updating technique was used for damage data obtained from reinforced concrete frame structures. The updated fragility curves were shown to be consistent with the previously obtained fragility curves from Singhal and Kiremidjian (1996). Shinozuka et al. (2000) presented both empirical and analytical fragility curves in this work. The empirical fragility curves were developed from damage data taken from the 1995 Kobe earthquake for 770 reinforced concrete columns. The analytical fragility curves were developed for two

bridges in the Memphis area subjected to ground motions of the same region using two-parameter lognormal distribution functions. Jeong and Elnashai (2004) developed a new methodology termed Planar Decomposition for deriving vulnerability functions for structures in three dimensions. A comparison of this new technique and the conventional approach was applied to a seismically excited one story reinforced concrete structure. This new approach produced vulnerability functions that, unlike conventional techniques, take torsional effects into account.

1.4.1 Fragility Curve Analyses of Linear Elastic Systems

In the event that a system stays within its linear region during some excitation, a fragility relationship may be developed through the use of modal superposition. The uncertainty in such an analytic procedure lies only in the structural modeling and response analysis method. Structures that are excited by moderate to strong motions tend to go beyond this region making a nonlinear analysis more appropriate. Irregular structures that are subjected to earthquake motions must also use a nonlinear analysis approach (Bai 2004).

1.4.2 Fragility Curve Analyses of Nonlinear Inelastic Systems

Under severe ground motions, nonlinear methods become a suitable, if not necessary, approach for analyzing systems. These methods can be either a nonlinear static analysis or a nonlinear dynamic analysis. For nonlinear analyses, modal superposition cannot properly

relate the structural response with the seismic demand. Although nonlinear static analysis is more commonly used by engineers, nonlinear dynamic analyses using specific ground motions are considered the more accurate approach (Shinozuka et al. 2000; Wen, Ellingwood, and Bracci 2004; Bai 2004; Taylor and Dyke 2006). Bai (2004) warned that more than one ground motion should be taken in this type of procedure, because the nonlinear approach could be highly sensitive to the characteristics of one ground motion. For a wide range of structural responses, seismic vibrations of low to high intensities that reflect the region should be used (Wen, Ellingwood, and Bracci 2004).

Using a nonlinear dynamic time history analysis, Shinozuka et al. (2000) developed fragility curves associated with specific damage states for two Memphis bridges. The fragility curves developed from variations of the bridges were combined to a fragility curve for a mixed population of bridges. In a study by Lew and Kunnath (2002), the efficacy of a nonlinear static analysis was compared to that of a nonlinear dynamic analysis. The four case study structures were a six-story steel moment frame building, a thirteen-story steel moment-resisting frame building and a twenty-story reinforced concrete moment frame building. The inelastic behavior of each of these structures were predicted and compared. The result was that for maximum displacements both static and dynamic nonlinear analyses were similar.

1.4.3 Fragility Curves and Mitigation Strategies

To protect structures from the debilitating effects of seismic activity, the engineering community has formulated design codes for structures. While these design codes have

shown to be effective measures for protection against earthquakes, buildings are still susceptible to damage. This is particularly the case for older structures that have been built before more accurate codes have been implemented and have also suffered from deterioration. In such cases, rehabilitation strategies are a necessary approach to protect these structures. Many times this responsibility falls in the hands of emergency management agencies and other such decision makers who must decide which structures are important for the community (i.e. hospitals, schools, bridges). To aid decision makers in their task, many researchers have developed fragility curve analyses to effectively show the impact of rehabilitation strategies on these critical facilities.

Bai (2004) performed fragility curve analyses on a case study structure subjected to seismic excitation on a global and member level. In this study, a reinforced concrete structure was retrofitted using shear walls, reinforced concrete column jacketing and by confining columns' plastic hinge zones through steel plates. The study showed that the fragility analyses based on parameters defined by FEMA 356 were enhanced by retrofitting the structure with shear walls and column jacketing for all of the limit states. The fragility analyses of the original structure and retrofitted structure with steel plates were nearly the same for the entire limit states investigated. Reinhorn, Barren-Correva, and Ayala (2002) investigated the influence of building properties on seismic fragility analyses for mitigation purposes. A model of a reinforced concrete frame structure was used. As in normal retrofitting, the building's stiffness, strength, and damping were altered to see the resulting effects on the fragility analyses. Increasing the strength and stiffness did not cause a significant improvement of the fragility curve analyses. However, by increasing the damping

the fragility curves had significant improvement. Wen, Ellingwood, and Bracci (2004) compared the fragility curve analysis of older structures through mitigation techniques. The first structure is an older reinforced concrete structure that has been characterized as having strong beam-weak column connections. The fragility curves of the reinforced concrete building were improved by column strengthening.

Kim and Shinozuka (2004) compared the fragility curve analyses of bridges before and after retrofit. The two bridge models chosen for this simulation are typical of southern California. The ground excitations are also representative of the Los Angeles area. The columns of both bridges were retrofitted with steel jacketing. It was shown that the retrofitted bridges were less likely to exceed the limit state in the fragility analyses. This was especially the case when more severe damage states were investigated. Pan, Agrawal, and Ghosn (2007) performed fragility analyses for steel highway bridges in the state of New York. The bridges were all designed according to New York state bridge design guidelines. The ground motions, while simulated, due to the scarcity of actual earthquake data were representative of rock motions applicable to the New York City region. The parameters of interest in this study were the flexural ductility capacity of the columns, the high type rocker bearing displacements, and the low type sliding bearing displacements. The study showed quadratic regression was significantly better than linear regression for large peak ground accelerations. In the work failure modes of individual components were also combined to obtain first order and second order bounds for the fragility of system failure.

Retrofit assessment through fragility analysis has recently extended to the use of control devices. Taylor, Barnawi, and Dyke (2007) investigated the system reliability of a nonlinear benchmark structure retrofitted with control devices through fragility analysis. The structure was a twenty story steel moment resisting frame structure designed within the SAC Steel Project for the Los Angeles area. The ground motions used were developed by Wen and Wu (2001). Active control devices using the H_2/LQG algorithm was chosen for this study. Various device configurations and control efforts were investigated. The study showed that fragility assessments were very similar when the control effort was kept constant despite the different device configurations. Furthermore, increasing the aggressiveness of the controller lowered the fragility curve and number of plastic hinges in the structure. A crossing of fragility curves near the end of the region of actual data was noted for the study. The researchers commented on the limited applicability of the results beyond this point. Casciati, Cimellaro, and Domaneschi (2008) proposed a control strategy using passive devices modeled using the Bouc-Wen hysteretic model for a benchmark cable-stayed bridge. The work focused on deck displacements, base moment, base shear, and forces in the cable. The results show a significant improvement in the base shear, base moment, and cable forces from the implementation of the passive devices.

1.5 Overview of Thesis

Identifying damage states through fragility relationships has become a rising trend for technical personnel to communicate the devastating effects of seismic events to emergency

management agencies and other decision makers. Fragility analyses can also show the impact of mitigation through rehabilitation strategies. MAE Center researchers have produced an array of literature regarding fragility curve analyses of structures that have been retrofitted with such methods as the addition of shear walls, column jacketing and confinement of plastic hinge zones with steel plates. There has also been some work on determining fragility relationships of structures that have passive and active control devices implemented on them (Taylor and Dyke 2006; Taylor, Barnawi, and Dyke 2007).

This thesis focuses on the development of fragility relationships of structures that have semi-active control systems. The research presented herein is part of the EE-1 Vulnerability Functions MAE Center Project to develop procedures for the formulation of relationships between ground motion severity and the probability of a set of limit states being reached and for the reduction of loss from different intervention approaches (http://mae.ce.uiuc.edu). The premise of this work is to investigate the reliability of structures retrofitted with semi-active control devices as a future option for the databases in the EE-1 Vulnerability Functions project.

In Chapter 2, the methodology regarding fragility curve analysis through a nonlinear regression analysis is discussed. The regression relates the structural demand to the seismic intensity applied to the structure. The structural demand can be qualitative or quantitative. The seismic intensity used in this work is developed by synthetic ground motions from Wen and Wu (2001). Included in this chapter is a sensitivity study of the nonlinear regression analysis. The chapter also discusses the methodologies used regarding control theory. This

section includes the H_2/LQG control law which is used to model the active devices and as the nominal controller for the modified clipped-optimal control algorithm. The passive and semi-active devices are MR dampers developed using the Bouc-Wen model.

Chapter 3 covers the development of fragility curves for a high rise building equipped with MR dampers as the semi-active control system. The high rise building model is a nonlinear 20 story steel moment-resisting frame structure. The fragility curves are developed from the structure's inter-story drifts, absolute accelerations, and base shears. The reliability of the controlled systems is then compared for each of the cases presented.

The focus of Chapter 4 is the development of fragility curves for a bridge equipped with semi-active control devices. The model used for this work is a cable-stayed bridge previously the subject of a benchmark control problem. The semi-active control devices used are MR dampers. The fragility curve analyses are developed for the structure's deck displacement, overturning moment, and deck shear. The system reliability of the bridge is then compared for each of the controlled and uncontrolled cases presented.

Chapter 5 summarizes the work of the thesis and recommends ideas for future investigations.

Chapter 2

Background

This chapter provides background information regarding the procedures used within this thesis to formulate a fragility analysis as well as the techniques used to model the control devices used herein. Development of a fragility curve is determined through a nonlinear regression analysis which relates the seismic intensity and structural demand. For this study the seismic intensity is given as ground motions and the structural demand is based on limit state capacities. A sensitivity study of the nonlinear regression is given upon discussion of the development of the fragility curve analysis.

Also included in this chapter is modeling of the MR damper using a Bouc-Wen hysteresis model (Spencer et al. 1997b; Jansen and Dyke 2001). The active control devices herein are considered to be ideal devices that provide the exact control forces commanded. The passive and semi-active control devices are modeled using the Bouc-Wen MR damper model. The desired forces of the MR damper cannot be controlled directly as they depend on the local responses of the structure where the devices are installed. However, the voltage applied to the MR damper can be controlled. The modified clipped-optimal algorithm, which varies the voltage from zero to some maximum, is presented herein with a nominal controller that utilizes the H_2/LQG.

2.1 Fragility Curve Analysis

Fragility curves define the probability of a particular set of limit states (LS) being reached or exceeded at a prescribed system demand ($D = d$) as shown in Equation 2.1.

$$F_R(x) = P(LS \mid D = d) \qquad (2.1)$$

For a seismic analysis, the system demand describes the intensity of a ground motion while the limit states are some degree of the structure's responses. The characteristics of the structure, representative earthquake intensities, and uncertainties in the capacity and demand are all included in the development of a fragility curve (FC). The central location of the FC is determined from the capacity of the system and the slope of the curve is dictated by the uncertainty (Wen, Ellingwood, and Bracci 2004).

Seismic fragility analyses require several different inputs: ground motion records, limit state capacities, nonlinear regression, and uncertainties. Ground motion data to be considered should be appropriate for the region of interest. Limit state capacities are some measure of local or global responses of the entire system. Nonlinear regression models are typically appropriate for systems subjected to moderate or severe seismic events. This is because parameters of interest such as inter-story drift, do not always behave linearly under an increase in seismic intensity for higher measures. Due to the probabilistic nature of fragility curves, uncertainties in the model, regression model, and the capacities should be incorporated in the final equation. More details of these components are expressed below.

2.1.1 Ground Motion Records

To develop seismic fragility curves, a number of ground motion records are needed. For regions of the world, such as California and Japan, that are highly active seismically acquiring a collection of earthquake excitation is feasible. It is thus reasonable to expect that many of these seismic events, both of high and low intensity, are recorded for future use in terms of mitigation purposes. In other areas such as the Mid America region, seismic events only occur in moderate levels. The infrequent level of high seismicity means a low number of recorded ground motions are available for fragility assessments. However, it is important to consider the infrequent, but important, event that an earthquake of high intensity will occur for mitigation purposes. Using ground motion data from specific regions is important for fragility curve development as studies have shown the regional variation of strong motion records (Hudson 1972; Brocherdt and Glassmoyer 1992; Gulio 2005). It was found that local geological soil conditions can impact the ground motion data. In such an event where earthquakes of a high intensity for certain regions are scarce, synthetic ground motions are often utilized. These simulated ground motions possess characteristics that are authentic to the soil conditions for the regions of interest.

Wen and Wu (2001) developed simulated ground motions for three Mid-America cities: Carbondale, Illinois, Memphis, Tennessee, and St. Louis, Missouri. These ground motions take into account uncertainties such as occurrence time, attenuation, magnitude, source location, and soil amplification through random variables and are simulated using information from the region's seismicity and up-to-date random-vibration ground motion

models (Wen et al. 2004). From this procedure a large number of ground motions are able to be developed for a given site. Suites of 10 uniform hazard ground motions (UHGM) corresponding to a probability of exceedance by matching the response spectra with the uniform hazard response spectra. These ground motions are designed such that the median response of the structural demand will give an accurate representation of a given probability of exceedance. Thus, a suite of 10 UHGM records allows the evaluation of the structural response of small probability of exceedance where typically thousands of structural analyses would have been needed. These ground motions which represent future earthquakes of various attenuations, distances, and magnitudes have been used by MAE center researchers for numerous studies (Jeong and Elnashai 2004; Wen et al. 2004; Padgett and DesRoches 2006; Taylor, Barnawi, and Dyke 2007). In particular, two sets of ground motions for the Memphis, TN area pertaining to a given probability of exceedance of 2% in 50 years and 10% in 50 years are used for this study.

Figure 2.1 refers to the higher intensity ground motions used in this study. These ground motions will be referred to later and are labeled Earthquakes (EQ) 1-10. The assignment of each of the ground motions is applied top to bottom and left to right. So, the left column contains EQ's 1-5 from top to bottom. The right column contains EQ's 6-10. Figure 2.2 refers to the lower intensity ground motions used in this study. The assignment of ground motions is applied like before. The left column contains EQ's 11-15. The right column contains EQ's 16-20.
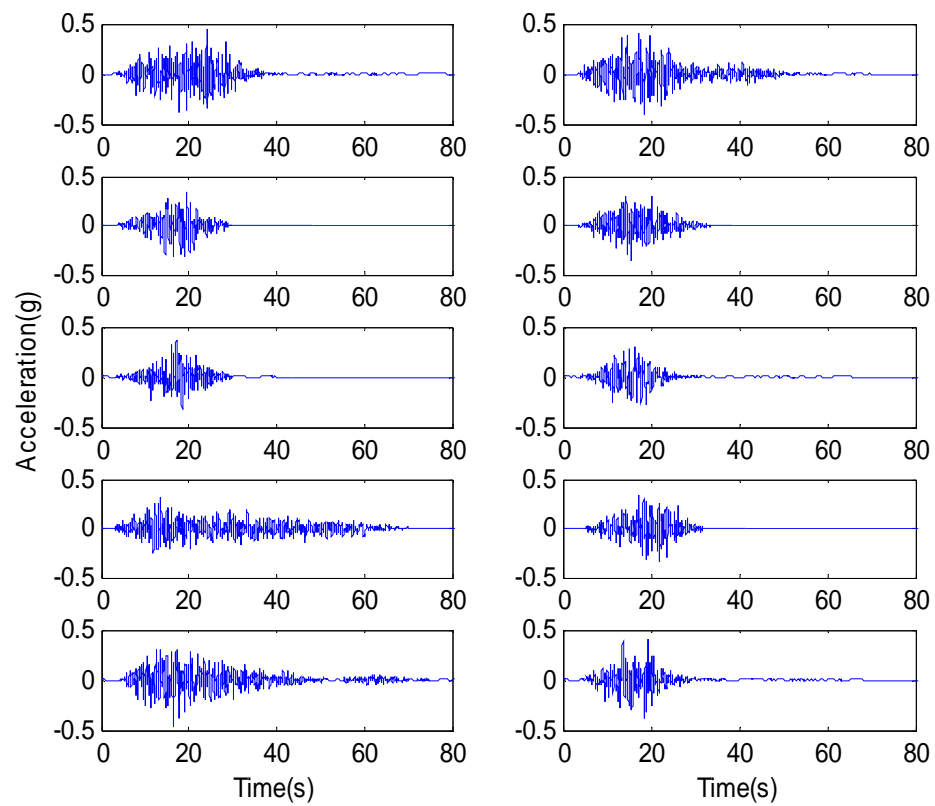
Figure 2.1 Wen and Wu (2001) Synthetic Ground Motions with a 2% Probability of Exceedance for Memphis, TN with Representative Soil Conditions
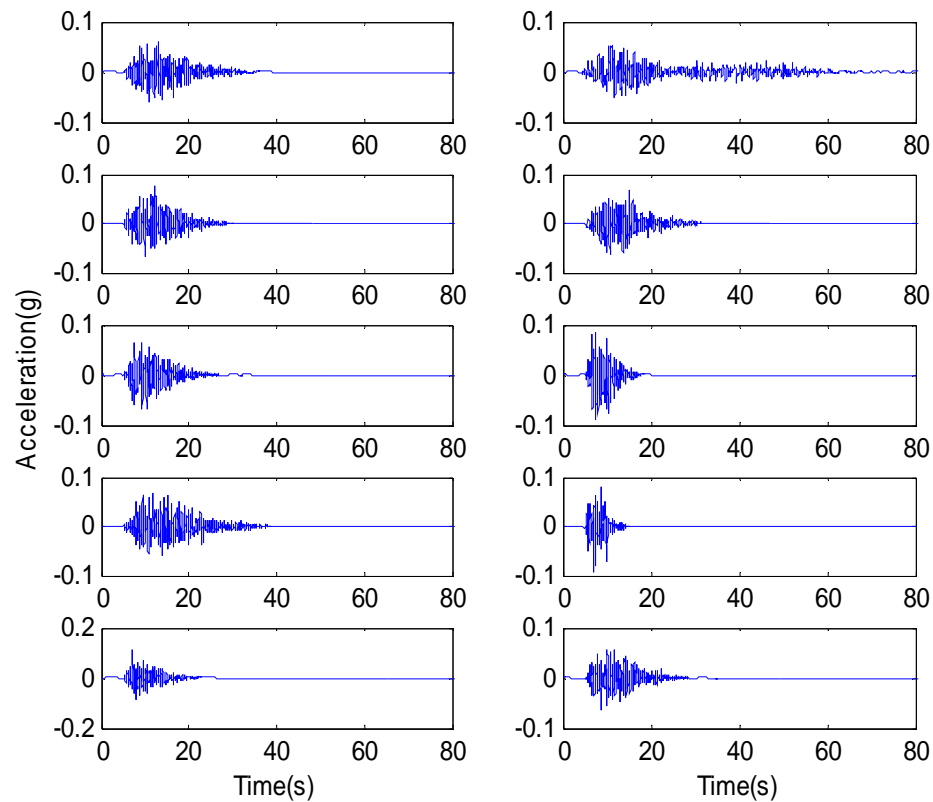
Figure 2.2 Wen and Wu (2001) Synthetic Ground Motions with a 10% Probability of Exceedance for Memphis, TN with Representative Soil Conditions

2.1.2 Limit States

Limit states serve as a threshold for determining the damage state of structures. In other words, they are considered to be the value at which a structural demand exceeds a specified level. These capacities may be a qualitative measure agreed upon by a community or some quantitative measure determined by mathematical means. One such example of a qualitative approach is noted by FEMA 356: Prestandard and Commentary for the Seismic Rehabilitation of Buildings. FEMA 356 is a collaborative effort between ASCE and FEMA

to redefine the guidelines for seismic rehabilitation of buildings into a national consensus standard. FEMA 356 has three categories of performance levels: Immediate Occupancy (IO), Life Safety (LS), and Collapse Prevention (CP). The IS structural performance state has been identified as having a post-earthquake damage state that remains safe to occupy, retains the original strength and stiffness of the structure and only suffers minor cracking. In the LS structural performance state, post earthquake damage is limited to significant damage to structure, but with some margin against either partial or total structural collapse. Some structural elements are allowed to be severely damaged, but cannot result in falling debris hazards in or outside of the building. Under this level, injuries are expected, but the overall risk of life-threatening injury should be very low. The CP performance level means the post-earthquake damage state in the building is on the verge of partial or total collapse. Significant damage has generally occurred in this state and a degradation of the strength and stiffness to the lateral load resisting system has also taken place. Large permanent drifts and, to some extent, a reduction of the vertical load carrying capacity of the structure has occurred as well. Significant risk of injury due to falling hazards may exist under this condition. Most minimum code requirements specify a performance level equivalent to the LS level provided above. FEMA 356 states a maximum inter-story drift limit for various structural types for each of the performance levels.

As stated earlier, limit states may also be provided in a quantitative sense. Although, there is no qualitative measure for absolute acceleration, this parameter has been an important component of evaluations on structures subjected to seismic excitation. Even in non-destructive cases, earthquakes can result in large accelerations that can be harmful. These

sudden effects can be discomforting to patients in hospitals and can damage valuable non structural components, such as equipment in communication towers (Sadek and Mohraz 1998). Another significant quantitative measure for evaluation of structures is base shear. The capacity of structures to resist base shear is an important feature in earthquake engineering. As most buildings are not designed to resist lateral loads, it is important for the structural components of any system to be able to resist shear at the bottom where the forces are the largest and chances of collapse are at its worst.

In bridges, large deck displacements could result in pounding between the deck and abutments causing severe damage to the superstructure. Deck shear is also another important concern because the cross sections of the tower at the deck experience large amounts of shear force. Also, a high enough deck shear (that exceeding the capacity of the component) could result in global system failure. Overturning moment is another response that is considered to be important in bridge design. As with the deck shear, a high enough overturning moment could result in global system failure.

For seismic assessment of structures, limit states, whether qualitative or quantitative are usually parameters that represent vital structural responses that could result in local or global failure of the system.

2.2 Nonlinear Regression Model

A regression analysis is often used to determine the probabilistic relationship between variables of interest. Regression analyses may be linear, multiple linear, and nonlinear. Nonlinear regression is an effective measure because engineering variables are not always linearly related (Ang and Tang 1975). This approach also serves as an appropriate method when there are clusters or a wide scatter of data. A relationship between the structural response demand and the seismic intensity is often selected based on the power-law form

$$D = aS^b \tag{2.2}$$

The nonlinear power law equation may logarithmically transformed into

$$\ln(D) = \ln(a) + b\ln(S) \tag{2.3}$$

With this simplified linear form, the unknowns a and b of the regression model can now be easily found to estimate a relationship between the structural response demand and the seismic intensity.

When the limit state is defined as a deterministic response, the fragility is calculated as

$$F_R = P(D \geq d_0 \mid S = s) = 1 - \Phi\left(\frac{\ln d_0 - \lambda_{D|S}}{\beta_T}\right) \tag{2.4}$$

where d_0 is the limit state capacity, $\lambda_{D|S}$ is a lognormal distributed parameter from the average value of the best fit power law equation, and β_T is the total uncertainty (Wen, Ellingwood, and Bracci 2004). Uncertainty of the building model, the power law equation, and the capacity should be included in the fragility analysis.

For this study, uncertainty in the fragility curve analysis will be divided into three categories: the modeling uncertainty (β_M), the demand uncertainty $(\beta_{D|S_a})$, and the capacity uncertainty (β_{CL}). The impact of these parameters on the fragility curve was considered by Taylor (2007).

2.3 Sensitivity of Nonlinear Regression Model

As mentioned earlier, the formulation of the nonlinear regression model is dependent on the relationship of the structural response demand to the seismic intensity. To investigate this relationship, a sensitivity study is performed on the demand and seismic intensity parameters. For purposes of this sensitivity study, an analytical model of the nonlinear moment-resisting 20 story steel frame structure described in Ohtori et al. (2004) is used. The seismic intensity will be represented either as the spectral acceleration (S_a) or the peak ground acceleration (PGA). The structural demand parameter will be the maximum inter-story drift for the structure. This parameter is calculated for each of the 20 Wen and Wu (2001) ground motions. The value of the maximum inter-story drift is increased for several

ground motions in the regression model. This parameter study seeks to consider how altering the parameter of interest affects the regression model. It is noted that the inter-story drifts are for the nonlinear benchmark 20 story building model without any control.

The sensitivity study is conducted by first taking the maximum inter-story drifts for the 20 Wen and Wu (2001) synthetic ground motions. The maximum inter-story drifts are plotted in relation to the peak spectral acceleration of the corresponding ground motion. A nonlinear regression is performed to determine the best curve fit for the points. This curve fit line is labeled the original curve. Next, the maximum inter-story drift associated with the smallest peak spectral acceleration is increased by 10 percent. A new best curve fit is determined for this adjustment. The maximum inter-story drift point is then increased to 30 percent and 50 percent. At each increase, a new best curve fit is developed. The influence of the change on the curve fit can be observed based on increasing the inter-story drift values. This procedure is repeated for the inter-story drift value associated with the median peak spectral acceleration value and the largest peak spectral acceleration value. After performing the sensitivity study using spectral acceleration as the seismic intensity measure, the sensitivity study is repeated using the curves associated with the peak ground acceleration values.

In the first part of this sensitivity study, the inter-story drift associated with the ground motion with the smallest peak spectral acceleration, $S_a = 0.0016\,g$ of the 20 earthquakes is increased. The results provided in Figure 2.3 seem to indicate that increasing the inter-story drift has little effect on the overall regression analysis from a preliminary observation. At a

closer inspection of the figure, however, it can be seen that the order of the curve fits becomes reversed. An inspection of the figure show that the curve fits converge and cross at some point along the seismic intensity range causing this reversal of the curve fits' order. It is noted that this point is near the dividing line between the section termed the actual data region and the section termed the extrapolated data region. The actual data region refers to the range of seismic intensities that correspond to actual inter-story drift values determined through simulation. The extrapolated data region refers to the range of seismic intensities where actual inter-story drift values do not exist. The dividing line is based on the largest spectral acceleration associated with the inter-story drifts, $S_a = 0.2451\,g$. The figure shows that at intensity values lower than this intensity measure, an increase in the inter-story value chosen will result in an upward shift of the curve fit associated with modifying this value. In the range after this point, the extrapolated region, an increase in the inter-story drift value will result in a downward shift of the curve fit.

The changes in the behavior of the nonlinear regression models from increasing the inter-story drift values also produces changes in the fragility curves associated with them as shown in Figure 2.4. A close inspection of the figure shows that in the actual data region increasing the inter-story drift value will lower the system reliability. However, in the extrapolated region increasing the inter-story drift value chosen for this part of the study will result in a higher system reliability.
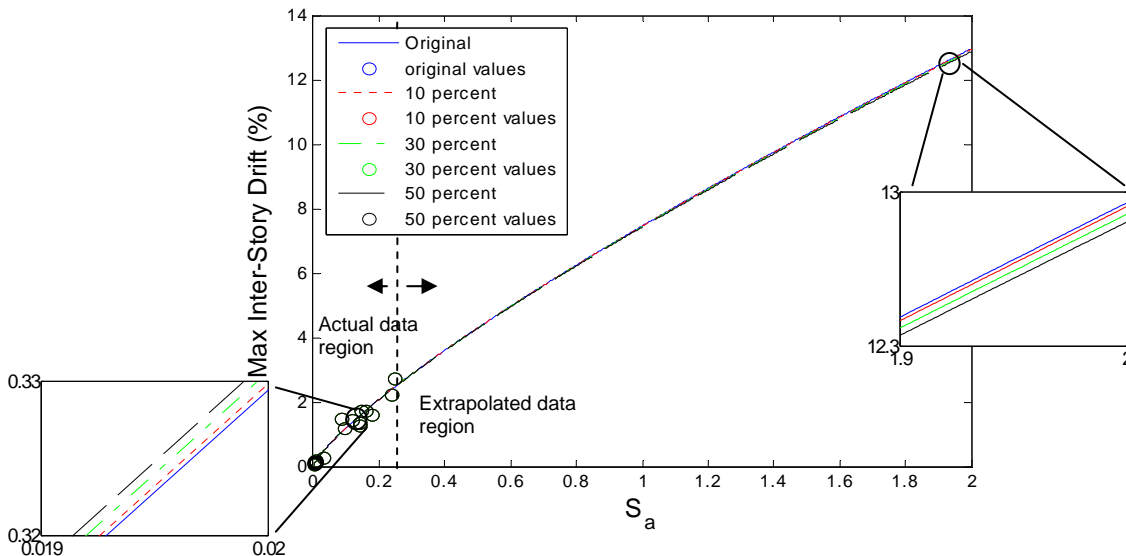
Figure 2.3 Nonlinear Regression varying First Inter-story Drift versus S$_a$
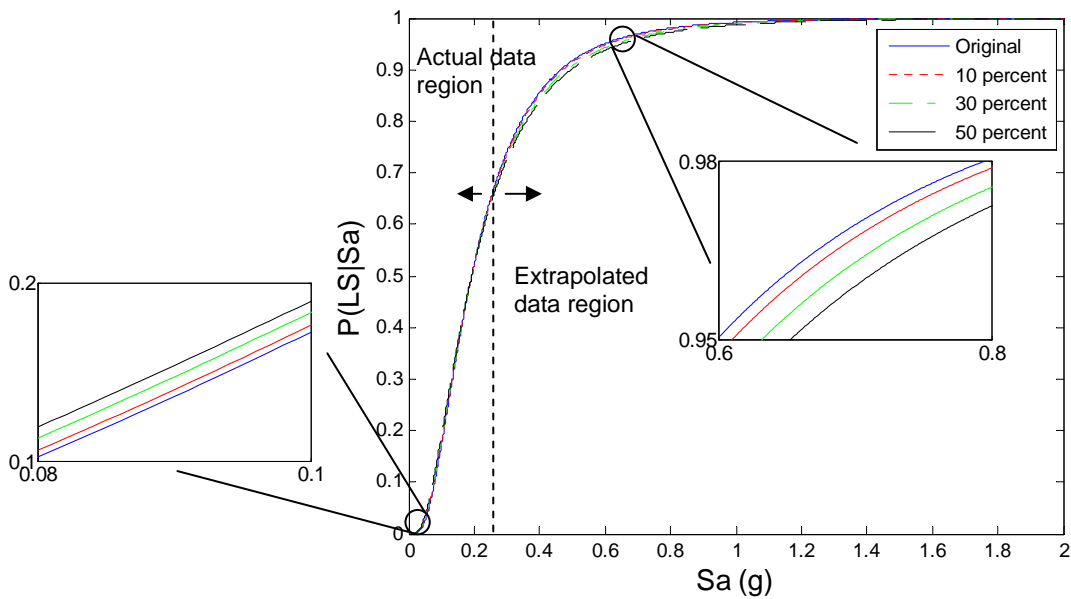
Figure 2.4 Fragility Curves varying First Inter-story Drift versus S$_a$

Next, the inter-story drift associated with the median value of the peak spectral accelerations, $S_a = 0.0859\,g$, was increased. The results are provided in Figure 2.5. The

curve fits in Figure 2.5 exhibit behavior similar to that of Figure 2.3. At values of spectral acceleration below the dividing line, increasing the value of the inter-story drift will result in an upward shift in the curve fit. At around $S_a = 0.2\,g$, the curve fits cross and the increase of the inter-story drift value results in the associated curve shifting downward.

The crossing and reversal exhibited by the curve fits in the nonlinear regression models above is repeated in the fragility analysis shown in Figure 2.6. As the inter-story drift is increased the system reliability is decreased for S_a values below $0.2\,g$. Beyond $S_a = 0.2\,g$, the figure shows in a close up inspection increasing the inter-story drift value associated with the median peak spectral acceleration results in a higher the system reliability.
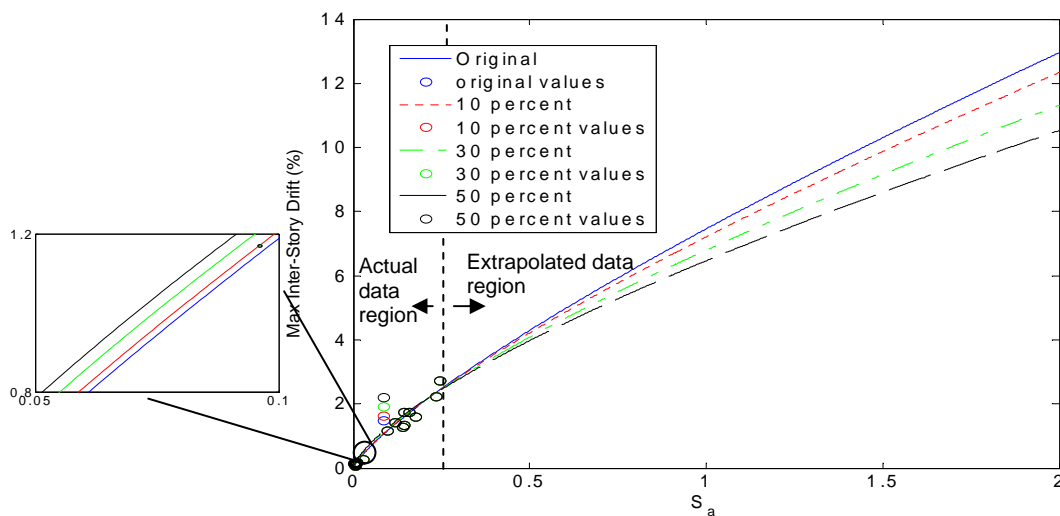
Figure 2.5 Nonlinear Regression varying Median Inter-story Drift versus S_a

38
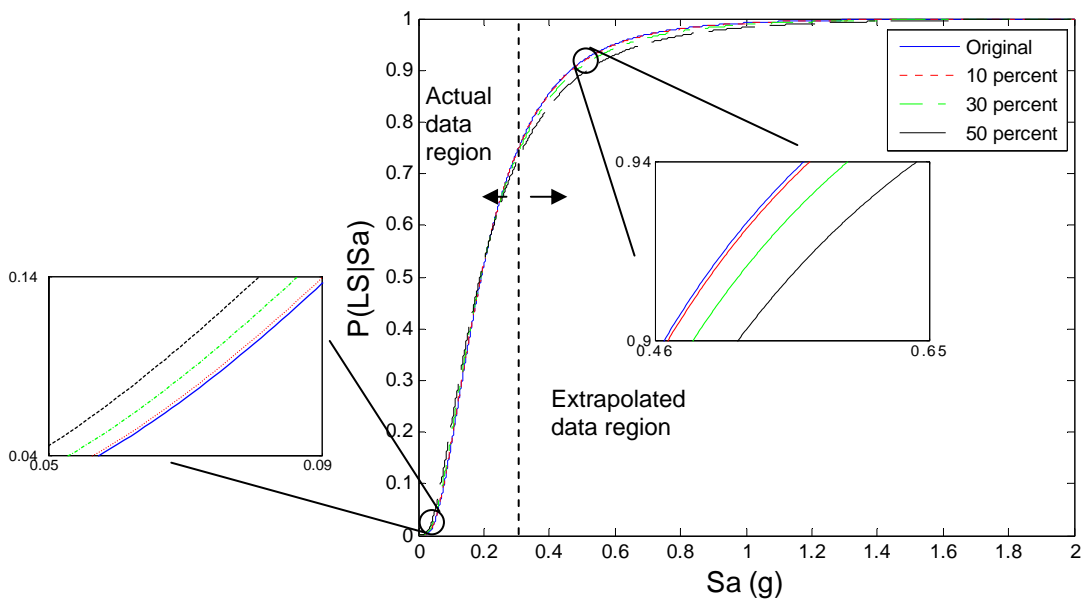
Figure 2.6 Fragility Curves varying Median Inter-story Drift versus S_a

In Figure 2.7, the value of the inter-story drift associated with the highest peak spectral acceleration, $S_a = 0.0859\,g$, is increased. The figure also indicates that the influence of the inter-story drift associated with the largest peak spectral acceleration is more significant than in the prior cases. The divergence in the curve fits is much greater in this figure than the others. Increasing the inter-story drift value results in a downward shift of the curve fits for this particular case for the seismic intensity range below $S_a = 0.15\,g$. Beyond this seismic intensity measure, an increase in the inter-story drift value will result in an upward shift of the curve fit.

The portion of the fragility curves in the actual data region show that increasing the inter-story drift value associated with the largest peak spectral acceleration will result in a decrease

in the system reliability as shown in Figure 2.8. An increase in system reliability occurs when the inter-story drift value is increased for the fragility curves in the extrapolated region. The only exception to this is for the original regression model and the fragility curve in which the inter-story drift value has been increased by 10 percent.
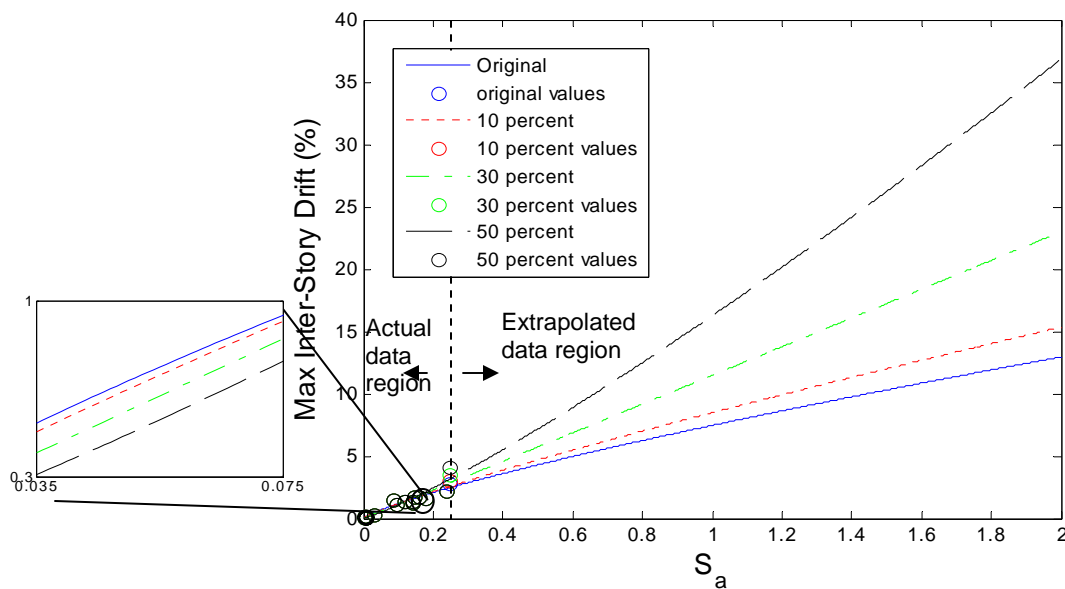
Figure 2.7 Nonlinear Regression varying Last inter-story Drift versus S_a

Figure 2.8 Fragility Curves varying Last inter-story Drift versus S_a

In an effort to evaluate whether a particular inter-story drift associated with an earthquake record was causing a major effect on the nonlinear regression model, another type of variation was examined. The first inter-story drift value in the series was increased by 10% and the others were kept the same. Next, the inter-story drift value associated with each peak spectral acceleration value was increased by 10% while the others were unmodified for each of the 20 curve fits. Nonlinear regression models were developed and fragility curve analyses were performed using the same procedures as before. The results in Figure 2.9 show that the nonlinear regression models do not seem to be significantly affected by an increase in the inter-story drift values for the actual data region. For the extrapolated data region, the curve fits become divergent as shown in Figure 2.10. There are two in particular that become divergent from the main group. The minor variance in the inter-story drifts of each earthquake does not seem to have a significant effect on the fragility curve analysis

shown in Figures 2.11-12. It is noted that varying a particular inter-story drift associated with an earthquake record ranging from a smaller to a larger intensity does not produce an overall trend for the curve fits or fragility curves based on an analysis.
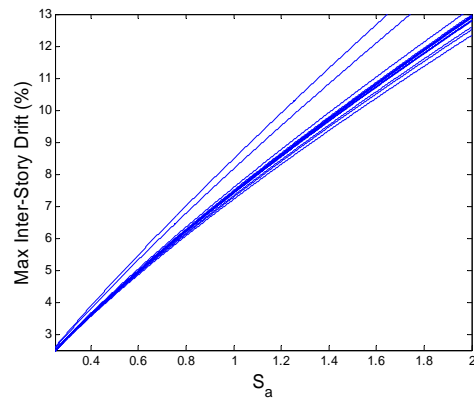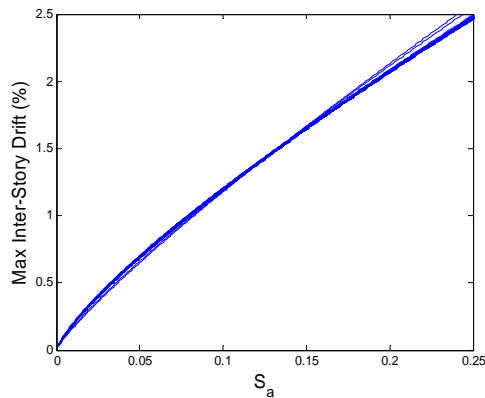
Figure 2.9 Nonlinear Regression (actual data) Figure 2.10 Nonlinear Regression (extrapolated data)
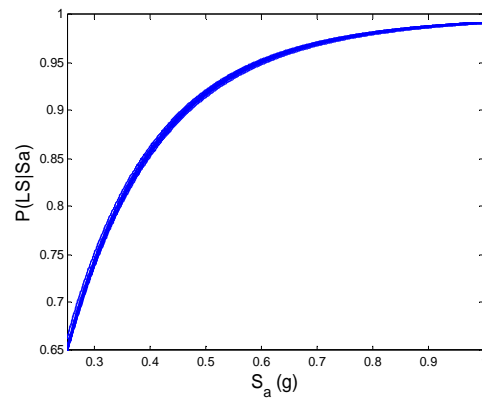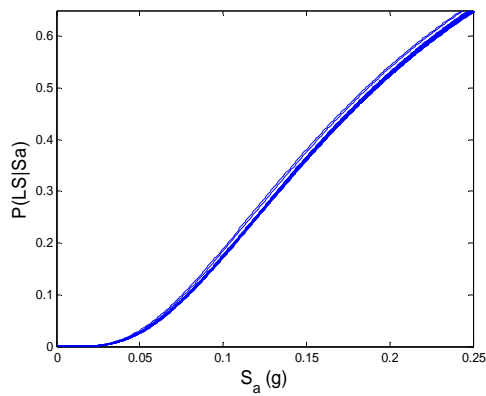
Figure 2.11 Fragility Curve (actual data)   Figure 2.12 Fragility Curve (extrapolated data)

For the next series of parameter studies, the same procedure for the developing the nonlinear regression curves is repeated, but this time the measure of seismic intensity is the peak ground acceleration (PGA). This parameter change is considered to demonstrate the influence of the type of demand on the resulting fragility analysis. It is noted that in under a

seismic demand of peak ground accelerations, the largest peak ground acceleration value, and therefore the dividing line between the actual data region and the extrapolated data region is $PGA = 0.4754\,g$.

In Figure 2.13, it seems that an increase in the inter-story drift associated with the smallest peak ground acceleration, $PGA = 0.054\,g$ in the sequence has little influence on the nonlinear regression model between the seismic intensity and the structural response demand within the actual data region. However, a closer inspection shows that increasing the inter-story drift value associated with the smallest peak ground acceleration value will result in a shift upward for the corresponding curve fits. In the extrapolated data region, an increase in this particular inter-story drift value will result in a downward shift of the curve fits. It is noted like in the series of parameter studies with spectral acceleration as the seismic intensity measure that the curve fits cross at some point and the order of the curves become reversed.

Similar to the curve fits described above, the fragility curves show a crossing and reversal of order as seen in Figure 2.14. The portion of the fragility curves in the actual data region show that by increasing the inter-story drift value, the system reliability is decreased. Increasing the inter-story drift value will result in a higher system reliability for the portion of the fragility curves located in the extrapolated region.

Figure 2.13 Nonlinear Regression varying First Inter-story Drift versus PGA
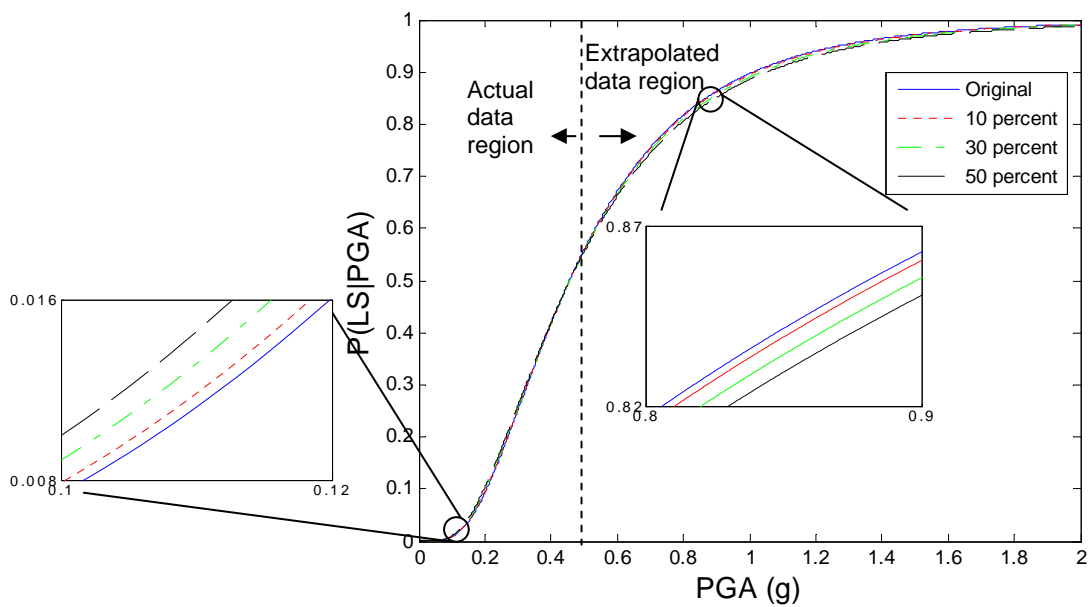
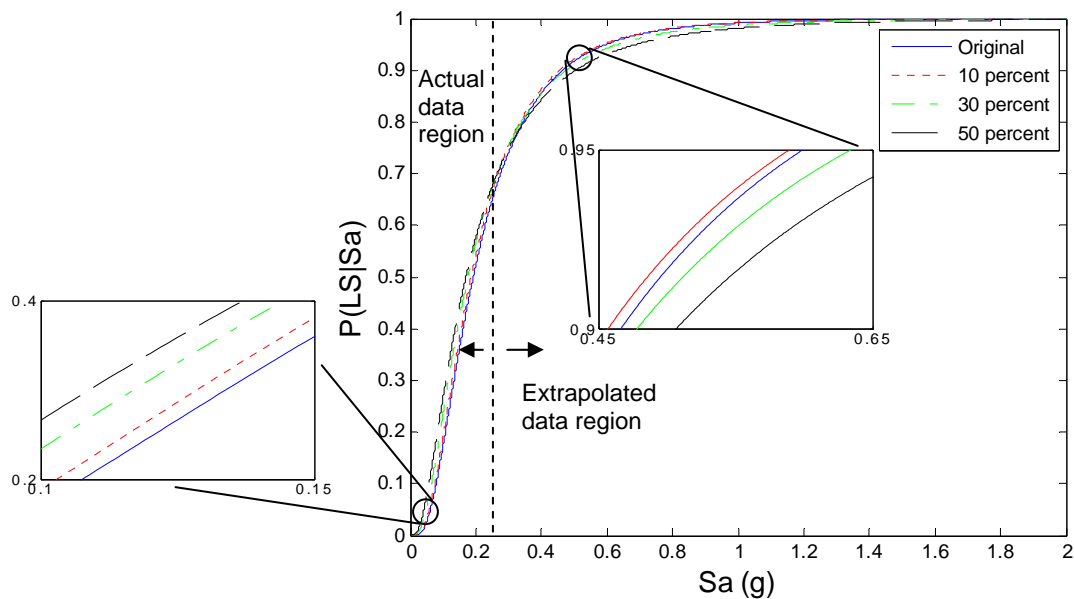**Figure 2.14 Fragility Curves varying First Inter-story Drift versus PGA**

The behavior exhibited by the curve fits from increasing the inter-story drift value associated with the median peak ground acceleration, $PGA = 0.2917\,g$ in Figure 2.15 is consistent with previous cases. In the actual data region, an increase in the inter-story drift value associated with the median peak ground acceleration will shift the curve fits upward. For the extrapolated region, the figure shows that an increase in the inter-story drift value will result in a downward shift of the curve fits.

The crossing and reversal of the order of the curve fits is most noticeable in the fragility curves associated with increasing the inter-story drift corresponding to the median peak ground acceleration as shown in Figure 2.16. The actual point of reversal is clearly very near the dividing line discussed earlier. In the region of actual data, an increase in the inter-story drift value will result in a decrease in the system reliability. Contrary to this, an increase in the inter-story drift value in the extrapolated data region will result in an increase in the system reliability.
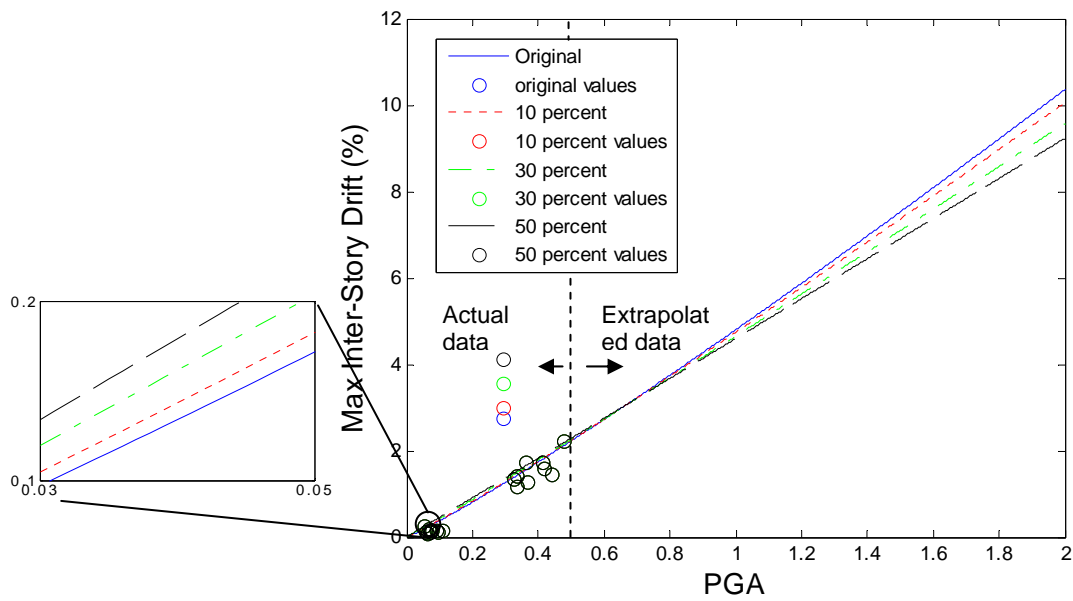
Figure 2.15 Nonlinear Regression varying Median Inter-story Drift versus PGA
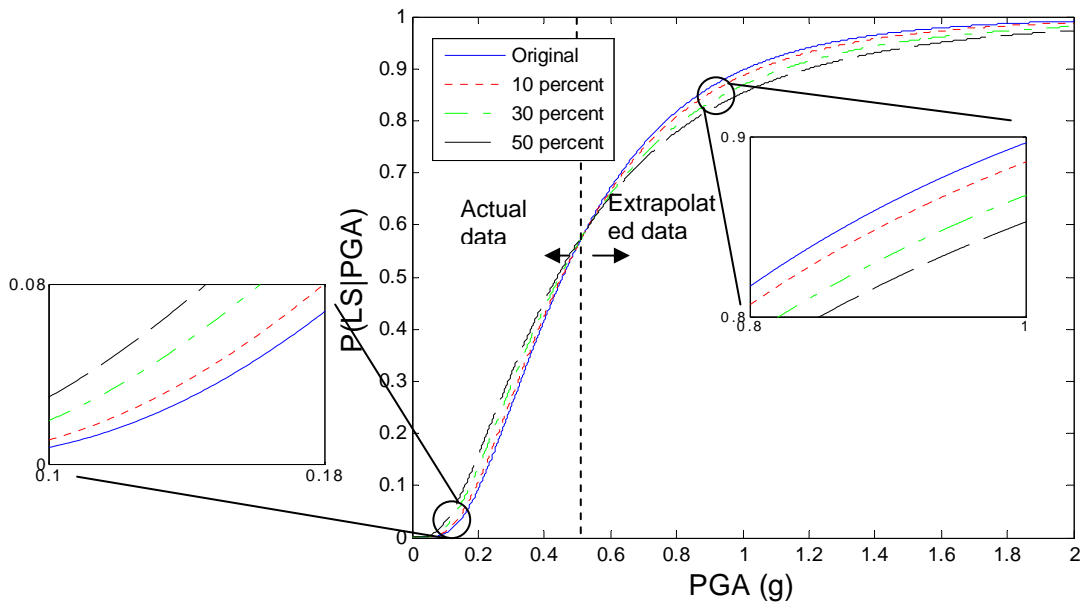

Figure 2.16 Fragility Curves varying Median Inter-story Drift versus PGA

The inter-story drift associated with the largest peak ground acceleration, $PGA = 0.4754\,g$, of the earthquake records is increased and its subsequent curve fits are plotted in Figure 2.17. Unlike many previous examples, increasing the inter-story drift value of the largest peak ground acceleration will result in a downward shift of the curve fit in the actual data region. The crossing of the curve fits and reversal of their order occurs at $0.3\,g$. After this threshold, the curve fit lines show that increasing the inter-story drift value associated with the largest peak ground acceleration will result in an upward shift of the curve fit. This influence of the inter-story drift on the curve fits for the peak ground acceleration as the seismic intensity is most evident in this figure.

The behavior exhibited by the nonlinear regression models has a corresponding effect on the fragility curve analysis as shown in Figure 2.18. The fragility curve analysis demonstrates that an increase of the inter-story drift value associated with the largest peak ground acceleration results in a higher system reliability for the actual data region. However in the extrapolated region increasing this inter-story drift value will result in a lower system reliability.
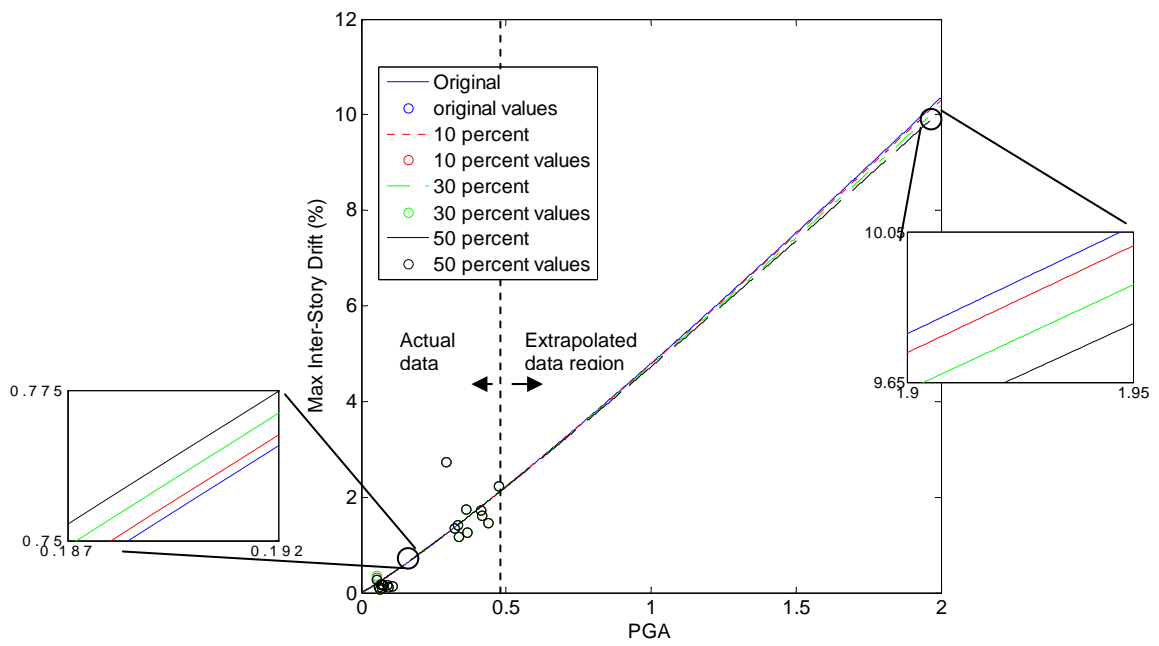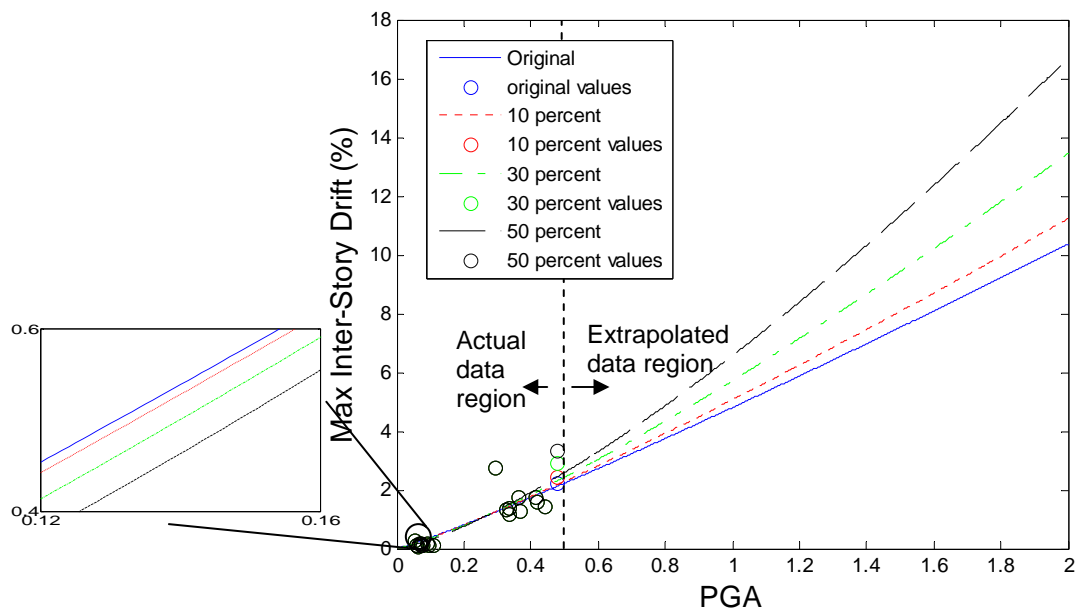
Figure 2.17 Nonlinear Regression varying Last Inter-story Drift versus PGA
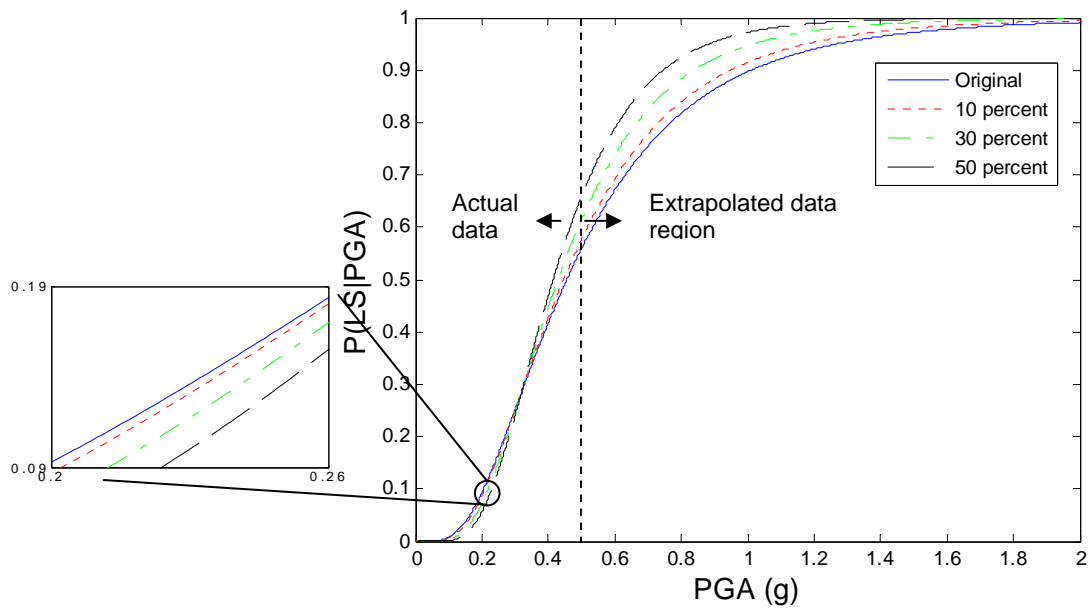
Figure 2.18 Fragility Curves varying Last Inter-story Drift versus PGA

In order to determine if the inter-story drift associated with a particular ground motion has more of an effect an analysis modifying each of the inter-story drifts was investigated. The process used to develop Figures 2.9-12 was used for Figures 2.19-22. The nonlinear regression models and fragility curves were taken with peak ground acceleration as the seismic intensity measure. Figure 2.19 shows us that the curve fits developed by the nonlinear regression models are not affected much by increasing the inter-story drift associated with each earthquake for the actual data region. However, the influence of each inter-story drifts is greater for the curve fits in the extrapolated region as each line shown in Figure 2.20 becomes more divergent.

The majority of the fragility curves in the actual data region are shown to be closely grouped for Figure 2.21. Only a couple of fragility curves are not clustered with the rest. The fragility curves in the extrapolated region are still closely grouped as shown in Figure 2.22. It is noted though that more fragility curves are divergent in the extrapolated data region. This portion of the study also shows that increasing the value of a particular inter-story associated with earthquake record ranging from a smaller to larger intensity does not result in an overall trend of the curve fits or fragility curves.

49
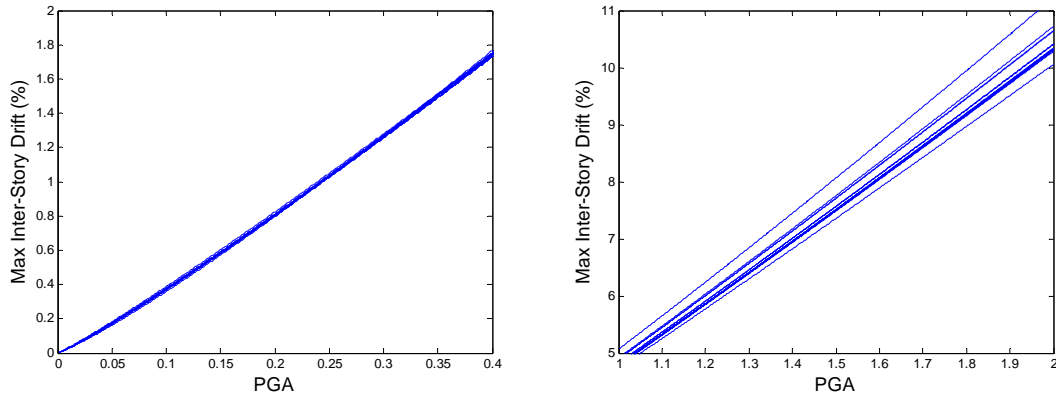
Figure 2.19 Nonlinear Regression (actual data) Figure 2.20 Nonlinear Regression (extrapolated data)
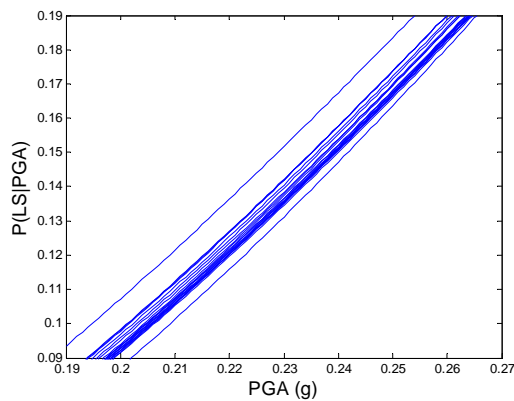
Figure 2.21 Fragility Curve (actual data)   **Figure 2.22 Fragility Curve (extrapolated data)**
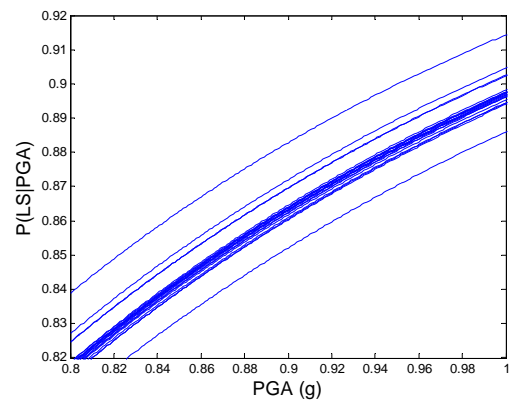
2.3.1 Summary

A parameter study is performed on the structural response demands and the seismic intensity measures. In this study, several trends were noted and are explained in this section. First, for both seismic intensity measures, spectral acceleration and peak ground acceleration, all of the nonlinear regression models and fragility analysis exhibited some form of reversal in the order of the curves when the seismic intensity was increased. While

in both cases, the point of this reversal differed it is noted that for each case this dividing line occurred on or near the limits of the actual data region. With the exception of increasing the inter-story drift value associated with the highest intensity measure, the actual data region showed an increase in the inter-story drifts resulted in an upward shift of the curve fits and a decrease in the system reliability for both seismic intensities. This increase in the inter-story drifts produced a downward shift of the curve fits and an increase in the system reliability for the extrapolated data region. This particular behavior seems at odds with what should be expected. It only seems reasonable that an increase in the inter-story drift values would produce an upward shift of the curve fits and increase the probability of exceeding the limit states (i.e. decreasing the system reliability).

Next, a slight variation in the inter-story drifts for both seismic intensities did little to change the fit in the actual data region. However, for the extrapolated region there was some divergence in the nonlinear regressions for both seismic intensities. The fragility curves were not changed much throughout the region. It was also shown that increasing an inter-story drift associated with a ground motion ranging from small to a large intensity measure will not produce an overall change in the curve fits or fragility curves like a steady increase of a particular inter-story drift as shown earlier.

In investigating all of the parameters included in the sensitivity study, it is shown that the choice of spectral acceleration or peak ground acceleration has little to do with the overall behavior of the nonlinear regressions and fragility curves. A variation in one inter-story drift can pose a major impact on the nonlinear regression. It is mentioned that Bai (2004) came

to a similar conclusion, as he mentioned the need for a significant number of samples to offset any large deviations in one value. Finally, the study has shown that the region corresponding to the actual data values is the more logical and practical area of observation for further analysis regarding fragility assessments.

2.4 Bouc-Wen MR Damper Model

MR dampers have shown a great deal of promise for civil engineering applications (Casciati 2008; Domaneschi 2005; Spencer et al. 1997a,b; Yoshida and Dyke 2004). The benefits of implementing these semi-active devices have been proven through both simulation and experimental verification. Accurate modeling of the MR damper's mechanical properties is necessary for predicting the behavior of the controlled system. Although, many models for the MR damper exist, this study employs the Bouc-Wen model. A schematic of a simple mechanical MR damper using the Bouc-Wen hysteresis model is shown in Figure 2.23. This particular model was developed and shown to accurately predict the behavior of the controlled system over a wide range of inputs in various experiments (Jansen and Dyke 2004; Yi et al., 2001).
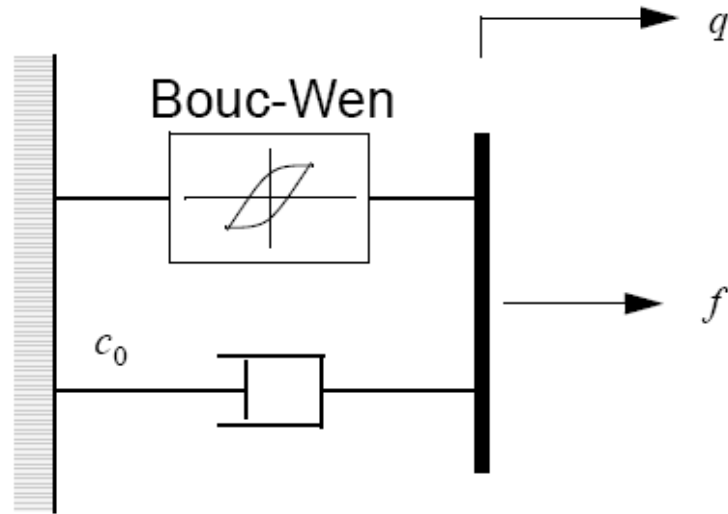
Figure 2.23 Mechanical Model of the MR damper

The equations governing the force f produced by this device model are

$$f = c_0 \dot{q} + \alpha z$$
$$\dot{z} = -\gamma |\dot{q}| z |z|^{n-1} - \beta \dot{q} |z|^n + A\dot{q}$$

(2.5)

where q is the displacement of the device, and z is the evolutionary variable that accounts for the history dependence of the response. By adjusting the parameters of the model $\gamma, \beta, n,$ and A, the linearity in the unloading and smoothness of the transition from the pre-yield to the post-yield region can be controlled. The functional dependence of the device parameters on the command input u is modeled as

$$\alpha = \alpha_a + \alpha_b u$$
$$c_0 = c_{0a} + c_{0b} u$$

(2.6)

Also, the current driver circuit of the MR damper introduces dynamics into the system. These dynamics are typically considered to be a first order time lag in the response of the devices to changes in the command input. These dynamics are accounted for with the first order filter on the control input given by

$$\dot{u} = -\eta(u - v)$$ (2.7)

where v is the command voltage applied to the control circuit.

2.5 Active and Semi-active Control Devices

In a seismically excited structure with m control devices whose forces are adequate to prevent the structural response from exiting the linear region, the equations of motion can be written as

$$\mathbf{M}_s\ddot{\mathbf{x}} + \mathbf{C}_s\dot{\mathbf{x}} + \mathbf{K}_s\mathbf{x} = \Lambda\mathbf{f} - \mathbf{M}_s\Gamma\ddot{x}_g$$ (2.8)

where $\mathbf{M}, \mathbf{C},$ and $\mathbf{K}$ are the mass, damping and stiffness matrices of the structure, $\mathbf{x}$ is a vector of the relative displacements of the structure, Λ is the influence matrix for the measured forces, $\mathbf{f} = [f_1, f_2,...f_m]^T$ is the vector of measured control forces, Γ is a vector of ones, and $\ddot{x}_g$ is a one-dimensional ground acceleration.

The equations expressed above can be written in state-space form as

$$\dot{\mathbf{x}}_s = \mathbf{A}\mathbf{x}_s + \mathbf{B}\mathbf{f} + \mathbf{E}\ddot{x}_g$$
$$\mathbf{y} = \mathbf{C}_y\mathbf{x}_s + \mathbf{D}_y\mathbf{f} + \mathbf{F}_y\ddot{x}_g + \mathbf{v} \qquad\qquad (2.9)$$
$$\mathbf{z} = \mathbf{C}_z\mathbf{x}_s + \mathbf{D}_z\mathbf{f} + \mathbf{F}_z\ddot{x}_g$$

where $\mathbf{A}, \mathbf{B}, \mathbf{E}, \mathbf{C}_y, \mathbf{D}_y, \mathbf{F}_y, \mathbf{C}_z, \mathbf{D}_z,$ and $\mathbf{F}_z$ are state space matrices, $\mathbf{y}$ is the vector of measured outputs, $\mathbf{v}$ is the measurement noise vector, $\mathbf{z}$ is the regulated output vector, and $\mathbf{x}_s$ is the state vector (Yi and Dyke 2000).

Furthermore, within this thesis no control-structure dynamics are included in the device models, although it is noted that this type of interaction would result in a significant effect on the physical system that should be accommodated for real world implementations (Dyke et al. 1995).

2.5.1 Active Control Law

An H_2/LQG control law has shown to be effective for structures affected by earthquake excitation (Dyke et al. 1995, 1996a, 1998) even in the case of nonlinear behavior (Yoshida and Dyke 2004, Yoshida 2004). In this approach, $\ddot{x}_g$ is taken as a stationary white noise,

and an infinite horizon performance is chosen that weights the regulated output vector, **z**,

i.e.,

$$J = \lim_{\tau \to \infty} \frac{1}{\tau} \left[\int_0^\tau \{ (\mathbf{C}_z\mathbf{x} + \mathbf{D}_z\mathbf{f})^T \mathbf{Q}(\mathbf{C}_z\mathbf{x} + \mathbf{D}_z\mathbf{f}) + \mathbf{f}^T\mathbf{R}\mathbf{f} \} dt \right]$$ (2.10)

where **R** and the elements of the weighting matrix **Q** are selected to appropriately weight the regulated outputs. Further, the measurement noise is assumed to be identically distributed, statistically independent Gaussian white noise processes, and $S_{\ddot{x}_g \ddot{x}_g} / S_{v_i v_i} = \gamma = 25$.

The control force provided by each active control device is given by

$$f_i(t) = u_i(t)$$ (2.11)

where $u_i(t)$ is the ith command force determined by the control algorithm. In other words, the measured forces for the active control devices are the desired forces from the control algorithm. This assumption indicates that the control devices are ideal.

The controller is presented in state space form as

$$\dot{\hat{\mathbf{x}}} = (\mathbf{A} - \mathbf{BK} - \mathbf{LC} + \mathbf{LDK})\hat{\mathbf{x}} + \mathbf{Ly}$$
$$\mathbf{u} = -\mathbf{K}\hat{\mathbf{x}}$$

(2.12)

The matrix $\mathbf{K}$ is the optimal gain matrix for the Linear Quadratic Regulator (LQR) with full state feedback which is expressed in state-space form as

$$\mathbf{K} = -\frac{1}{2}\mathbf{R}^{-1}\mathbf{B}^T\mathbf{P}$$

(2.13)

where $\mathbf{P}$ is the solution of the control algebraic Riccati equation (CARE) given by

$$\mathbf{PA} + \mathbf{A}^T\mathbf{P} - \frac{1}{2}\mathbf{PBR}^{-1}\mathbf{B}^T\mathbf{P} + 2\mathbf{Q} = 0$$

(2.14)

In most real world problems, all the states are not available for measurement. Therefore, observer design techniques are developed to estimate the full state vector from only partial information developed from a measured outputs that capture enough information regarding the system dynamics. The vector $\hat{x}$ is the estimated state vector using the Kalman filter. The matrix $\mathbf{L}$ is the observer gain matrix for the Linear Quadratic Gaussian (LQG) where

$$\mathbf{L} = \mathbf{R}^{-1}\left(\gamma\mathbf{F_y}\mathbf{E}^T + \mathbf{C_y}\mathbf{S}\right)^T$$

(2.15)

The parameter matrices $\mathbf{R}, \mathbf{S},$ and $\mathbf{E}$ with appropriate dimensions are detailed in Spencer, Dyke and Deoskar (1998). Also, the characteristics of the ground excitation are not incorporated into the control design problem, although this has been found to be successful for active control design in prior studies (Dyke et al. 1996a).

2.5.2 Semi-active Control Law

Semi-active devices require the use of a force feedback component in the controller design due to the fact that a control force cannot be directly commanded; the force produced by the device is based strongly on the response of the structure to which it is attached. Thus Equation 2.11 does not hold here and the control force must be measured.

With the use of the force measurement, the nominal controller is presented as

$$\dot{\hat{\mathbf{x}}} = (\mathbf{A} - \mathbf{LC})\hat{\mathbf{x}} + \mathbf{Ly} + (\mathbf{B} - \mathbf{LD})\mathbf{f} \qquad (2.16)$$

where $\mathbf{f}$ is the measured forces generated by the MR dampers.

For semi-active control

$$\mathbf{u} = -\mathbf{K}\hat{\mathbf{x}}$$
$$f_i(t) \neq u_i(t)$$

Therefore the force output is not the command, or desired, force given by the H_2/LQG control law. Instead, the force produced by the MR damper in the simulation is fed into the nominal controller for control action determination.

2.6 Modified Clipped Optimal Control Algorithm

The control algorithm for the MR damper does not directly command the forces to be produced. Instead, the current or voltage applied to the MR circuit is adjusted to induce the MR damper to apply the desired force. In the original clipped optimal control algorithm (Dyke et al. 1996b) a command voltage of either $0V$ or some prescribed maximum voltage level, V_{max} is applied to the device. This algorithm would be classified as a bang-bang controller. A modified version of this control algorithm was later proposed by Yoshida (2003). In this variation, the voltage can assume any value between $0V$ and the maximum voltage, V_{max}. The control voltage, denoted V_{ci} is determined using a linear relationship between the applied voltage and the maximum force of MR damper as shown in Figure 2.24. This particular algorithm is based on some nominal controller that determines the desired forces. For the purposes of this study, H_2/LQG controllers described in Chapters 3 and 4 will be used due to its success in the past of determining control performance. In the event the desired force exceeds the maximum force of the MR damper, the maximum voltage is applied. This approach limits the control force applied to the structure.
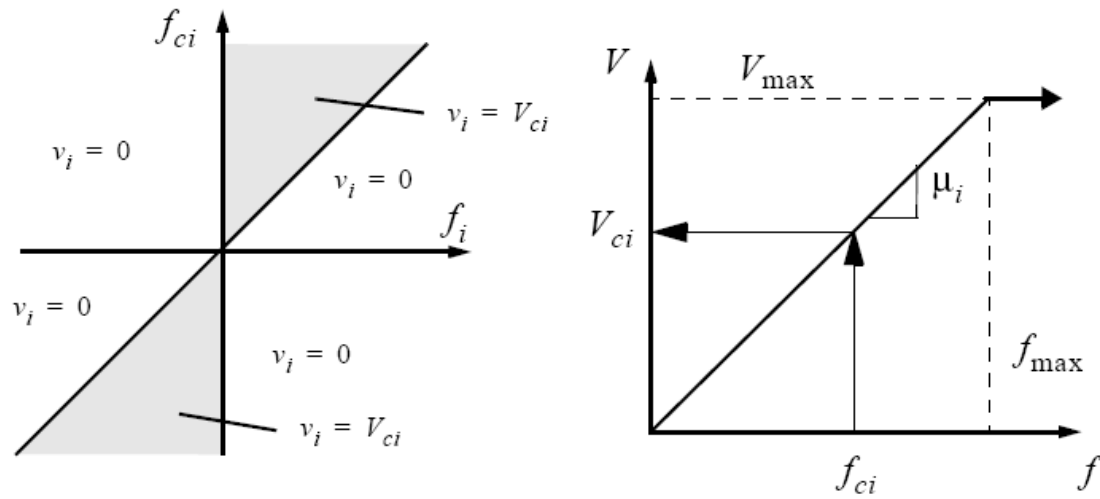
Figure 2.24 Graphical Representation of the Modified Clipped Optimal Control Algorithm

The equation governing the control action is thus written as

$$v_i = V_{ci} H\big(\{f_{ci} - f_i\} f_i\big) \tag{2.17}$$

where

$$V_{ci} = \begin{cases} \mu_i f_{ci} & \text{for } f_{ci} \le f_{max} \\ V_{max} & \text{for } f_{ci} > f_{max} \end{cases} \tag{2.18}$$

where f_{max} is the maximum force produced by the control device and μ_i is the coefficient relating the voltage to the force.

Chapter 3

Fragility Curve Analysis of a 20 Story Building Model

This chapter discusses the development of fragility curves for the 20 story nonlinear benchmark structure described in Ohtori et al. (2004). The model is a moment-resisting steel frame structure retrofitted with control devices. The limit states are based on qualitative and quantitative measures of structural responses calculated from the numerical model of the structure. These capacity measures are discussed in further detail in this section. Control designs are proposed for the active and semi-active devices. A comparison of the fragility curves for the unretrofitted and retrofitted structure with passive, active, and semi-active control devices are presented herein. An evaluation of the peak values of the responses is included in this chapter. A comparison of the control effort from several control systems is also provided in this chapter.

3.1 Model Description

The model proposed for this work is the 20 story nonlinear benchmark steel moment-resisting frame (MRF) structure designed for the SAC project. SAC is a joint venture between three nonprofit organizations: The Structural Engineers Association of California (SEAOC), the Applied Technology Council (ATC), and California Universities for Research

in Earthquake Engineering (CUREE). The structure was designed for the SAC Phase II Steel Project by Brandow & Johnston (1996). Although the structure was not constructed, it was designed to meet seismic codes for a typical high-rise building in the Los Angeles area.

The steel MRF structure is 30.48 m (100 ft) by 36.58 m (120 ft) in plan with an elevation of 80.77 m (265 ft). The bays are 6.10 m (20 ft) on center in both directions. The N-S direction consists of 5 bays while the E-W bay consists of 6 bays. The benchmark structure has 20 levels above ground and two basement levels. The floor-to-floor heights for the basement are 3.65 m (12 ft). The ground floor itself is 5.49 m (18 ft). Typical floor-to-floor heights for the above ground levels (measured from center of beam to center of beam for analysis purposes) are 3.96 m (13 ft).

The columns are 345 MPa (50 ksi) steel. The interior are wide flange, while the corner columns are box columns. Column splices, which are seismic splices to carry bending and uplifting forces, are located throughout the floor levels. The beams are 248 MPa (36 ksi) with wide flange and act compositely with the floor slab.

The seismic mass of the structure consists of various components including the steel framing, floor slabs, ceiling/floor, mechanical/electrical, partitions, roofing, and a penthouse located on the top. The seismic mass for both N-S MRFs of the ground level is 5.32×10^5 kg (36.4 kips s^2/ft), for the first level is 5.63×10^5 kg (38.6 kips s^2/ft), for the second to 19th level is 5.52×10^5 kg (37.8 kips s^2/ft), and for the 20th level is 5.84×10^5 kg (40.0 kips s^2/ft).

In-plane finite element models are developed for the N-S MRFs. These MRFs are chosen

because they are the weak direction of the
structure. The mass matrix is developed from
lumped masses located at nodes throughout the
structure. The nodes are located at beam-column
connection points. Structural member
nonlinearities are taken into account from strong
seismic motion. A bilinear hysteresis model is used
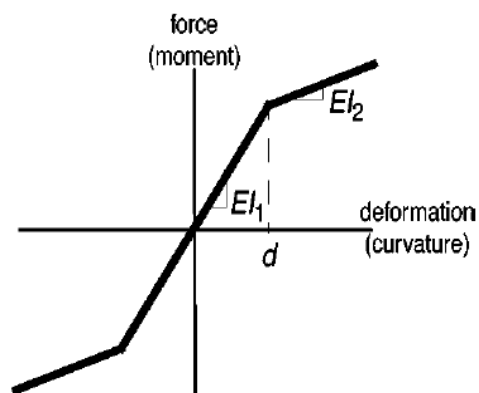
Figure 3.1 Bilinear Hysteresis Model

to describe the member behavior in this event is shown in Figure 3.1. The beam and column

members are described as plane-frame elements. The damping matrix is determined based

on Rayleigh damping. The first 10 natural frequencies are: 0.261, 0.753, 1.30, 1.83, 2.40,

2.44, 2.92, 3.01, 3.63, and 3.68 Hz.
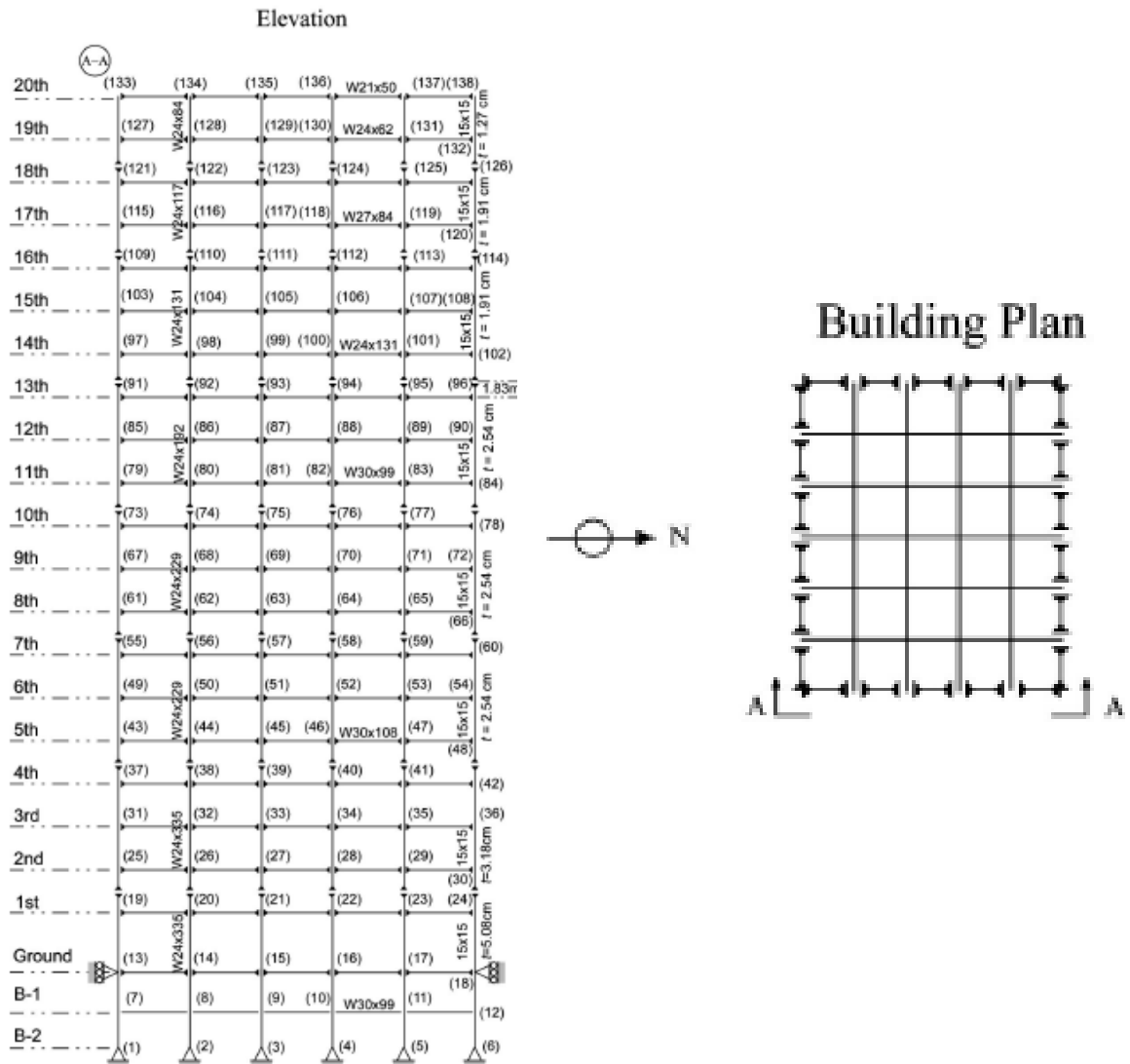
Figure 3.2 Twenty story Nonlinear Moment Resisting Steel Frame Benchmark Building

3.2 Limit States of the Numerical Model

Three different global limit states are chosen for the fragility analyses. These limit states serve to identify some damage reflected on the structure. Inter-story drift, base shear, and absolute acceleration are the limit states considered for this study.

As stated in Chapter 1, FEMA (2000) categorizes three different structural performance levels for inter-story drift capacity. A performance level of life safety was chosen because it confers with most design codes for this study. The life safety limit state is defined by FEMA (2000) to be 2.5% transient drift and 1% permanent drift for moment-resisting steel frames.

A quantitative measure for the limit state corresponding to the base shear was determined because no qualitative measure exists. The measure was chosen as the capacity of the steel members located at the base. The AISC Steel Manual (2001) was used to calculate the capacity of the base shear. The manual provides a shear strength analysis for steel members. This approach was applied to the columns at the base of the structure. The nominal shear strength is calculated as 13,141 kN (2954 kip) for the columns at the base of the structure.

The limit state corresponding to the absolute acceleration does not have a qualitative measure, so a quantitative measure was again chosen. A reasonable value for the absolute acceleration is needed due to the lack of available information provided on design criteria involving this measure. A moderate level of absolute acceleration on the uncontrolled structure is selected. The mean value of the absolute acceleration of the uncontrolled structure subjected to the suite of 2% probability in a 50 year period ground motions is the capacity. The limit state capacity is thus determined to be 0.63 g.

3.3 Control Design

The numerical model discussed above was retrofitted with four different control systems. The design of each of the control systems are discussed in this section. A controller based purely on acceleration feedback is used to drive the actuator in two of the smart control system cases. The MR damper approach also utilizes a force feedback measurement from force transducers located on each device. The actuators are oriented horizontally and are rigidly attached between adjacent floors. The phenomenological model of the MR damper discussed in Chapter 2 is used for numerical simulations. Details regarding each of the control systems implemented are discussed in this section.

3.3.1 Sensors

Accelerometers are chosen for the sensors in this study due to their reliability and inexpensive measurements of absolute accelerations. Accelerometers are simulated on floors 2, 4, 6, 8, 10, 12, 14, 16, 18, 20. The accelerometers are considered to be ideal sensors. Accelerometers are sufficient for determining the control effort for the active control system. The sensors can be modeled in state space form as

$$\mathbf{y}^s = \mathbf{D}_s \mathbf{y}_m \tag{3.1}$$

where $\mathbf{D}_s = [\mathbf{I}]$. The vector of measured responses is

$\mathbf{y}_m = [\ddot{x}_{a2}\ \ddot{x}_{a4}\ \ddot{x}_{a6}\ \ddot{x}_{a8}\ \ddot{x}_{a10}\ \ddot{x}_{a12}\ \ddot{x}_{a14}\ \ddot{x}_{a16}\ \ddot{x}_{a18}\ \ddot{x}_{a20}]^T$. A schematic is shown below in Figure 3.2 to illustrate the sensors input in the numerical model.
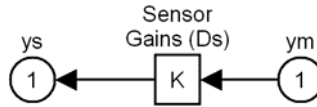
Figure 3.3 Simulink Block Diagram of the Sensor Model for Active System

Force transducers for each of the control devices are also used for the semi-active control systems. These sensors in addition with the accelerometers are needed to determine the control effort for the semi-active case. The sensors can be written in state-space form as

$$\mathbf{y}^s = \mathbf{D}_s \begin{bmatrix} \mathbf{y}_m \\ \mathbf{f}_m \end{bmatrix} \qquad (3.2)$$

where the vector of measured forces applied to the structure is $\mathbf{f}_m = [f_{m1}\ f_{m2} \dots f_{mn}]^T$ and

$$\mathbf{D}_s = \begin{bmatrix} \mathbf{I} & \mathbf{0} \\ \mathbf{0} & \mathbf{I} \end{bmatrix}$$

A schematic is shown below in Figure. 3.3 to illustrate the implementation of the sensor model.
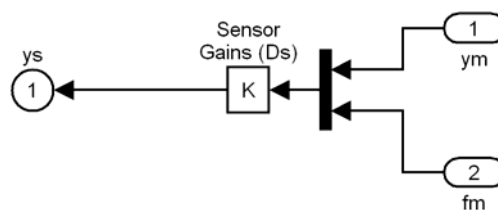
Figure 3.4 Simulink Block Diagram of the Sensor Model for Semi-active System

3.3.2 Control Devices

Hydraulic actuators are chosen for the active control systems in this study. Typically in control design, device constraints are a major concern that needs to be addressed. These limitations could include device stroke, velocity, or force output. For the study, the active devices are considered to be ideal actuators with a maximum force output of 1,000 kN (224.8 kip). Four devices are implemented on each of the first four floors. Two devices are placed on each of the remaining 16 floors, for a total of 48 devices.

MR dampers are used for the passive and semi-active control systems in this study. The approach used for modeling of the MR damper was presented in Chapter 2. Yoshida (2003) developed parameters for the MR damper model to have a capacity of 1000 kN (224.8 kip) and are given as: α_a = 1.0872e5 N/cm, α_b = 4.96116e5 N/(cm·V), n = 1, A = 1.2, γ = 3 cm^{-1}, β = 3 cm^{-1}, and η = 50 sec^{-1}. The parameters are based on an identified shear-mode MR damper experimentally tested at Washington University (Yi et al. 2001) that has been scaled up to produce a maximum force capacity of 1000 kN (224.8 kip) at $V_{max} = 10V$. The scaled up MR damper is estimated to have a maximum power requirement of 50 Watts,

according to the manufacturer. Device constraints such as stroke and velocity are neglected for the MR damper. The device placement scheme described for the active control system is also used for the passive and semi-active control systems for purposes of comparison.

Two passive control systems are developed for this study and are defined as the "passive-off" and "passive-on" cases. The passive-off control system consists of the MR damper described above where a constant voltage of $0\ V$ is applied. The passive-on control system is developed by applying a constant voltage of $4\ V$ to the MR damper.

3.3.3 H_2/LQG Controller

An H_2/LQG controller is chosen for the active and the semi-active control systems in this study. The controller is based on a linear, reduced-order model found in the benchmark files. The reduced model has 20 states (Ohtori et al. 2004).

Parametric studies were determined for both the active and semi-active control systems with various weighting matrices $\mathbf{Q}$, corresponding to various regulated output vectors, $\mathbf{y}$. Variations of the $\mathbf{R}$ matrix were also investigated. For both control systems, the controllers using the reduced-order building model were subjected to the twenty Wen and Wu (2001) synthetic ground motions discussed in Chapter 2. Best possible control designs for improving system reliability of the inter-story drift, base shear, and absolute acceleration

were evaluated. The amount of control force utilized was another design consideration in identifying the best designs.

Parametric studies showed that a regulated output corresponding to the displacements on each of the floors of the building, $\mathbf{y} = [\mathbf{x}]^T$, produce an effective controller for the active control system. Various different weightings for the $\mathbf{Q}$ matrix were investigated. The studies show that the best weighting matrix for the regulated responses is $\mathbf{Q} = q \cdot \mathbf{I}_{20x20}$ where q = 2e13. The weighting matrix $\mathbf{R}$ is selected as $\mathbf{R} = \mathbf{I}_{20x20}$ (Taylor, Barnawi, and Dyke, 2007).

Parametric studies of the semi-active control system revealed that a regulated output corresponding to the absolute accelerations of each floor, $\mathbf{y} = [\ddot{x}_a]^T$ results in an effective controller. Various weightings were considered to determine a suitable controller. As a result, the weighting matrix for the regulated responses should be $\mathbf{Q} = q \cdot \mathbf{I}_{20x20}$ where q = 1e13. The development of the weighting matrix is based on a study by Yoshida (2003) and is selected as $\mathbf{R} = diag\left(\left[n_1^2 \; n_2^2 \ldots n_{20}^2\right]\right)$ where n_i is the number of devices on the ith floor.

3.4 Numerical Results for the Benchmark Building

The benchmark building is evaluated for system reliability through fragility curve analyses using the limit states described earlier in the chapter. The fragility curves are evaluated close

to the highest seismic intensity of the suite of ground motions utilized. Results from parameter studies in Chapter 2 show that data extrapolated beyond this region could result in inappropriate conclusions. A comparison of passive, active, and semi-active control systems are provided. In addition, a comparison of the peak and time history responses of the chosen parameters is given. Finally, the root-mean-square (RMS) control efforts for the active, passive-on, and semi-active cases are tabulated for on the most severe earthquakes in the suite of ground motions.

3.4.1 Fragility Curve Analyses

A comparison of fragility curves of the benchmark building retrofitted with various control systems is provided in Figure 3.4. The life safety performance level for inter-story drift provided by FEMA (2001) is decided as the limit state capacity for these fragility curves. The structure prior to retrofit has the worst performance, followed by the passive-off control system case for this fragility analysis. Interestingly, the fragility curves of the unretrofitted and passive-off control cases converge and both systems possess a reliability of 35% at the high end of the spectral acceleration. The semi-active control system provides a system reliability of 58%. The active control system case slightly improves the system with a reliability of 61%. The passive-on control system provides the best performance for the inter-story limit state with a system reliability of 63%.
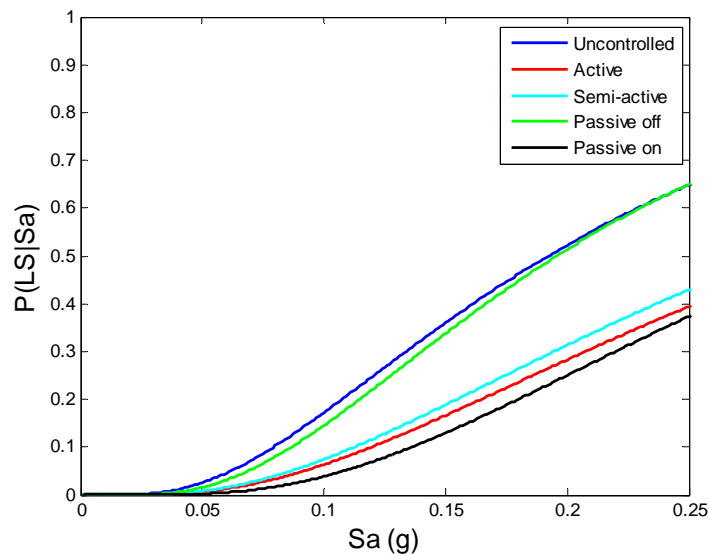
Figure 3.5 Fragility Curve Analysis of Inter-story Drifts

The fragility curve analysis based on the base shear limit state capacity in Figure 3.5 shows that retrofitting the structure with the active control system decreases the building's performance leading to a system reliability of 35% from the original model. The passive-on control case provides a system reliability of 41%. The uncontrolled building provides a system reliability of 44%. The passive-off and semi-active control systems provide a system reliability of 46% for a $S_a = 0.25$ g. However, the semi-active control case provides the better performance for the range of seismic intensity investigated.

The a and b parameters for the power-law form of the nonlinear regression models for inter-story drift are provided in Table 4.1.

Table 3.1 Parameters of nonlinear regression models using inter-story drift

	Uncontrolled	Active	Passive off	Passive on	Semi-active
a	7.45	4.73	7.94	5.38	6.36
b	0.80	0.72	0.85	0.84	0.26
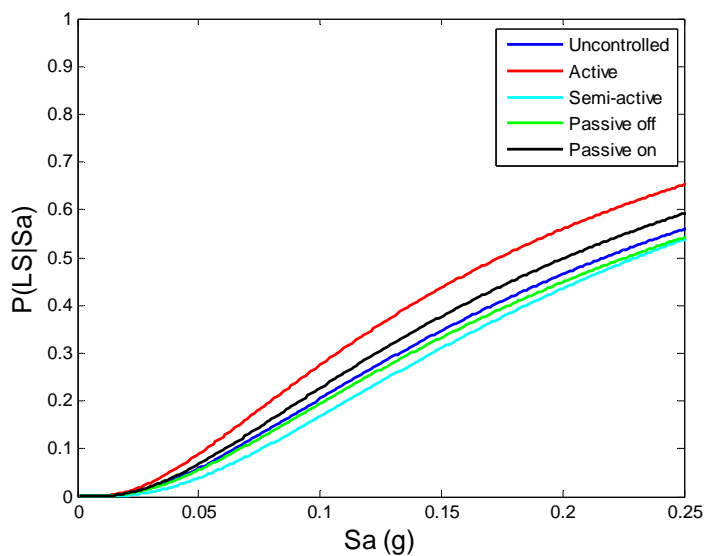
Figure 3.6 Fragility Curve Analysis of Base Shear

The fragility curve analysis for the absolute acceleration of the 20 story benchmark building is provided in Figure 3.6. The uncontrolled building has the worst performance with a system reliability of 36%. The passive-off control system slightly improves the performance of the benchmark building, providing a system reliability of 38%. The active control system greatly improves performance with a system reliability of 49%. The passive-on case further improves the performance a system reliability of 51%. The semi-active control case, however, gives the best performance with a system reliability of 55%.

The a and b parameters for the power-law form used in the nonlinear regression models using base shear as the limit state capacity are provided in Table 3.2.

Table 3.2 Parameters of nonlinear regression models using base shear

	Uncontrolled	Active	Passive off	Passive on	Semi-active
a	3.00E+07	3.55E+07	3.00E+07	3.00E+07	3.12E+07
b	0.54	0.57	0.56	0.51	0.59
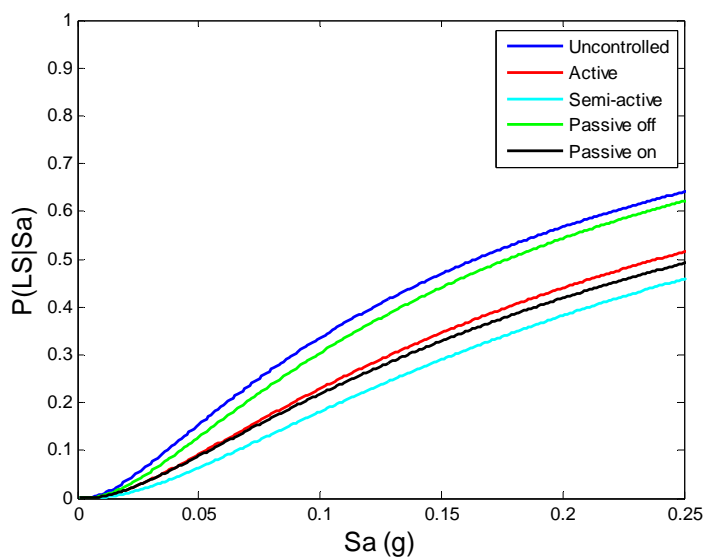
Figure 3.7 Fragility Curve Analysis of Absolute Acceleration

The a and b parameters for the power-law form for the nonlinear regression models using absolute acceleration as the limit state capacity are given in Table 3.3.

Table 3.3 Parameters of nonlinear regression models using absolute acceleration

	Uncontrolled	Active	Passive off	Passive on	Semi-active
a	1.49	1.27	1.51	1.15	1.17
b	0.47	0.48	0.50	0.44	0.48

3.4.2 Peak and Time History Responses of the Benchmark Building

Comparisons of the peak responses for each of the ground motions are provided in order to fully investigate each of the control systems for the benchmark building. Comparisons of representative time history responses for the active and semi-active controlled benchmark building are also evaluated. Time histories are provided for both a high and low intensity ground motion. The comparisons also serve to validate the effectiveness of the fragility curve analyses provided above. The comparisons are evaluated for inter-story drift, base shear, and absolute acceleration.

The uncontrolled building has the highest inter-story drifts for the suite of earthquakes in Figure 3.7 with the exception of two ground motions. The passive-off control system has the second worst performance for the inter-story drifts. The active control system has the third highest collection of inter-story drifts for the suite of ground motions. The semi-active control system has the second best performance for the controlled cases, outperforming the active case in all but four cases. According to the studies shown in Chapter 2, the influence of various individual points (take earthquake number 8 for instance) could result in the lower system reliability for the semi-active case. The passive-on control system provides the best performance by providing the lowest inter-story drift for a majority of the ground motions.
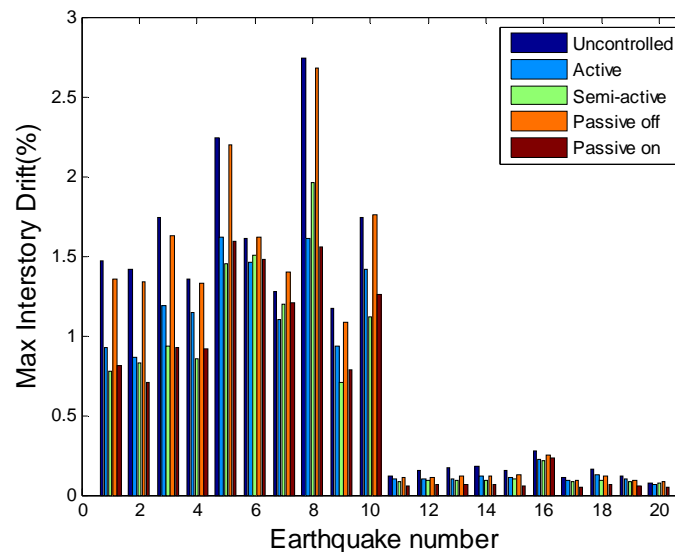
Figure 3.8 Peak Responses of Inter-story Drifts for Ground Motions

A comparison of the time history responses for the top floor inter-story drift for Earthquake 5 is shown in Figure 3.8. The time history responses for inter-story drift have been reduced by the active and semi-active control systems. The semi-active control systems shows better performance over the active control system during the earlier portion of this high intensity ground motion. During the smaller, latter attenuations the semi-active and active control systems provide the same level of performance for the benchmark building.

Another comparison is given in for Earthquake 17 in Figure 3.9. The beginning of this particular ground motion shows that the uncontrolled case performs as well as the controlled structures. However, the active and semi-active control cases provide a significant and consistent reduction in inter-story drift for majority of the ground motion's duration. It is also noted that both control systems possess similar time history responses for this earthquake.
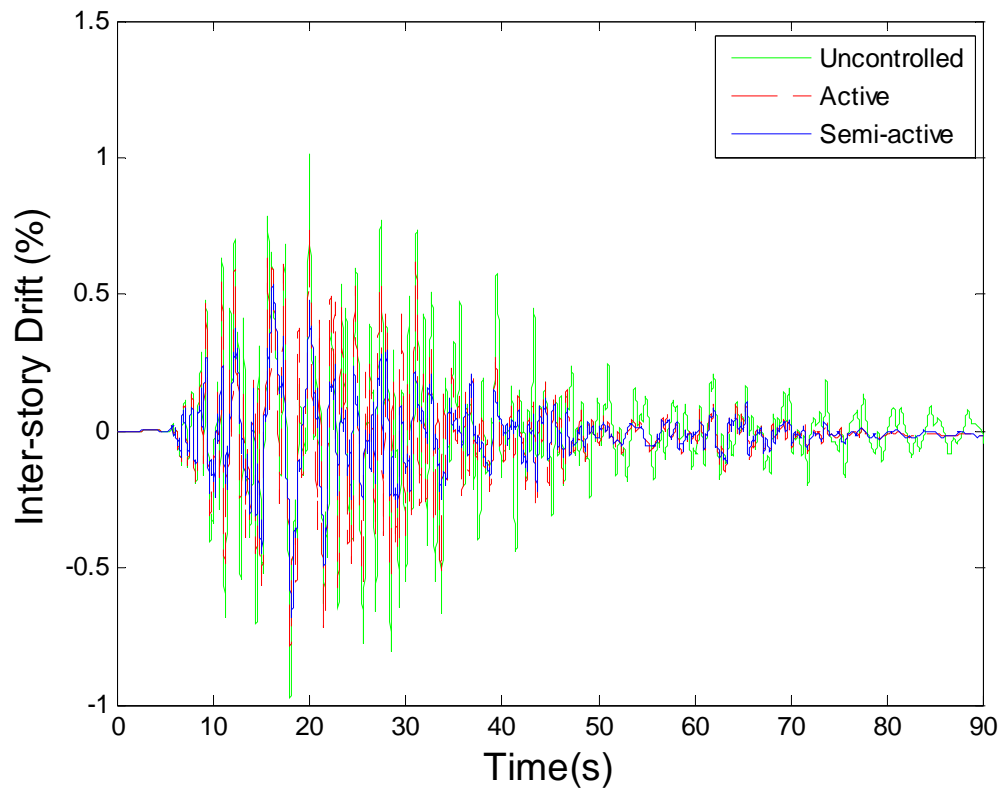
Figure 3.9 Time History Responses of Inter-story Drift for Earthquake 5
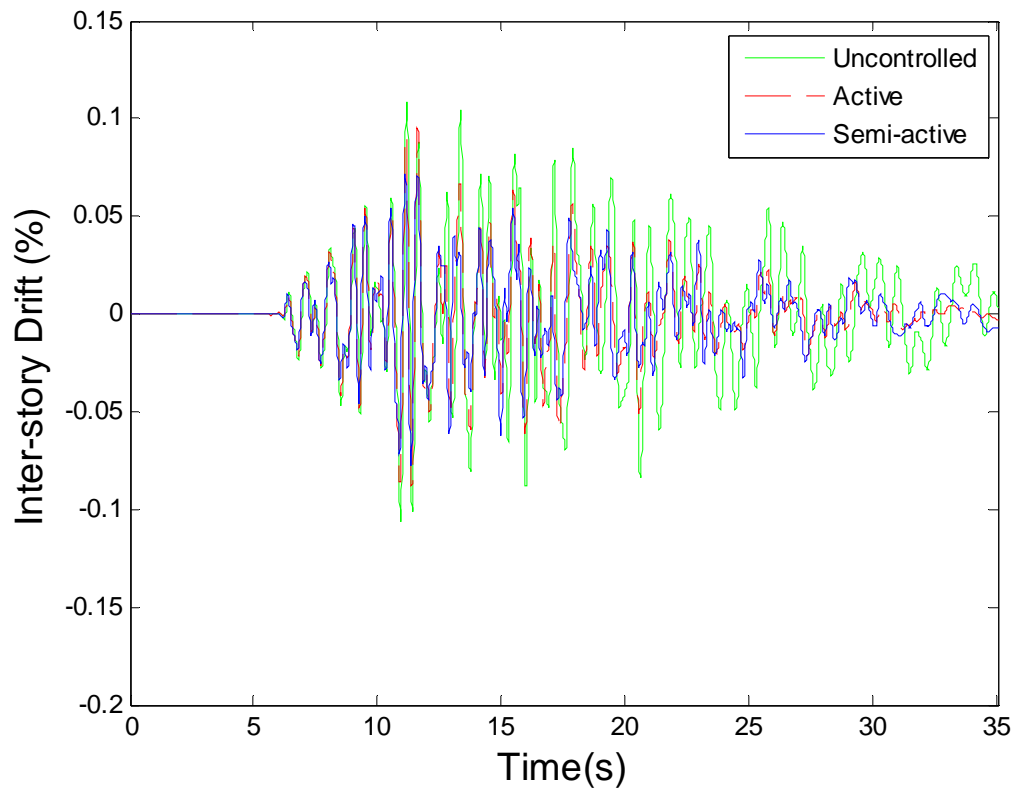
Figure 3.10 Time History Responses of Inter-story Drift for Earthquake 17

A comparison of the base shear imposed on the benchmark building for each of the retrofitted cases is provided in Figure 3.10. The active control case has the largest base shear for all of the higher intensity ground motions and a number of the lower intensity measures. The passive-on case has the largest base shear for the lower intensity earthquakes and the second largest for the higher intensity ground motions. The passive-off case has the second best performance overall in terms of base shear. The semi-active case has the best performance providing the lowest base shear for a majority of the ground motions used.
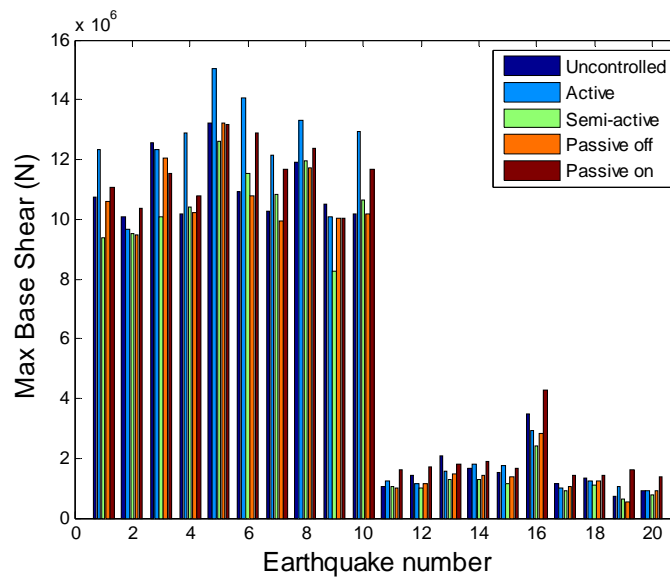
Figure 3.11 Peak Responses of Base Shear for Ground Motions

A comparison of the active and semi-active controlled building's time histories for base shear are given in Figure 3.11. Results show that the controlled structures for both smart systems offer some mitigation for this high intensity measure. This reduction in base shear is mainly for the latter half of the ground motion's duration. The semi-active control system provides a reduction of the base shear peak responses over the uncontrolled and actively controlled structures.

In a comparison of the active and semi-active control systems for the benchmark structure using a low intensity ground motion, the base shear over Earthquake 17 shown in Figure 3.12 has been reduced by a moderate amount. This reduction is primarily in the second half of the ground motion's duration. During the more intense portion of this ground motion, the base shear associated with the semi-active control system is shown to have the best performance.
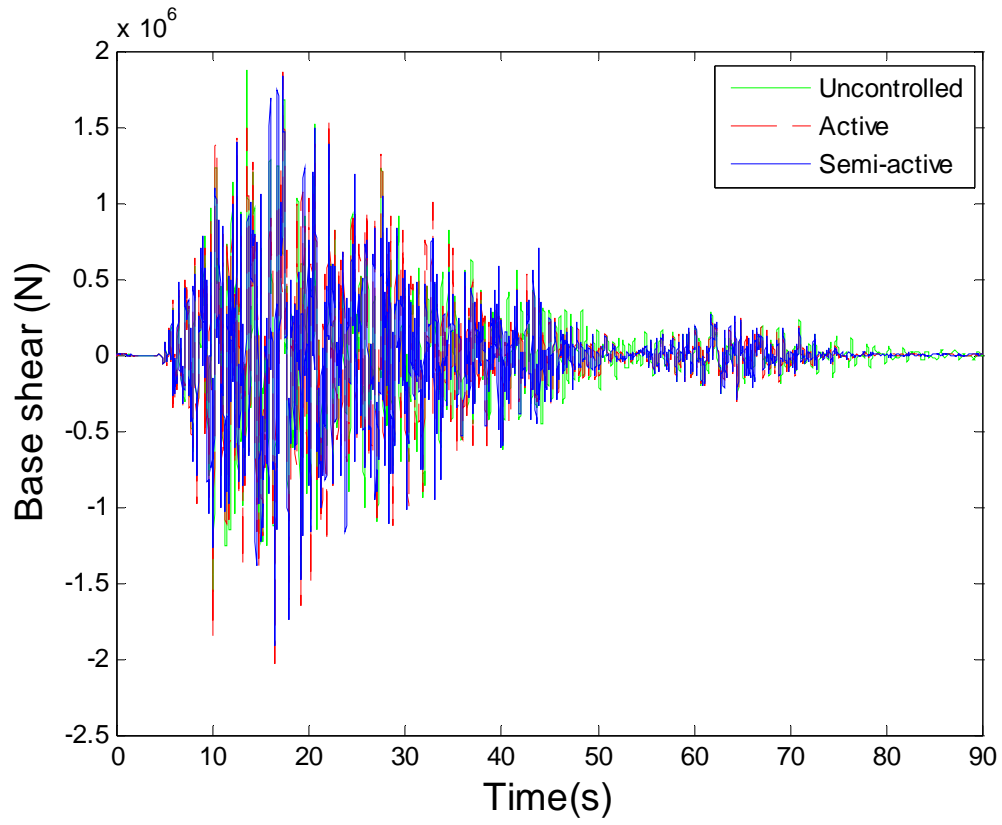
Figure 3.12 Time History Responses of Base Shear for Earthquake 5
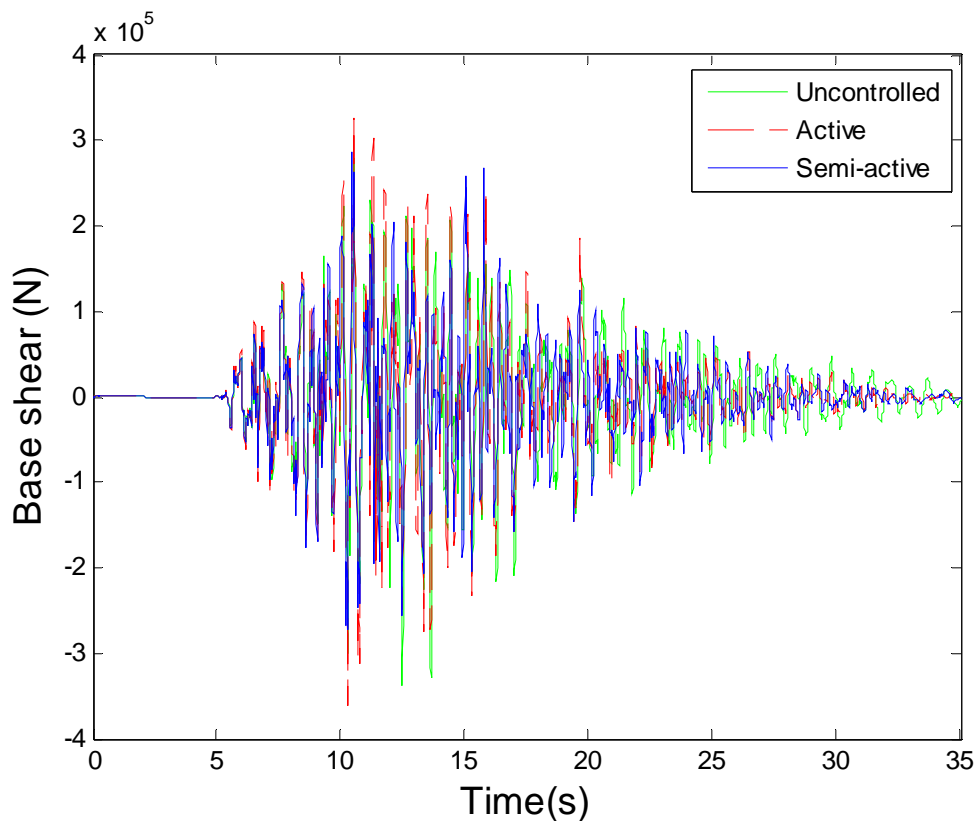
Figure 3.13 Time History Responses of Base Shear for Earthquake 17

The peak responses of the absolute accelerations are given in Figure 3.13. The building prior to retrofit yields the highest absolute acceleration for a majority of the ground motions. The passive-off control system has absolute acceleration values similar to the uncontrolled case for the higher intensity ground motions and fairly high responses for the lower intensity measures. The passive-on case has the highest peak responses for the lower intensity ground motions and moderately high responses for the higher intensity ground motions giving it the third worst performance. The active control system provides the second best performance in terms of peak responses by maintaining among the smaller responses for all of the lower intensity ground motions and for nearly half of the higher intensity earthquakes. The semi-

active control system has the lowest peak responses giving it the best performance of the controlled cases with the exception of five ground motions.
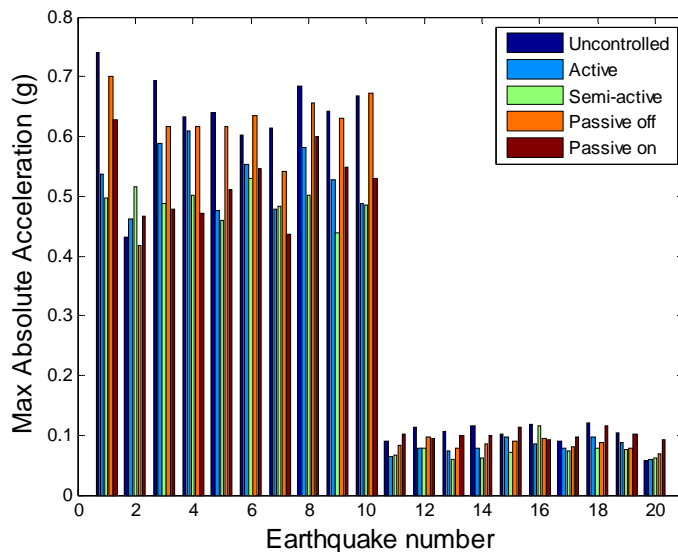
Figure 3.14 Peak Responses of Absolute Acceleration for Ground Motions

The comparisons of the time history responses shown in Figure 3.14 show the significant improvement the active and semi-active control systems have over the uncontrolled structure for absolute acceleration located on the top floor of the benchmark building. The two control systems provide reductions in both the peak and overall responses for this high intensity ground motion. The semi-active control yields the best performance for the time history responses.

In Figure 3.15, the active and semi-active controlled building is shown to have smaller absolute accelerations than the unretrofitted building throughout the time history of this low intensity ground motion. The active and semi-active control systems are able to attenuate

the time history responses to minimal values unlike the uncontrolled case. The semi-active

case is provides lower responses throughout the majority of this ground motion's duration.
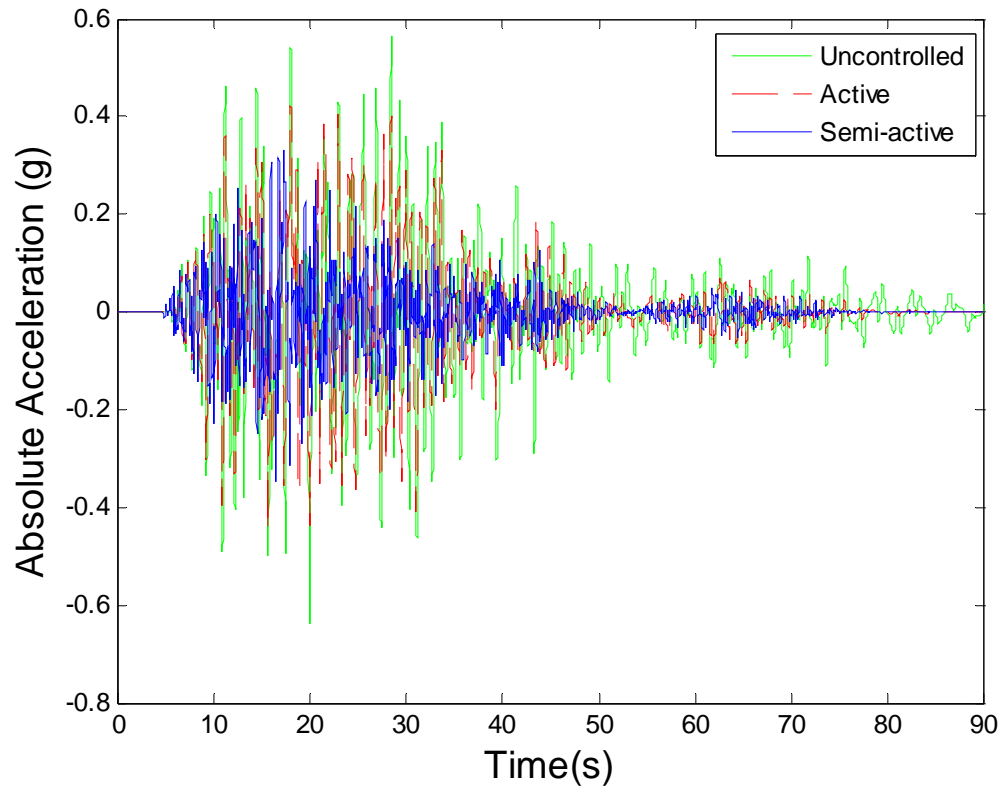
Figure 3.15 Time History Responses of Absolute Acceleration for Earthquake 5
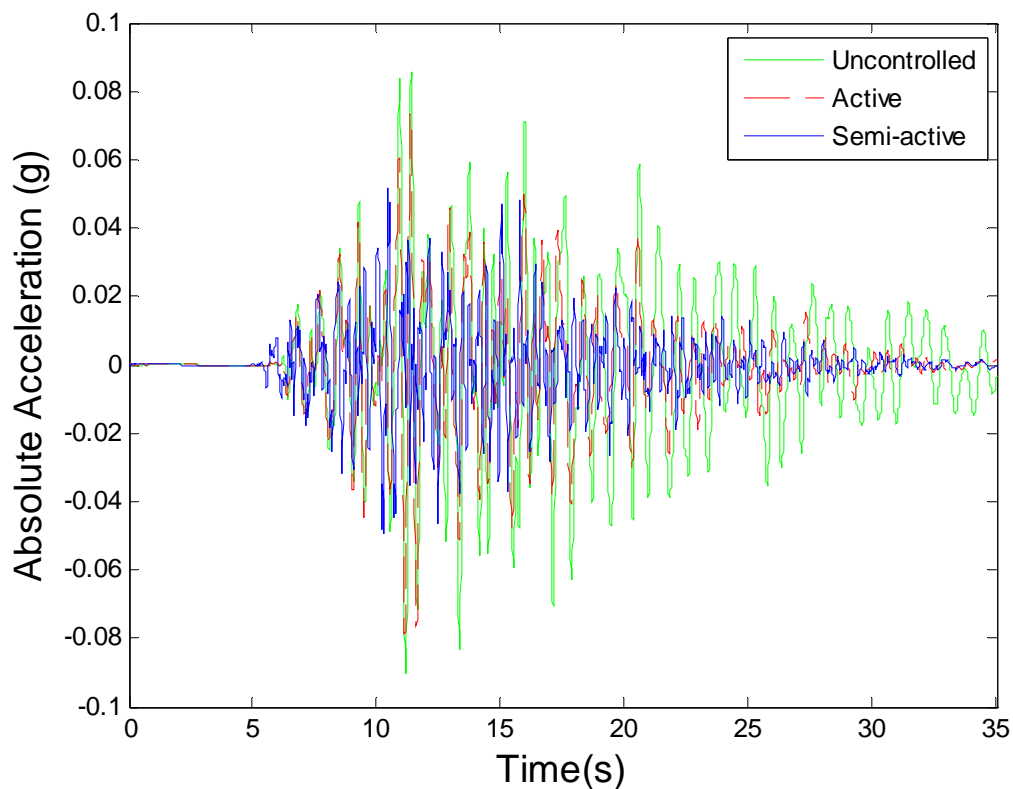
Figure 3.16 Time History Responses of Absolute Acceleration for Earthquake 17

3.4.3 Comparison of Control Effort Required

The amount of control forces produced is another design consideration. The life of a control device is dependent on its usage and the cost is determined by the magnitude of the forces generated by that device. Smaller control devices are generally less expensive and if their full capacity is not used often, they will likely last longer. From an economic standpoint, it is prudent to choose devices which will produce moderate control forces while effectively mitigating the responses of the structure during a seismic event. Table 3.4 shows the mean of the RMS control efforts per device at the eight damper locations for the three

most effective control cases. The values have been determined for the building excited by Earthquake 5. Results in the table show a similar amount of control force applied to the structure over the time history for the active and passive-on control systems. The semi-active case, however, requires a control effort of only one-seventh of the other cases.

Table 3.4 RMS Values of Control Forces (kN)

Passive-on	Active	Semi-active
225	242	34

3.5 Summary

This chapter focused on the development of fragility relationships for a full scale building under several retrofit strategies. The full scale building used in this study was a 20 story nonlinear benchmark building with a moment-resisting steel frame. The fragility analyses of the benchmark building were based on global structural parameters determined to be integral to system functionality. Inter-story drift, base shear, and absolute acceleration were defined as the limit state parameters. The retrofit strategies proposed for this study were all control systems implemented as supplemental dampers throughout the structure. The types of control systems used were passive, active, and semi-active. An acceleration feedback strategy was utilized for the design and implementation of all of the control systems. In addition, a force feedback measurement was needed for implementation of the semi-active control system. The devices for the active case were ideal hydraulic actuators and were controlled using an H_2/LQG control law. The Bouc-Wen model was used for the passive and semi-active devices. The semi-active devices were controlled using the modified clipped-

optimal control algorithm. In addition, a comparison for the peak responses was investigated for the various mitigation techniques proposed to determine the effectiveness of the fragility assessments. A comparison of the control effort used in several control cases was also investigated.

The semi-active control system was determined to have the best overall performance in comparing various control systems in terms of system reliability through fragility assessments. This control case outperformed all of the other cases in two of the three limit states and was moderately efficient in the third limit state. Although, the active and passive-on control cases were shown to be more efficient in terms of inter-story drift, the major drawback to these two systems was their poor performance in terms of base shear. In all three cases, the semi-active control case showed improvement over the uncontrolled building.

An investigation of the peak and time history responses of the limit state parameters showed that the fragility curve analyses accurately describes the behavior exhibited by the structure over the suite of ground motion records. There was a strong correlation between controlled systems that had higher reliability and those that performed better in terms of peak responses. The time history responses proved to have more ambiguity for the investigated parameters. The semi-active case showed better performance than the active case for the inter-story drift for both the high and low seismic intensities. This result is contrary to the fragility assessment. The base shear time history responses were very similar for the semi-active and active control cases. In the fragility assessment, the semi-active case shows a

significant improvement over the active control case. The time histories for the absolute acceleration, however, showed a lot of similarity with the fragility assessment in terms of the active and semi-active control responses. It is noted that the time history responses were for 2 out of the 20 representative ground motions and that analyses of the entire suite of ground motions is needed to properly compare the time history responses to the fragility assessments.

The semi-active case has the smallest control effort given in a comparison of the three retrofit strategies investigated. This particular case yielded a system reliability similar to the other cases, if not better, while only using a fraction of the control effort used by the others. The smaller effort needed would allow for less costly devices and potentially lead to less wear on the devices.

Chapter 4

Fragility Curve Analysis of a Cable-Stayed Bridge Model

This chapter considers the development of fragility relationships for the benchmark structure described in Dyke et al. (2003). The model is a cable-stayed bridge that is retrofitted with control devices. Limit states are developed for the model based on the dimensions of the structure and member strength analyses. Further details regarding the limit state capacities are provided in this chapter. Control designs are proposed for the active and semi-active control systems. System reliability of the unretrofitted and retrofitted structure with passive, active, and semi-active control systems are investigated and compared. An evaluation of the peak responses of the limit state parameters is presented. An investigation of the effect on the cables is provided for each of the control systems proposed. A comparison of the control effort of several control systems is also included.

4.1 Model Description

The model proposed for this work is the Bill Emerson Memorial cable-stayed bridge which spans the Mississippi River near Cape Girardeau, Missouri. The structure was designed by the HNTB Corporation with seismic events strongly considered due to the location of the

structure in the New Madrid seismic zone. The bridge is also a critical facility as it is principal crossing over the Mississippi River.

The Bill Emerson Bridge is comprised of two towers, 128 cables, and 12 additional piers in the Illinois approach as shown in Figure 4.1. The Illinois approach is neglected for the numerical model used in this study. The main span is 350.6 m (1150 ft) while the side spans are 142.7 m (468 ft). A cross section of the bridge is shown in Figure 4.2. The bridge has a total width of 29.3 m (96 ft) with four lanes of traffic and two bicycle lanes straddling the car lanes. The deck of the bridge consists of steel beams and concrete slabs. The two towers have a height of 102.4 m (336 ft) at Pier 2 and 108.5 m (356 ft) at Pier 3. The cross section of the towers varies throughout its height. Further description of the cross sections can be found in Dyke et al. (2003). Each of the towers supports 64 cables of high-strength, low-relaxation steel. The cable anchorage is attached to steel girders beneath the deck slab.
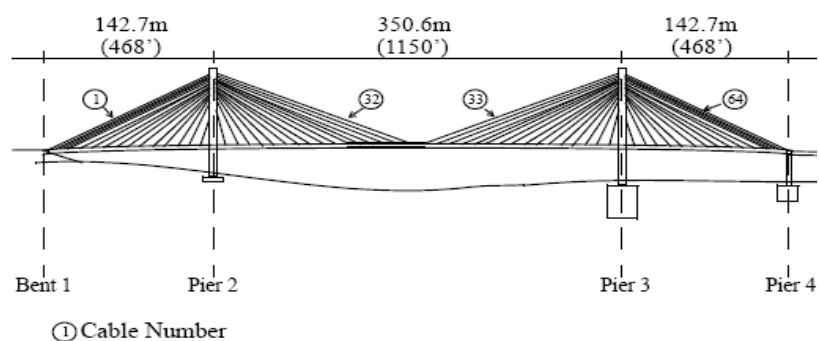
Figure 4.1 Drawing of the Bill Emerson Bridge
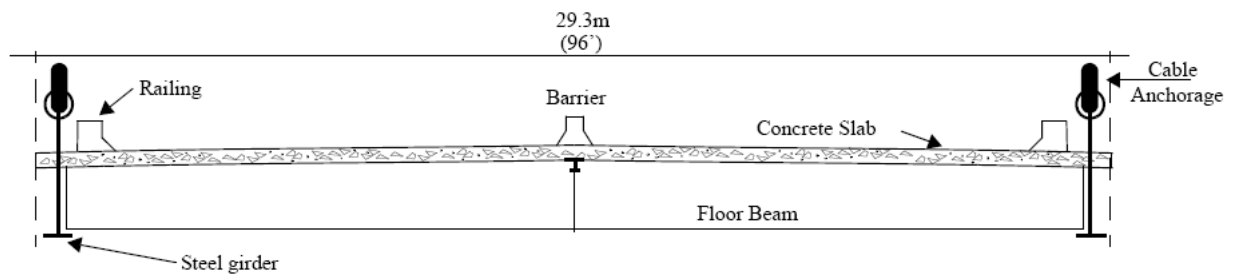
Figure 4.2 Cross Section of Bridge Deck

The beams are made from ASTM A709 grade 50W steel with f_y of 344 MPa (50 ksi). The slabs are comprised of prestressed concrete with f_c' of 41.36 MPa (6 ksi). The cables are comprised of ASTM A882 grade 270 steel. The cables are also covered with a polyethylene piping to resist corrosion.

The mass of the deck is comprised of the steel beams, rigid concrete slabs, barriers, and railings. The total mass of the deck per unit length is assumed to be 2,645.7 kg/m (5,831 lbs/ft).

Two numerical models are used for analysis purposes in this study (Dyke et al. 2003). Both of the models used are linear. Typically, fragility assessments are performed on structures that behave nonlinearly. The first model is for the bridge model without control devices implemented. Instead, sixteen 6.67 MN (1,500 kip) shock transmission devices are applied between the tower and deck. These devices are employed in the longitudinal direction of the bridge and allow for expansion of the deck for temperature changes. These devices also lock up and are modeled as rigid links in the event of seismic activity. The first ten frequencies of this numerical model are 0.29, 0.37, 0.47, 0.52, 0.58, 0.65, 0.67, 0.70, 0.71, and 0.72 Hz.

The second model consists of the bridge in a configuration to allow control system implementation. The devices may be placed longitudinally between the deck and the tower like the first model. The connections between the tower and the deck are disconnected for this model to facilitate insertion of a realistic device model. The lack of connections results in the model being more flexible than the first model. The first ten frequencies for the second model consisting of the structure alone are 0.16, 0.27, 0.37, 0.45, 0.50, 0.57, 0.62, 0.65, 0.70, and 0.71 Hz.

4.2 Limit States of the Numerical Model

Three limit states are chosen for conducting fragility analyses for the bridge model. Some parameters of interest are common for cable-stayed bridges (Walther et al. 1999; Bontempi et al. 2003; Iemura and Pradono 2003; Domaneshi 2005). The parameters of interest are deck displacement, deck shear, and overturning moment and these are considered for this study.

An appropriate measure of deck displacement must be considered due to the lack of a widely accepted design criterion. Because the length of the gaps between the deck and tower are probably dependent on the actual length of the structure a limit state is conceived based on some proportion of the bridge's length. A very low percentage of the bridge's length is considered as a precautionary measure. Here a limit state of 0.01% is chosen for the deck displacement.

A quantitative measure is developed for the capacity of the deck level shear in the towers. A strength analysis to determine a suitable value is performed upon the cross section at the interface where the deck meets the tower. An analysis is developed using ACI (2005) in conjunction with information provided from construction plans because the towers are composed of reinforced concrete. The analysis shows that a limit state of 17,833 kN (4009 kips) is suitable for this study and is within the threshold of the tower's actual capacity.

The limit state for overturning moment also is calculated through a quantitative approach. The moment developed at the footings of one of the piers of the bridge is determined to be the overturning moment. A strength analysis is calculated using ACI (2005) and construction plans provided to develop the limit state capacity because this area is comprised of reinforced concrete. A limit state capacity of 335,863 kN-m (247,657 lb-ft) is determined for the overturning moment.

4.3 Control Design

The second model of the cable-stayed bridge is retrofitted with four different control systems. Accelerometers and displacement sensors are employed for the smart control systems utilized. In addition, the control system that has MR dampers also uses force transducers for feedback. The devices are applied longitudinally between the deck and the towers as shown in Figure 4.3. The phenomenological model of the MR damper is described

earlier in Chapter 2. Further details regarding the control systems are provided in this section.
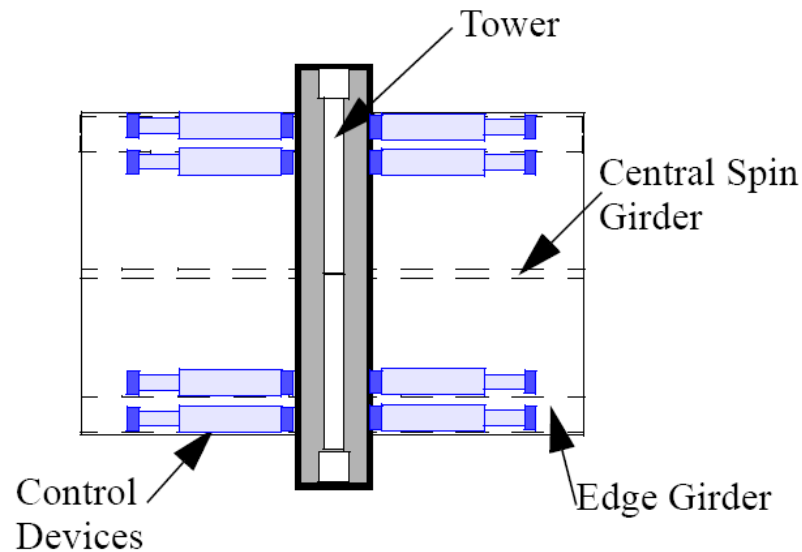
Figure 4.3 Schematic of Device Location

4.3.1 Sensors

The active and semi-active control systems use five accelerometers and four displacement sensors for a total of nine sensors. The placement and location of the sensors are the same for both control systems. The accelerometers are oriented in the longitudinal direction of the structure. Four of the accelerometers are located on the top of the tower legs. The fifth accelerometer is located at the midspan of the deck. The displacement sensors are also oriented longitudinally along the bridge. Two displacement sensors are positioned between the deck and Pier 2 while the other two are located between the deck and Pier 3. The accelerometers and displacement sensors are considered to be ideal sensors. The control

forces determined for the active control system are dependent only on these sensors. The

sensors for the active control system can be modeled in state-space form as

$$\mathbf{y}^{s} = \mathbf{D}_{s}\mathbf{y}_{m} \tag{4.1}$$

where $\mathbf{D} = [\mathbf{I}]$; $\mathbf{y}_{m} =$ measured responses from the accelerations and displacements. A

schematic illustrating the implementation of the sensors in the numerical model is described

in Figure 4.4.
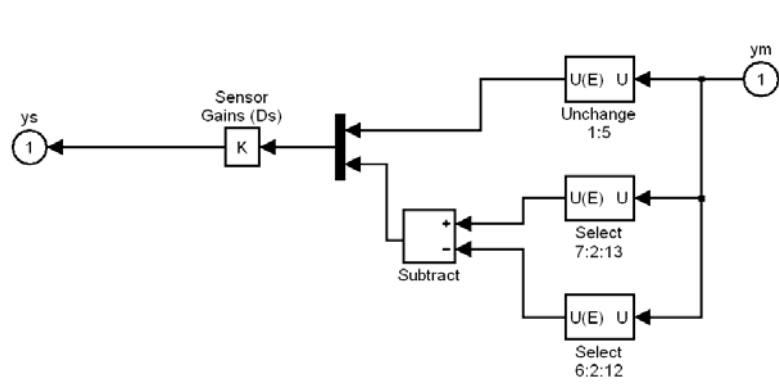
Figure 4.4 Simulink Block Diagram of the Sensor Model for Active System

For the semi-active control system a force feedback component is needed to develop the

control forces to drive the devices. The equation used in the numerical model for the sensor

implementation can be expressed in state-space form as

$$\mathbf{y}^{s} = \mathbf{D}_{s}\begin{bmatrix}\mathbf{y}_{m}\\\mathbf{f}_{m}\end{bmatrix} \tag{4.2}$$

where the measured forces applied to the structure are given as $\mathbf{f}_m = \begin{bmatrix} f_{m1} & f_{m2} & \dots & f_{mn} \end{bmatrix}^T$ and

$$\mathbf{D}_s = \begin{bmatrix} \mathbf{I} & \mathbf{0} \\ \mathbf{0} & \mathbf{I} \end{bmatrix}$$

A schematic of the sensor implementation for the numerical model is provided in Figure 4.5
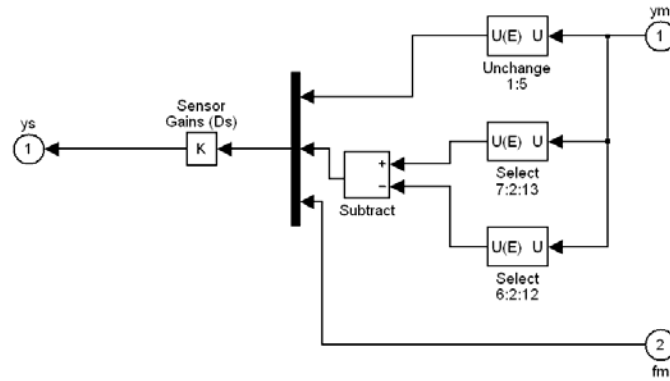
Figure 4.5 Simulink Block Diagram of the Sensor Model for Semi-active System

4.3.2 Control Devices

Hydraulic actuators are chosen as the control devices for the active control system. The constraints of the devices need to be taken into account for an accurate control design. These constraints can include device stroke, velocity, and force output. Ideal actuators with a maximum force output of 1000 kN (224.8 kip) are considered for the active control system in this study. Four actuators located are between the deck and Bent 1, eight of the actuators are placed between the deck and Pier 2, eight are placed between the deck and Pier 3, and four are between the deck and Pier 4, for a total of 24 hydraulic actuators.

MR dampers are chosen as the control devices for both the passive and semi-active control systems. The particular MR damper model chosen is discussed in Chapter 2. The parameters for this particular device was developed by Yoshida (2003) and given as: $\alpha_a = 1.0872\mathrm{e}5$ N/cm, $\alpha_b = 4.96116\mathrm{e}5$ N/(cm$\cdot$V), $n = 1$, $A = 1.2$, $\gamma = 3$ cm^{-1}, $\beta = 3$ cm^{-1}, and $\eta = 50$ sec^{-1}. These parameters are based on an identified shear-mode MR damper experimentally tested at Washington University (Yi et al. 2001) and scaled up to have a maximum output of 1000 kN (224.8 kips) at a $V_{\max} = 10$ V. The power requirement for such a device was determined to be 50 Watts according to the manufacturer. Device constraints such as stroke and velocity need not be considered for the MR damper due to its unique force development procedure. The MR damper develops control forces by applying a magnetic field so concerns such as fluid movement or the extent device pushes in hydraulic actuators are nullified. The placement and location of the MR dampers for the passive and semi-active control systems are the same as the active control system.

Two passive control systems are considered for this study. The first passive system is termed the "passive-off" case and is defined by applying a constant voltage of 0 V to the MR damper. The second passive system is termed the "passive-on" case and is defined by applying a constant voltage of 4 V to the MR damper.

4.3.3 H$_2$/LQG Controller

An H$_2$/LQG controller is chosen for both the active and semi-active control systems. The controller is developed for a linear reduced-order model of the bridge provided in the benchmark files. The reduced-order model has 30 states (Dyke et al. 2003).

An investigation of the $\mathbf{Q}$ and $\mathbf{R}$ weighting matrices is conducted to properly design the controllers in this study for both the active and semi-active control systems. Parametric studies are performed for each of the weighting matrices for the reduced-order model subjected to earthquake excitations developed by Wen and Wu (2001). The best possible designs are developed for each of the control systems in terms of increasing system reliability for the deck displacement, deck shear, and overturning moment while using an appropriate amount of control force.

Parametric studies show that for the active control system a regulated output of the deck displacements at Bent 1 and Pier 4 will produce an effective controller. An investigation regarding the weighting for the $\mathbf{Q}$ matrix is performed. Results show that the weighting matrix for the regulated response output should be $\mathbf{Q} = q \cdot \mathbf{I}_{4x4}$ where $q = 2.5e6$. The weighting matrix corresponding to the control forces is set to $\mathbf{R} = \mathbf{I}_{8x8}$ is sufficient.

The most effective controller is produced by selecting a regulated output of the deck shears located at Pier 2 and Pier 3 for the semi-active control system. Development of an appropriate weighting on the $\mathbf{Q}$ matrix is analyzed next. The parameter study conducted for

the weighting matrix corresponding to the regulated output results in a weighting matrix of

$\mathbf{Q} = q \cdot \mathbf{I}_{4x4}$ where $q = 1$. The weighting matrix for the control forces is set to $\mathbf{R} = \mathbf{I}_{8x8}$.

4.4 Numerical Results for the Benchmark Bridge

The retrofitted and original bridge models are evaluated for system reliability through fragility assessments under the limit states described earlier in this chapter. An analysis of the bridge's peak responses using the limit state parameters is evaluated next. The number of cables that exceed an appropriate tension range throughout the seismic events is observed. Finally, the control effort exhibited by several control systems is investigated.

4.4.1 Fragility Curve Analyses

A comparison of fragility analysis for the benchmark bridge using the control systems discussed earlier is provided below in Figure. 4.6. These fragility curves have a limit state covers spans to a displacement that is a small percentage of the deck length. The seismic intensities extend to a range that corresponds with the region of actual data. The fragility curve analysis shows a clear distinction between the system reliability of each of the controlled structures. The passive-off case has the lowest system reliability with 51%. The active control system provides a system reliability of 64%. The passive-on control system has a system reliability of 78%. The semi-active control system provides the best performance for the retrofitted structure with a system reliability of 83%. However, it is

observed that the unretrofitted structure's performance far exceeds the others with a system reliability of 98%.
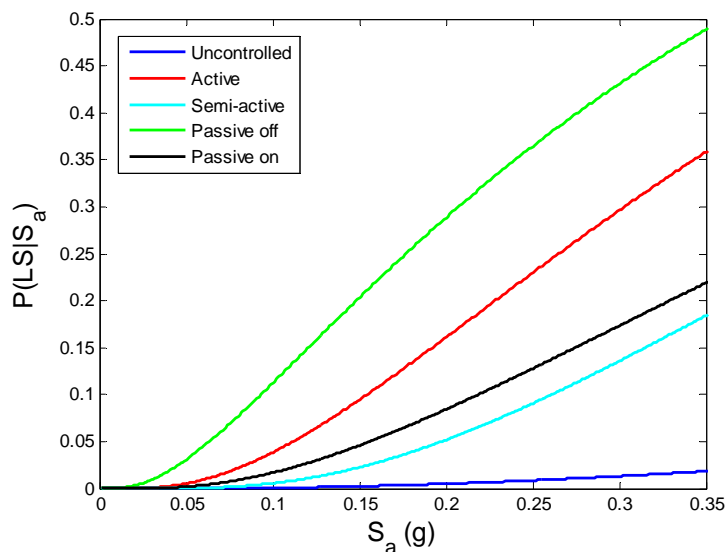
Figure 4.6 Fragility Curve Analysis of Deck Displacement

A fragility analysis of the various controlled systems for the deck shear is provided in Figure 4.7. A reversal in terms of performance for two sets of fragility curves is noted for this analysis. The first set is for the passive-off and active control systems. The passive-off has a higher system reliability for lower intensities, while the active control system has a higher system reliability for the higher intensities. The system reliability of the passive-off case is a little over 80%, while the system reliability of the active control system is nearly 82% at the highest intensity measure considered for the analysis. The second set of retrofit cases that display a reversal in terms of performance are the uncontrolled system and the passive-on control system. The passive-on control system results in a higher system reliability for the cable-stayed bridge for the lower intensities. This behavior is reversed near the end of the seismic intensity range with the unretrofitted structure having a better performance. The

passive-on case has a higher system reliability of 92.5% and the uncontrolled system is slightly better with a system reliability of 93% at the highest seismic intensity considered for the analysis. The semi-active control system has the best performance of all the cases with a system reliability around 96%.

The a and b parameters for the power-law form of the nonlinear regression models using deck displacement as the limit state capacity is provided in Table 4.1.

Table 4.1 Parameters of nonlinear regression models for deck displacement

	Uncontrolled	Active	Passive off	Passive on	Semi-active
a	0.30	1.06	1.31	0.82	0.83
b	0.54	0.71	0.71	0.78	0.75
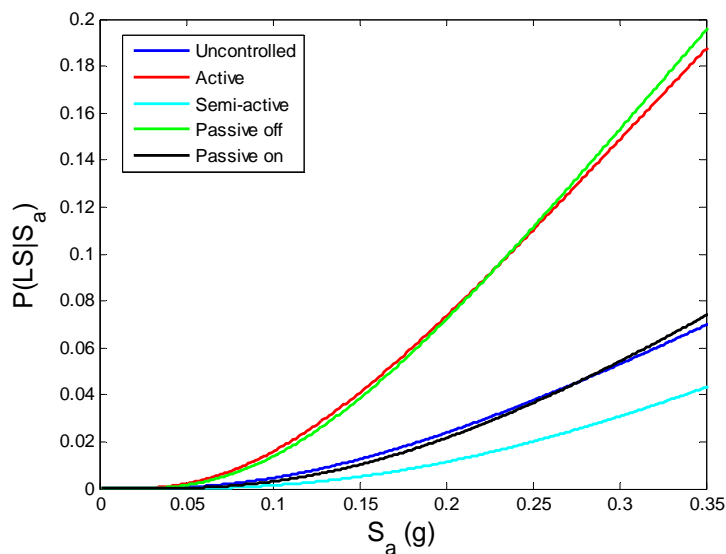
Figure 4.7 Fragility Curve Analysis of Deck Shear

The *a* and *b* parameters for the power-law form for the nonlinear regression models using deck shear as the limit state are provided in Table 4.2.

Table 4.2 Parameters of nonlinear regression models for deck shear

	Uncontrolled	Active	Passive off	Passive on	Semi-active
a	1.32E+04	1.96E+04	2.07E+04	1.45E+04	1.26E+04
b	0.5	0.55	0.59	0.56	0.52

Fragility curves using the overturning moment limit state are compared for the bridge model under the proposed retrofit strategies in Figure 4.8. The uncontrolled case has the worst performance with a system reliability of 0% at the end of the seismic intensity range. Although the active and passive-off control systems have roughly the same system reliability of 9%, there is no clear deciding factor in terms of performance. The passive-off control case is shown to have better performance for lower seismic intensities. On the other hand, the active control case is shown to have better performance for the higher seismic intensities. The passive-on case improves the performance over these two cases with a reliability of 22%. The best performance, however, is achieved by the semi-active control system with a system reliability of 28%.
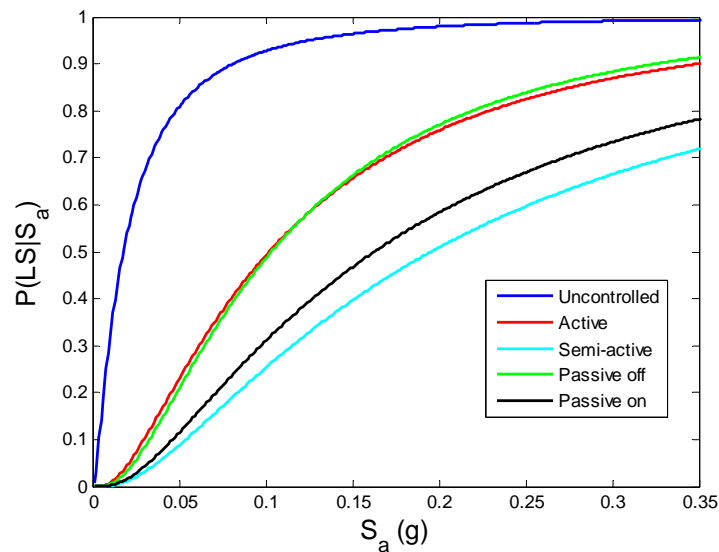
Figure 4.8 Fragility Curve Analysis of Overturning Moment

The *a* and *b* parameters for the power-law form for the nonlinear regression models using overturning moment as the limit state capacity are provided in Table 4.3.

Table 4.3 Parameters of nonlinear regression models for overturning moment

	Uncontrolled	Active	Passive off	Passive on	Semi-active
a	3.04E+06	1.18E+06	1.35E+06	8.79E+05	8.10E+05
b	0.55	0.55	0.61	0.53	0.54

4.4.2 Peak Responses of the Benchmark Bridge

Peak responses of the cable-stayed bridge retrofitted using the control systems are compared in this section. A comparison of the peak responses also serves as a measure to test the validity of the fragility curve analyses performed in the above section.

A comparison of the peak responses for the deck displacement is shown in Figure 4.9. The passive-off case shows the highest deck displacements in terms of both actual value and number of occurrences, giving it the least mitigating effect. The active case shows very high peak values for the higher intensity ground motions and some of the lower intensity ground motions as well. The semi-active case has values similar to the passive-on case at lower intensities, but does not perform as well for higher intensity ground motions. The passive-on case typically has the lowest values for the lower intensity ground motions and among the lowest for the higher intensity measures. The uncontrolled system, however, has the best performance by far with the lowest peak values in terms of deck displacement for the higher intensity ground motions.
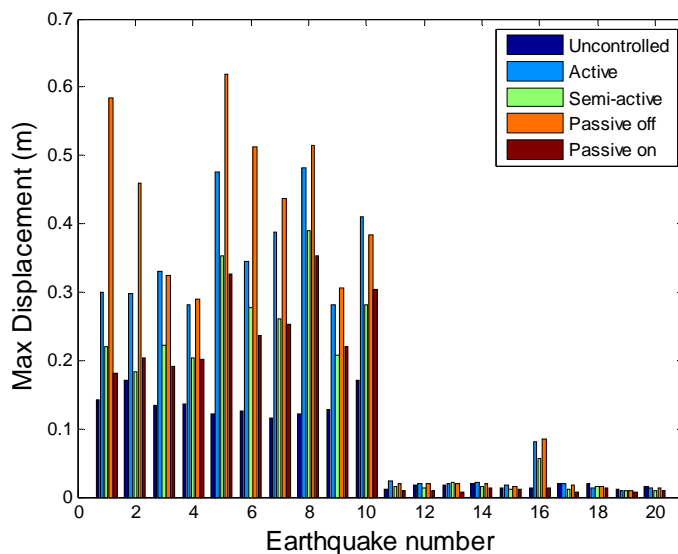
Figure 4.9 Peak Responses of Deck Displacement for Ground Motions

A comparison of a representative time history responses for deck displacement is provided for the active and semi-active controlled bridge model in Figure 4.10. The comparison evaluates the displacement of Bent 1 excited by Earthquake 5. Results show that the active

and semi-active control systems actually increase the displacement located in Bent 1. In comparison, the semi-active control case provides less of an increase than the active control case.

A comparison of the deck displacement time history responses on Bent 1 excited by Earthquake 17 is provided in Figure 4.11. The active and semi-active control cases are also compared in this analysis. The active control case is shown to reduce the overall displacement, if not all of the larger responses for the time history. The semi-active control case provides the best mitigating effect by reducing the deck displacement responses throughout the entire time history.
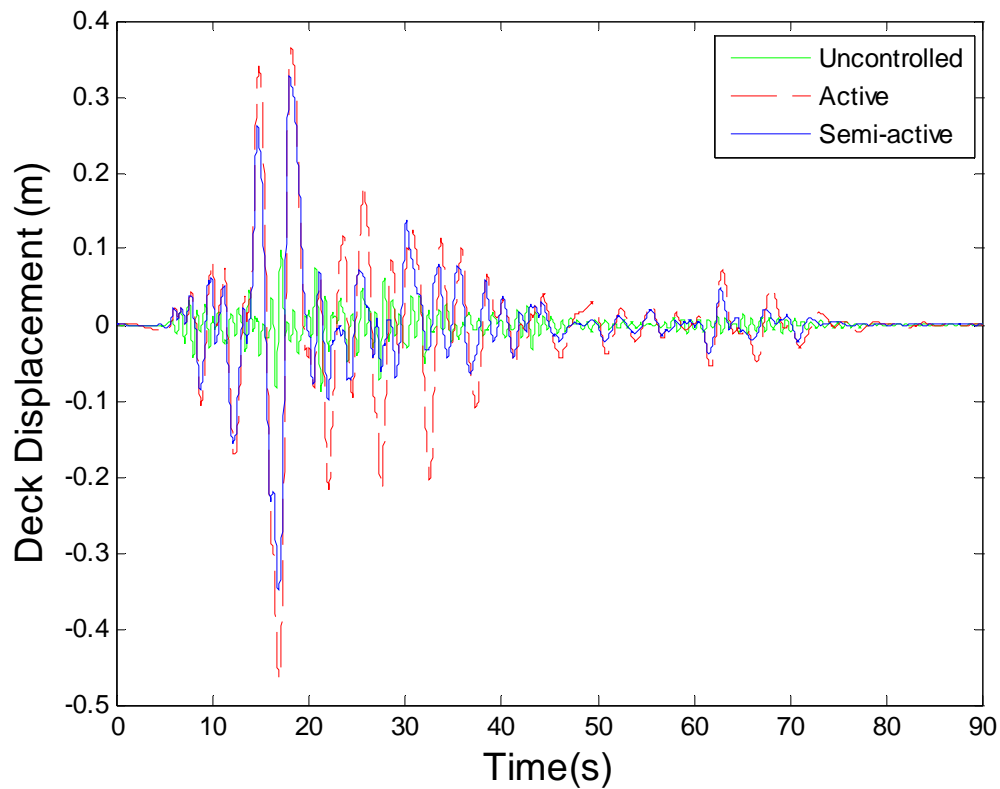
Figure 4.10 Time History Response of Deck Displacement for Earthquake 5

Figure 4.11 Time History Response of Deck Displacement for Earthquake 17

A comparison of the peak responses for the deck shear is performed in Figure 4.12. Determining the highest overall responses is difficult for this case. The higher intensity ground motions show that the passive-off case has a slight lead over the active case in terms of the highest peak responses. Conversely, the peak responses for the active cases are slightly higher than the passive-off case for the lower intensity measures. The debate over higher overall responses is extended to the uncontrolled and passive-on cases which comprise the middle range of peak values. There is constant changing of the two control systems as the higher values making determining which is higher overall very difficult. The semi-active controlled bridge is the most consistent of all the mitigation options. This

control system, with several exceptions, has the lowest peak responses for the deck shear and thus the best performance.
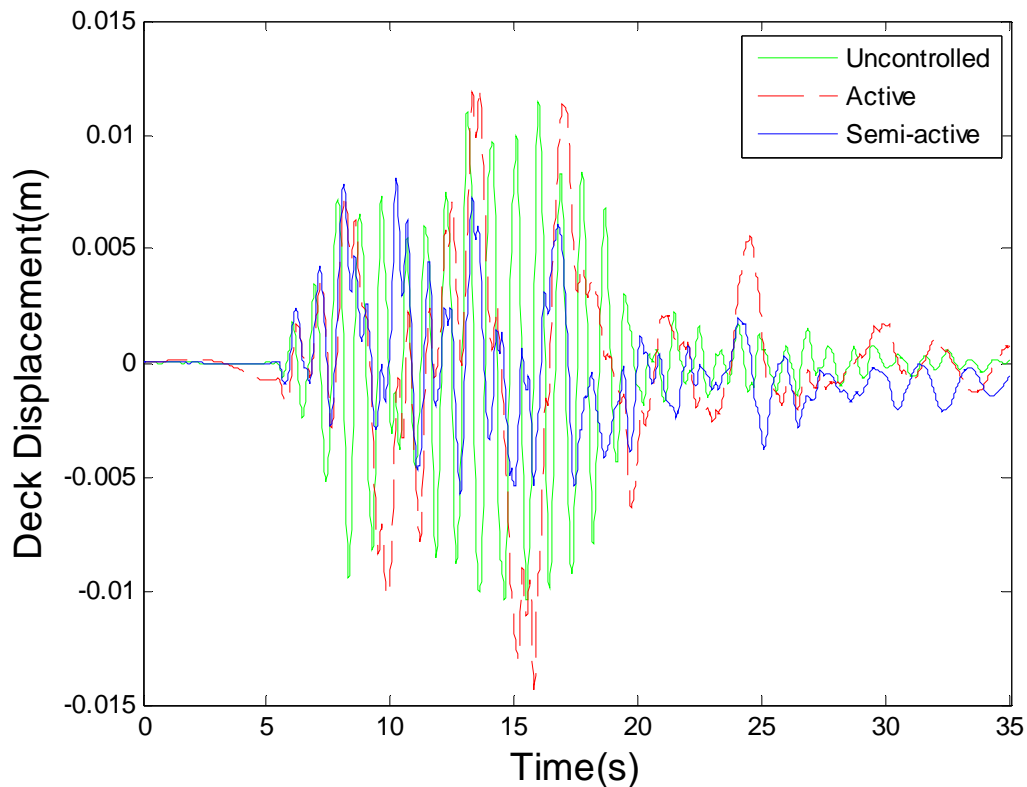

Figure 4.12 Peak Responses of Deck Shear for Ground Motions

A comparison of a representative time history responses of the deck shear for the active and semi-active controlled bridge model is provided in Figure 4.13. The time history response shown is the shear at the deck-tower connection over Pier 2 excited by Earthquake 5. The active control system is shown to have a detrimental effect on the deck shear throughout the entire time history. This effect actually increases the deck shear imposed on the tower connection over the uncontrolled bridge model. The semi-active control case provides a moderate mitigation effect for the bridge model under this seismic event.

 Another comparison of the deck shear over Pier 2 is evaluated in Figure 4.14 for the active and semi-active controlled bridge models. The bridge model is excited by Earthquake 17 in this analysis. Implementing the active control system increases the deck shear in the bridge

model several times that of the uncontrolled structure. The semi-active control case is shown to match or reduce the deck shear imposed on the tower of the uncontrolled case.

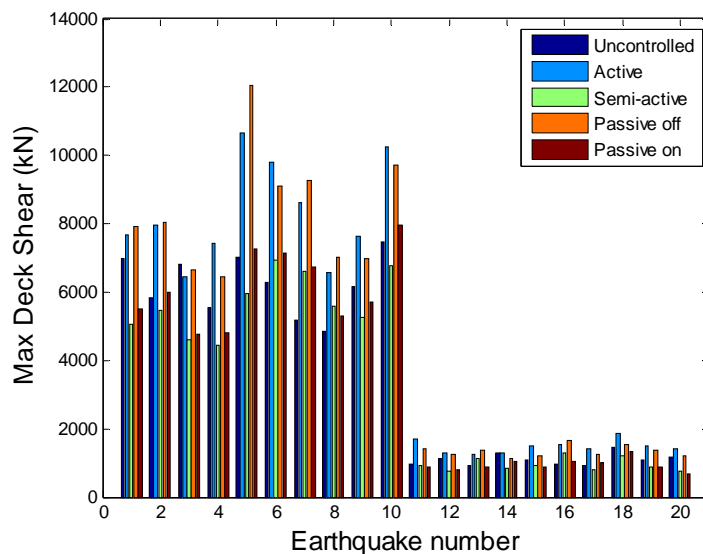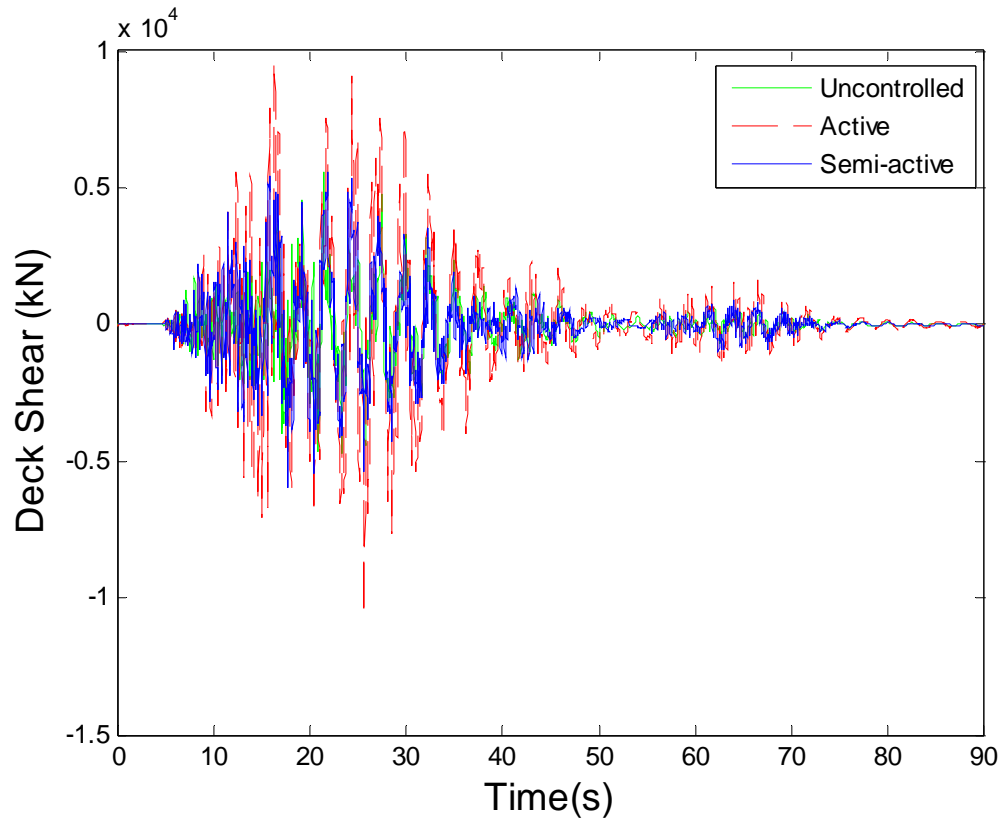**Figure 4.13 Time History Response of Deck Shear for Earthquake 5**
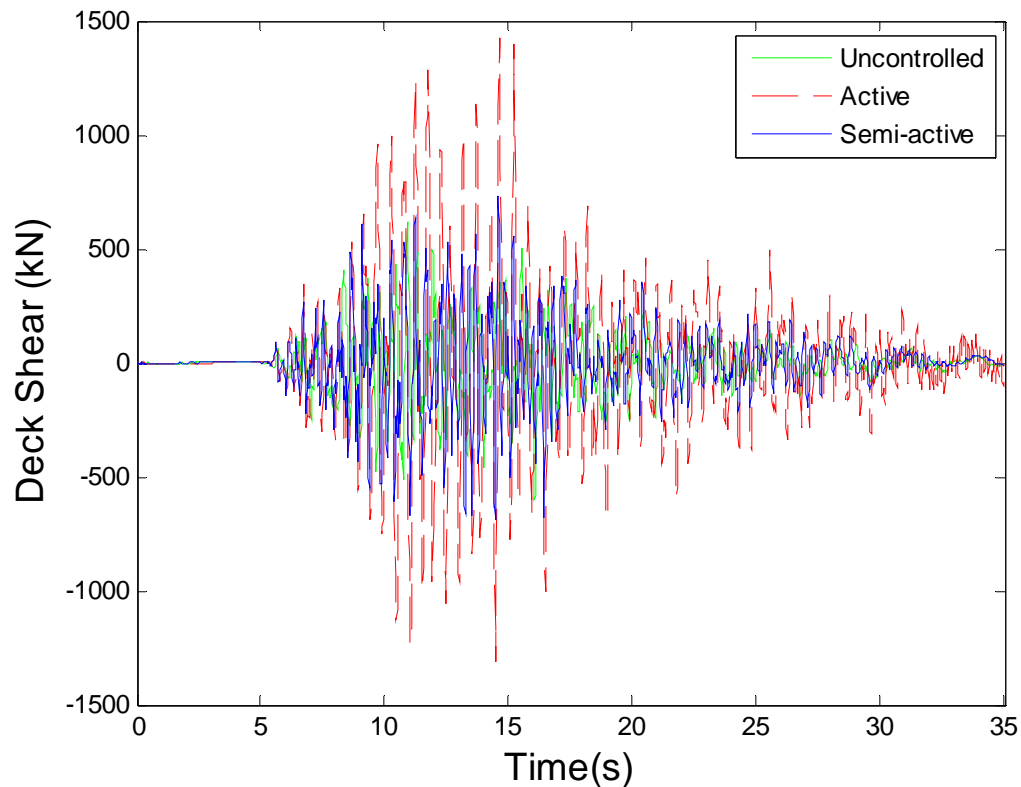
Figure 4.14 Time history Response of Deck Shear Earthquake 17

A comparison of the overturning moment peak responses for each of the control cases is presented in Figure 4.11. The uncontrolled building is the most obvious case and also the highest. The active control system has the least mitigating effect for the control options provided. The passive-off case has peak responses that are in the middle range of the various bridge cases for nearly all of the lower intensity and some of the higher intensity ground motions investigated. The passive-on case has the second best performance. This particular mitigation strategy has overall lower peak responses than any case other than the semi-active case. The semi-active control system has the best performance, having the lowest peak responses for the suite of ground motions.
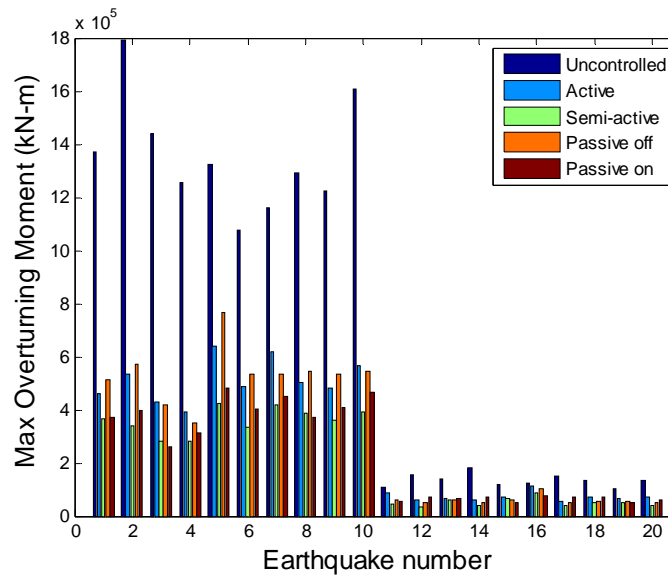
Figure 4.15 Peak Responses of Overturning Moment for Ground Motions

A comparison of the time history responses for overturning moment is shown in Figure 4.16 for the active and semi-active controlled bridges. The overturning moment response is the moment at the base of the tower over Pier 2 excited by a high intensity ground motion. The figure displays the mitigating effect of the active and semi-active control systems on the bridge model. The semi-active control case is shown to have a greater reduction of the time history responses than the active control system.

The time history responses for overturning moment excited by a low intensity ground motion are compared for the active and semi-active cases in Figure 4.17. The active and semi-active control systems offer a significant reduction of the responses for the first half of the ground motion's duration. The active controlled bridge tends to have responses that are higher than the uncontrolled case for the latter portion of the time history. The semi-active

109

case, on the other hand, continues to reduce the time history responses of the bridge model

over the uncontrolled structure.
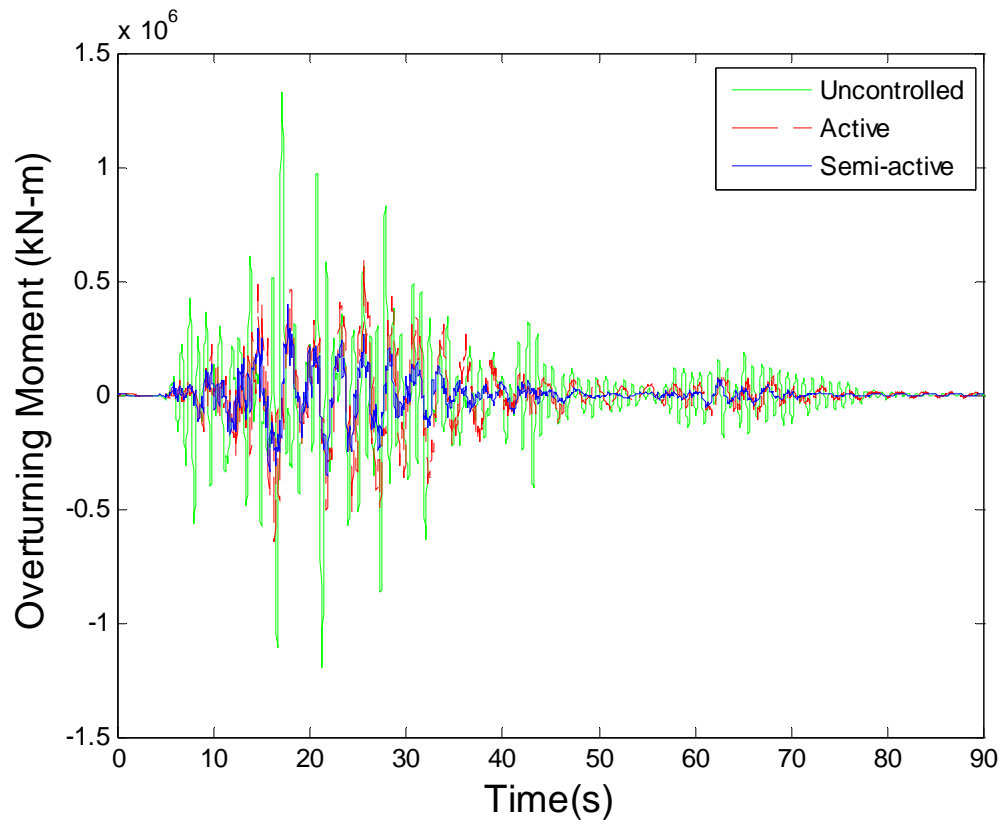
Figure 4.16 Time History Response of Overturning Moment for Earthquake 5
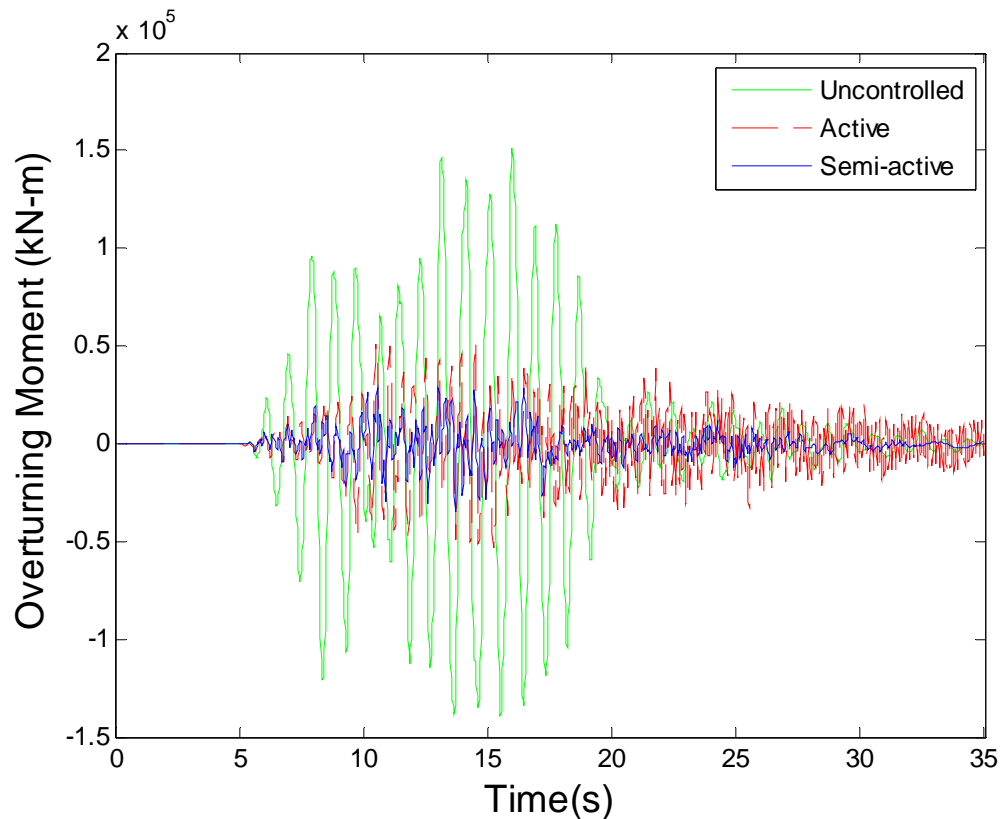
Figure 4.17 Time History Response of Overturning Moment for Earthquake 17

4.4.3 Cable Tensions in Acceptable Range

The cables of the cable-stayed bridges are an important component in the control designs considered. The cables could fail if the tension is too high and cause massive damage to the superstructure or vehicles crossing the bridge during a seismic event. Too much slack in some of the cables would significantly increase the forces in other cables. Therefore, it is important that the cables stay within an acceptable range of tension to prevent this from occurring. Additionally, exceedance of an acceptable range would result in an invalid model.

The acceptable range of tension is defined in the benchmark files for the cable-stayed bridge. An investigation of the number of cables that exceed this region is conducted for the unretrofitted and retrofitted bridge cases as shown in Table 4.1. Each case is subjected to Earthquake 10, which happens to be the ground motion that causes the most exceedance of cables. The uncontrolled bridge suffers the largest number of exceedances with 66 cables going slack, which is roughly half of the cables on the bridge. The active case reduces this number, but still has 24 cables that are not in the acceptable region. The MR damper cases work well in limiting the number of cables that exceed the acceptable region. The passive-off case confines the cables outside of the acceptable region to 18. Both the passive-on and semi-active controlled bridges offer optimal performance by restricting all of the cables from exceeding the acceptable range.

Table 4.4 Cables exceeding Acceptable Region

Uncontrolled	Active	Passive-off	Passive-on	Semi-active
66	24	18	0	0

4.4.4 Comparison of Control Effort Required

The amount of control effort used by the control devices is also a design consideration. Minimization of device usage and control forces applied can possibly prolong the life of the control devices. Thus, development of control designs that require smaller devices which may not have to use full capacity will generally be less expensive. In this example, the three most effective control designs were considered from an economic standpoint based on their control efforts for the bridge model excited by Earthquake 5. Table 4.1 shows the mean of

the RMS control forces per device at the 8 different locations. Results show the passive-on control case has the highest RMS control effort with a value of 277.7 kN. The semi-active control case comes in second with a RMS control effort of 254.4 kN. The lowest control effort required of 104.9 kN is developed by the active control system. An investigation of more aggressive active controllers showed that even a slight increase in the weighting for the active control system would result in instability.

Table 4.5 RMS Values of Control Forces (kN)

Passive-on	Active	Semi-active
277.7	104.9	254.4

4.4.5 Summary

This chapter focused on the development of fragility relationships for a cable-stayed bridge structure retrofitted using control devices. The bridge model used for this study is the Bill Emerson Memorial Bridge located near Cape Girardeau, Missouri. The bridge model was subjected to ground motions indicative of the New Madrid Seismic Zone. The ground motions were provided by Wen and Wu (2001). The fragility relationships were based on global parameters that were meant to determine system functionality. These global parameters served as the limit states: deck displacement, deck shear, and overturning moment. Passive, active, and semi-active control devices served as the retrofit options. Sensors for both smart systems included accelerometers and displacement sensors. Force transducers were also used for the semi-active control system to properly determine the necessary control forces. The active control system used hydraulic actuators and an

H_2/LQG controller to drive and calculate the control forces. Both the passive and semi-active cases used MR dampers as control devices. The Bouc-Wen hysteresis model described in Chapter 2 was employed in both cases. Determination of the control forces for the semi-active case was achieved using an H_2/LQG control law and the modified clipped optimal algorithm. In addition, an investigation of the peak responses was conducted to evaluate the effectiveness of the fragility analyses. Further investigations were performed to determine if a necessary allowance of cables were being restricted to the acceptable region and to that an appropriate amount of control effort was being used.

A comparison of the various mitigation techniques employed for the cable-stayed bridge revealed that the semi-active case had the best performance for two of the fragility assessments while the uncontrolled case had the best system reliability for the remaining fragility assessment. Despite its benefit in one fragility assessment, the uncontrolled case's performance in the other assessment is moderate to very poor. In fact, the uncontrolled system provides no system reliability in one of the assessments for higher intensity ground motions. On the other hand, the semi-active control still offers a suitable amount of system reliability for the assessment in which it does not have the best performance. In fact, the semi-active case has the best performance for the numerical model used in that assessment which is more flexible. Therefore, it is determined that the semi-active control has the best overall performance for the cases presented in the fragility assessments.

A comparison of the peak and time history responses of the limit state parameters showed that the fragility assessments accurately describe what the behavior of the cases over the

suite of ground motions. The various cases show the same performance level throughout each of the comparisons in all but one case for the peak responses. The time history responses for the deck displacement yield similar conclusions for the structure excited by Earthquake 5. The retrofitted structures have better performance for the structure excited by Earthquake 17. The semi-active and uncontrolled cases for the time history responses show closer results than the fragility assessment. The results from the time history analysis and fragility analysis show very good correlation. It is noted that the fragility assessment is based on the entire suite of ground motions and the time history only takes two ground motions into account, so finding good correlation is difficult. Overall, the semi-active case is shown to have the best performance in terms of peak and time history responses.

The confinement of the cables within an acceptable tension range was another design consideration. The semi-active case and the passive-on cases were shown to keep the cables within the acceptable region better than any other cases. In fact, all of the MR damper cases were among the highest cases.

The control force used by the control devices was another important concern from an economic standpoint. The passive-on and semi-active cases produce similar results in control effort. The active control case generates the lowest amount of control effort required. The active case, however, fails to perform as well as the semi-active control case in almost every analysis. Increasing the control effort to provide better results for the active control case result in an unstable controller. It is also noted that these analyses are performed without issues such as measurement noise.

Chapter 5

Conclusions

A methodology has been presented for examining seismically excited structures with semi-active control systems through fragility curve analyses. Numerical models of both a nonlinear high-rise steel moment-resisting frame building and a cable-stayed bridge were used in this study to demonstrate the methodology. Each structure was retrofitted with various control strategies: passive, active, and semi-active control. Fragility curve analyses of each control case were conducted and compared for the structures.

Chapter 1 provided background information on fragility curves and structural control. This information included not only a look at fragility curves from a general standpoint, but as an effective and practical measure in terms of examining structures for seismic mitigation. A concise literature review of structural control was provided as well. Studies showed the mitigating effect of structures retrofitted with passive, active, and semi-active control systems.

The actual methodology used to examine the numerical models provided comprises most of Chapter 2. A nonlinear regression model was used to develop the fragility relationships. The limit states for the building model and bridge model as well as ground motion data were presented here. The phenomenological model for the Bouc-Wen MR damper model is discussed in this section. The passive cases were modeled by implementing MR dampers.

An H_2/LQG control law was used for the active and semi-active cases. This controller was used in conjunction with a decision block for the semi-active control system to form the modified clipped-optimal control algorithm. In addition, a sensitivity study was conducted for the nonlinear benchmark building. The study investigated the influence of data values used for the nonlinear regression model as well as the type of demand provided. Results showed that curve fits and fragility curves evaluated below the largest peak seismic intensity measure (actual data region) provided logical conclusions thus limiting the range of appropriate investigation to seismic intensities in the actual data region as used in this thesis. The choice of spectral acceleration or peak ground acceleration proved to be inconsequential to the behavior of the fragility assessments.

Chapter 3 presented a numerical study of a nonlinear benchmark building. The building model used was the 20 story steel moment-resisting frame building designed for the SAC Phase II Steel Project. Fragility analyses were conducted for the structure excited by 20 synthetic ground motions developed by Wen and Wu (2001) for the Memphis, TN area. Three different limit states were evaluated: inter-story drift, base shear, and absolute acceleration. Fragility assessments were conducted for the structure retrofitted with passive, active, and semi-active control devices. The fragility relationships showed that the semi-active control system provided the greatest system reliability. Additional support of the fragility relationships were provided through analyses of the limit state parameters for each of the control cases in terms of peak responses and time histories. The semi-active control case provided superior performance at a fraction of the control effort provided by the passive-on and active control cases.

Chapter 4 discusses the fragility assessment of a benchmark cable-stayed bridge. The numerical model used for simulation was the Bill Emerson Memorial bridge located near Cape Girardeau. The model was excited using the 20 Wen and Wu (2001) ground motions for the Memphis, TN area. Fragility curves were developed for the bridge under these excitations for the deck displacement, deck shear, and overturning moment limit state capacities. The fragility relationships showed that semi-active control provided the best system reliability for two of the cases. Retrofitting the structure only decreased the system reliability for the remaining fragility analyses. However, not retrofitting the structure resulted in catastrophic effects in some cases. Strong correlation was shown between the fragility assessments and the peak responses and time histories of the various control cases, thus supporting the fragility analysis approach. A study of the tension in the cables showed that the passive-on and semi-active case prevented all of the cables from exceeding an acceptable range. The active control case required the smallest amount of control effort, but failed to provide sufficient performance in many cases.

This thesis demonstrates the possibility of emerging techniques of consequence based engineering with established methodologies such as structural control. Not only does this thesis support previous work regarding the efficacy of control devices through fragility analyses, but it serves to showcase the promise of semi-active control for mitigation purposes of different types of civil structures.

On a grand scale, fragility assessments allow engineers to bridge the communication gap between themselves and decision makers for discussions regarding emergency management.

Fragility curves allow for an accurate, quick, and easy way for engineers to explain the benefits associated with retrofitting crucial civil structures in a community through techniques such as structural control to decision makers.

5.1 Future Work

This thesis investigated the use of control systems as a retrofit strategy for civil engineering structures through fragility assessments. Both numerical studies showed the benefit of control systems under a suite of ground motions for the limit states provided. The work provided will be made available for MAE center researchers in the future. In addition, this work utilizes ground motions indicative for the Mid-America region which is beneficial for MAE center goals. One of the MAE centers goals in which the work herein is an integral part is the development of MAEviz. MAEviz is software which performs seismic risk assessments and mitigation analyses such as cost-benefit ratios and user defined scenarios. The work herein will be used for providing control systems as a retrofit option for certain structures in a community.

It is noted that this work is only one series of investigations providing control devices as a seismic mitigation tool through fragility assessment. More work should be developed in terms of the devices, control algorithms, limit states, and structures themselves to provide an in depth look at the capability of fragility assessments using structural control.

The types of devices and their placement in a structure is an important consideration for investigation in a related work of this study. Much like the MR dampers, newer devices are being developed and fragility assessments may serve as another measure to test their capabilities for future practical implementation. Placements based on engineering judgment or genetic algorithms could result in strategies that optimize performance and reduce device cost.

Similar to control devices, various types of control algorithms can be used to investigate their effectiveness. Because fragility assessments usually encompass a number of earthquake motions, the robustness of a control algorithm may well be determined through fragility assessments.

Different types of limit state capacities are another variable for investigation through fragility assessments. As shown in this thesis, different types of structures are subject to failure in different ways, therefore different limit state capacities should be investigated. Moreover, decision makers may determine that system reliability should be evaluated through different limit states.

More types of structures would also be a suitable variable under the methodology proposed. Models of structures such as hospitals, schools, and fire stations would be very important to investigate for any community. Also, structures were only investigated from a numerical standpoint. The advent of new methodologies such as Fast Hybrid Testing (FHT) at Colorado University NEES will allow for fragility assessments of partial experimental

models, which could result in the methodology being used for full experimental implementation in the future.

While many various topics have yet to be explored, this thesis provides a foundation for the development of various control strategies as retrofit options for seismic risk assessment through fragility curve analyses.

References

Abdel-Rohman, M. and Leipholz (1979), "Automatic Active Control" Structural Control: Proceedings of the International IUTAM Symposium on Structural Control, Ontario, Canada, June 4-7.

Abrams, D.P., (2002). "Consequence-based engineering approaches for reducing loss in mid-America," Linbeck Distinguished Lecture Series in Earthquake Engineering, University of Notre Dame.

ACI (2005), Building Code Requirements for Structural Concrete, prepared by American Concrete Institute.

Agrawal, A.K., Yang, J.N., and He, W.L. (2003), "Applications of Some Semiactive Control System to Benchmark Cable-Stayed Bridge" *Journal of Structural Engineering: Special Issue on Structural Control.* **129**(7), pp. 884-894.

AISC (2001), LRFD Manual of Steel Construction: Third Edition, prepared by the American Institute of Steel Construction.

Ang, A. and Tang, W. Probability Concepts in Engineering Planning and Design. Volume I-Basic Principles. John Wiley & Sons, Ltd: New York, 1975.

Bai, J.W. (2004), *Seismic fragility and retrofitting for a reinforced concrete flat-slab.* Masters Thesis. Texas A & M University, College Station, Texas.

Bontempi, F., Casciati, F., and Giuduci, M. (2003), "Seismic response of a cable-stayed bridge: active and passive control systems (Benchmark Problem)" *Journal of Structural Control: Special Issue on Cable-stayed Bridge Seismic Benchmark Control Problem.* **10**, pp. 169-186.

Borcherdt R.D. and Glassmoyer, G. (1992), "On the characteristics of local geology and their influence on ground motions generated by the Loma Prieta earthquake in the San Francisco Bay region, California," *Bulletin of the Seismology Society of America*, **82**(2), pp. 603-641

Brandow and Johnston Associates (1996). Consulting Structural Engineers, Los Angeles. SAC Steel Project. (1994), Technical Office, Richmond, California. 94804-4698. http://www.sacsteel.org/.

Casciati, F., Cimellaro, G.P., and Domaneschi, M., Seismic Fragility of a Cable-stayed bridge when retrofitted by hysteretic devices. Computers and Science (2008), doi:10.1016/j.compstruc.2008.01.012

Domaneschi, M. (2005). *Structural Control of Cable-stayed Suspended Bridges.* Doctoral Dissertation. University of Pavia, Pavia, Italy.

Dyke, S.J., Spencer, Jr., B.F., Quast, P., and Sain, M.K., (1995), "Role of Control-Structure Interaction in Protective System Design" *Journal of Engineering Mechanics,* **121**(2), pp. 322-338.

Dyke, S.J., Spencer, Jr., B.F., Quast, P. Sain, M.K., Kaspari, Jr. D.C. and Soong, T.T. (1996a), "Acceleration Feedback Control of MDOF Structures" *Journal of Engineering Mechanics,* **122**(9), pp. 907-918.

Dyke, S. J., Spencer Jr., B. F., Sain, M. K. and Carlson, J. D. (1996b), "Modeling and Control of Magnetorheological Dampers for Seismic Response Reduction." *Smart Materials and Structures,* **5**, pp. 565–575.

Dyke S.J., Spencer Jr. B.F., Quast, P., Kaspari, Jr., D.C. and Sain M.K. (1996c), "Implementation of an Active Mass Driver Using Acceleration Feedback Control" *Microcomputers in Civil Engineering: Special Issue on Active and Hybrid Structural Control,* **11**, pp. 305-323.

Dyke S.J., Spencer Jr. B.F., Sain, M.K., and Carlson, J.D., (1998), "An Experimental Study of MR Dampers for Seismic Protection", *Journal of Smart Materials and Structures: Special Issue on Large Civil Structures,* **7**(5), pp. 693-703.

Dyke S.J., Caicedo J.M., Turan G, Bergman L.A., and Hague S. (2003), "Phase I Benchmark Control Problem for Seismic Response of Cable-Stayed Bridges" *Journal of Structural Engineering: Special Issue on Structural Control,* **129**(7), pp. 857-872.

FEMA (2000), Prestandard and Commentary for the Seismic Rehabilitation of Buildings (*FEMA 356*), prepared by the ASCE for the Federal Emergency Management Agency, Reston, VA.

Giulio, G.D., Azzara, R.M., Cultrera, G., Giammarinaro, M.S., Vallone, P., and Rovelli, A. (2005), "Effect of Local Geology on Ground Motion in the City of Palermo, Italy, as Inferred from Aftershocks of the 6 September 2002 Mw 5.9 Earthquake," Bulletin of the Seismological Society of America, **95**(6), pp. 2328-2341.

Hudson D.E. (1972), "Local distribution of strong earthquake ground motions" Bulletin of the Seismological Society of America, **62**(6), pp. 1765-1786.

Iemura, H. and Pradono, M., (2003), "Application of pseudo-negative stiffness control to the benchmark cable-stayed bridge" *Journal of Structural Control: Special Issue on Cable-stayed Bridge Seismic Benchmark Control Problem,* **10**, pp. 187-203.

Iemura, H. and Pradono, M. (2005), "Simple algorithm for semi-active seismic response control of cable-stayed bridges" *Earthquake Engineering and Structural Dynamics*, **34**, pp. 409-423.

Jansen L.M. and Dyke SJ. (2000). "Semi-Active Control Strategies for the MR Damper: A Comparative Study" *Journal of Engineering Mechanics,* **126**(8), pp. 795–803

Jeong, S.-H., and Elnashai, A.S., (2004), "Fragility Analysis Using a New 3-D Damage Index" *2004 Ancer Annual Meeting*, Honolulu, Hawaii, July 28-30.

Jung, H.-J., Spencer Jr., B.F., and In-Won, L. (2003). "Control of Seismically Excited Cable-Stayed Bridge Employing Magnetorheological Fluid Dampers", *Journal of Structural Engineering: Special Issue on Structural Control.* **129**(7), pp. 873-883.

Kafali, C., and Grigoriu, M. (2004). "Seismic Fragility Analysis" *Proceedings of the Ninth ASCE Specialty Conference on Probabilistic Mechanics and Structural Reliability*, July 26-28.

Kim, S.H. and Shinozuka, M. (2004), "Development of fragility curves of bridges retrofitted by column jacketing" *Probabilistic Engineering Mechanics,* **19**(1-2), pp. 105-112.

Lew, H.S. and Kunnath, S.K. (2002), "Assessment of Structural Systems Evaluation Methods Based on Local Seismic Demands" *Innovations in Design with Emphasis on Seismic, Wind and Environmental Loading, Special Publication SP-209-42*, American Concrete Institute, Farmington, Michigan, pp. 771-790.

"Magnetorheological fluid." <u>Wikipedia, The Free Encyclopedia</u>. 5 May 2008, 10:19 UTC. Wikimedia Foundation, Inc. 24 May 2008. <http://en.wikipedia.org/wiki/MR_fluid>

Melchers, R.E. <u>Structural Reliability Analysis and Prediction: Second Edition.</u> John Wiley & Sons, Ltd: Chichester, 1999.

Ohtori, Y., Christenson, R., Spencer, B.F. and Dyke, S.J. (2004), "Benchmark Control Problems for Seismically Excited Nonlinear Buildings" *Journal of Engineering Mechanics*, **130**(4), pp. 366-385.

Pan, Y., Agrawal, A.K., and Ghosn, M. (2007), "Seismic Fragility of Continuous Steel Highway Bridges in New York State" *Journal of Bridge Engineering*, **12**(6), pp. 689-699.

Park, K.-S., Jung, H.-J., Spencer Jr., B.F., and Lee, I.-W. (2003), "Hybrid control systems for seismic protection of a phase II benchmark cable-stayed bridge", *Journal of Structural Control: Special Issue on Cable-stayed Bridge Seismic Benchmark Control Problem,* **10**, pp. 231-248.

Reinhorn, A.M., Barron-Correva, R., and Ayala, A.G. (2002), "Global Spectral Evaluation of Seismic Fragility of Structures," Proceeding of 7th U.S. National Conference on Earthquake Engineering, Boston, M.A, July, 22-25.

Sadek, F. and Mohraz, B. (1998). "Semiactive Control Algorthims for Structures with Variable Dampers," *Journal of Engineering Mechanic*, **124**(9), pp. 981-990.

Shinozuka, M., M.Q. Feng, J. Lee, and T. Naganuma (2000), "Statistical Analysis of Fragility Curves" *Journal of Engineering Mechanics*, 126(12), pp. 1224-1231.

Singhal, A. and Kiremidjian, A.S. (1996), "Method for probabilistic evaluation of seismic structural damage" *Journal of Structural Division*, ASCE, **122**(12), pp. 1459-1467.

Singhal, A. and Kiremidjian, A.S. (1998), "Bayesian Updating for Fragilities with Application to RC Frames" *Journal of Structural Engineering*, **124**(8), pp. 922-929.

Sodeyama, H., Suzuki, K., and Katsuaki, S. (2004) "Development of Large Capacity Semi-Active Seismic Damper Using Magneto-Rheological Fluid", *Journal of Pressure Vessel Technology*, **126**, pp. 105-109.

Spencer Jr., B.F., Carlson, J.D., Sain, M.K. and Yang, G. (1997a) "On the current status of magnetorheological dampers: Seismic protection of full-scale structures" *Proceedings of the American Control Conference*, Washington, D.C.

Spencer Jr., B.F., Dyke, S.J., Sain, M.K. and Carlson, J.D. (1997b) "Phenomenological model of magnetorheological damper" *Journal of Engineering Mechanics*, **123**(3), 230-238.

Spencer, Jr. B.F., Dyke, S.J., and Deoskar, H.S. (1998), "Benchmark Problems in Structural Control: Part 1-Active Mass Driver System" *Earthquake Engineering and Structural Dynamics: Special Issue on the Benchmark Structural Control Comparison*, **27**, pp. 1127-1139.

Taylor, E., and Dyke, S. (2006). "Development of Fragility relationships for Smart Structures" Proceedings of 4th World Conference on Structural Control & Monitoring, San Diego, California July 11-13.

Taylor, E. (2007), *The Development of Fragility Relationships for Controlled Structures*. Masters Thesis. Washington University, St. Louis, Missouri.

Taylor, E., Barnawi W., and Dyke S.J (2007). "Development of Fragility Relationships for Smart Structures" Proceedings of the World Forum on Smart Materials and Smart Structures Technology, Chongqing and Nanjing, May 22-27.

USGS (2008a) "Historic Earthquakes" U.S. Geological Survey, Retrieved from http://earthquake.usgs.gov.

USGS (2008b) "Earthquake Hazard in the Heart of the Homeland" U.S. Geological Survey, Retrieved from http://pubs.usgs.gov/fs/2006/3125/

Walther, R., Houriet, B., Isler, W., Moia, P., Klein, J. Cable stayed bridges: Second Edition. Thomas Telford Publishing: London. 1999.

Wen, Y.K. and Wu, C.L. (2001), "Uniform hazard ground motion for mid-America cities" EERI *Earthquake Spectra*, **17**(2), 359-84.

Wen Y.K., Ellingwood, B.R. and Bracci, J. (2004), "Vulnerability Functions Framework for Consequence-based Engineering" MAE Center DS-4 Report, Mid-America Earthquake Center, UIUC.

Wen, Y.K., and Ellingwood, B.R. (2005), "The Role of Fragility Assessment in Consequence-Based Engineering" EERI *Earthquake Spectra*, **21** (3), 861-877.

Yao, J.T.P., "Concept of Structural Control" Journal of the Structural Division, (1972), **98**(ST7), 1567–1574.

Yi, F., Dyke, S. J., Caicedo, J. M., and Carlson, J. D. (2001), "Experimental Verification of Multi-Input Seismic Control Strategies for Smart Dampers" *Journal of Engineering Mechanics*, **127**(11), pp. 1152-1164. 1164.

Yoshida, O., (2003), *Torsionally Coupled Response Control of Earthquake Excited Asymmetric Buildings: Development and Application of Effective Control Systems Using Smart Dampers.* Doctoral Dissertation. Washington University, St. Louis, Missouri.

Yoshida, O., Dyke, S.J., Giacosa, L.M., and Truman, K.Z. (2003), "Experimental Verification of Torsional Response Control of Asymmetric Buildings Using MR Dampers", *Earthquake Engineering & Structural Dynamics*. **32**(13), pp. 2085-2105.

Yoshida, O. and Dyke, S.J. (2004), "Seismic Control of a Nonlinear Benchmark Building Using Smart Dampers" *Journal of Engineering Mechanics*, **130**(4), pp. 386-392.

Vita

Waleed T. Barnawi

Date of Birth	September, 14 1981
Place of Birth	Tulsa, Oklahoma
Degrees	B.S. Civil Engineering, May 2006
	M.S. Civil Engineering, August 2008
Professional Societies	American Society of Civil Engineers
	National Society of Black Engineers
	Multi-Disciplinary Center for Earthquake Engineering Research
	Mid-America Earthquake Center
	Earthquake Engineering Research Institute

Publications

Dyke, S., Gao, X., and Barnawi, W., "Fast Hybrid Testing of Magneto-Rheological Damper Control of Benchmark Building" *Proceedings of the 2008 ASCE Engineering Mechanics Institute Conference*, Minneapolis, MN, May 18-21, 2008.

Barnawi, W. and Dyke, S., "Fragility Curves of a Benchmark Cable-Stayed Bridge with Smart Devices" *Proceeding of the 2008 ASCE Engineering Mechanics Institute Conference*, Minneapolis, MN, May 18-21, 2008.

Barnawi, W. and Dyke, S., "Fragility Based Relationships of a 20-story Benchmark Building with Smart Device Implementation" *Proceedings of the 2008 ASCE Earth and Space Conference*, Long Beach, CA, March 3-5, 2008.

Barnawi, W., Hendel, M., Truman, K., and Dyke, S. "Experiences in Globalization in Engineering Modules for the K-12 Classroom", *Proceedings of the 2007 ICEER Conference*, Victoria, Australia, December 2-7, 2007.

Barnawi, W., Dyke, S., Truman, K., Taylor, E., and Anderson, L. "Earthquake engineering modules for K-12 education" http://mase.wustl.edu/wusceel/ucist/TeachingModules/K-12

Taylor, E., Barnawi, W., and Dyke, S., "Development of Fragility Relationships for Smart Structures" *Proceedings of the World Forum on Smart Materials and Smart Structures Technology*, Chongqing and Nanjing, May 22-27, 2007.

Barnawi, W., Walsh, K., Abdullah, M., and Lee, T. "Investigating Appropriate Conditions for Passive and Semi-Active Control Devices" *Proceedings of the Research Experience for Undergraduates in Japan Symposium*, Tokyo, August 5, 2005.

August 2008

Short Title: Fragility Curves with Semi-active Devices   Barnawi, M.S. 2008